8-2019

Hydrogeologic and Geomorphic Processes in a Wastewater Spray Irrigated Agricultural System Located In a Karstic Seasonably-Cold Climate

Timothy J. Daniel
Clemson University, timothy.daniel93@gmail.com

HYDROGEOLOGIC AND GEOMORPHIC PROCESSES IN A WASTEWATER SPRAY IRRIGATED AGRICULTURAL SYSTEM LOCATED IN A KARSTIC SEASONABLY-COLD CLIMATE

A Thesis
Presented to
the Graduate School of
Clemson University

In Partial Fulfillment
of the Requirements for the Degree
Master of Science
Hydrogeology

---

by
Timothy John Daniel
August 2019

Accepted by:
Christophe Darnault, Committee Chair
Lawrence Murdoch
Ron Falta

ABSTRACT

Wastewater reuse, particularly via the use of spray irrigation of treated effluent, is a common practice worldwide and can help lessen the impact of the overconsumption of water resources. The increased recharge to the subsurface that enhances weathering and erosion during the irrigation application process makes it important to characterize any changes in the land surface over time. The Living Filter at Pennsylvania State University receives on average 1.5 million gallons per day (MGD) of secondary treated wastewater effluent year round. This Living Filter has been in continuous operation in some capacity for the past 55 years without any significant issues related to geomorphologic processes. For over 50 years, nitrate as nitrogen (NO_3-N) concentrations in the karstic groundwater system have fluctuated with time due to variations in the application rate of the effluent and concentration within the effluent. Although nitrate concentrations previously exceeded the federal maximum contamination levels (MCL) of 10 parts per million (ppm) in groundwater monitoring wells in and around the living filter, they are now below the MCL of 10 ppm ever since the early 2000's.

The objective of chapter two of this study was to identify and relate any bedrock fracture traces and surface depressions to any surficial or geomorphologic processes currently underway.

The objective of chapter three this study is to (1) model groundwater flow in the karst landscape to examine the hydraulic response of the aquifer to the recharge by wastewater irrigation of the Living Filter and (2) simulate the fate and transport of nitrate in the karst aquifer resulting from wastewater irrigation of the Living Filter site.

For chapter two, a manual process was developed in order to determine the trend and location of several fracture traces within the Astronomy site section of the Living Filter. The Living Filter is underlain by a massive dolomite with fractures trending near N-S that were previously documented using photogrammetry. A semi-automated isolation scheme was next used to identify and correlate closed hillslope depressions to the location of fracture traces in the Living Filter. A predominant but slight NE-SW trend was observed among fractures at N5E in the area north of the Pennsylvania Furnace Anticline. A high occurrence of depressions was noted in the area of fractures compared to non-fractured bedrock. The depressions in this area were found to have a net gain of 8,000 ft^2 the result of which was from the net loss of 5,000 ft^2 within the agricultural portion of the site and a net gain of 13,000 ft^2 within the forested portion of the site. Cross sections of several depressions within cropped areas indicated a lower angle slope corresponding to a V-shape while depressions within forested areas were characterized by a traditional U-shape and previously established steeper slope.

For chapter three, a framework was developed to model the impact of treated wastewater and disposal of large volumes of wastewater for irrigation in agriculture and forestry land uses on groundwater nitrate contamination in a karst landscape of the Spring Creek Watershed, central Pennsylvania, in order to understand the long term contributions of nitrate to the unconfined karst aquifer below the “Living Filter” site. This study uses a numerical simulation model to examine groundwater flow and nitrate fate and transport in the karst landscape of the Spring Creek Watershed, central Pennsylvania, in response to aquifer recharge by wastewater irrigation of the Living Filter site. The

simulation of nitrate fate and transport in the aquifer was conducted by developing a groundwater mass transport model using MODFLOW and MT3DMS. A number of predictive simulations for year 2015 and 2035 were carried out to evaluate the impact of treated wastewater and disposal of large volumes of wastewater for irrigation in agriculture and forestry land uses on groundwater nitrate contamination and concentrations. The calibrated groundwater model yielded a Root Mean Square Error of 5.41 for the area of irrigation and 24.67 for the entire modelled area. Results of the water quality model show that the aquifer recharge by wastewater reuse irrigation does not produce nitrate levels above 10 $mg \cdot L^{-1}$ in the karstic landscape of the Spring Creek Watershed, thus meeting the regulatory standards for nitrate in groundwater. Results also demonstrated the sustainability of wastewater reuse irrigation practices for agriculture and forestry land uses.

These results will enhance the current understanding of the different morphologic characteristics of both forested and agricultural depressions in karst topography along with the nitrate dynamics of karstic wastewater effluent recharge systems. The workflows implemented here can be implemented in similar sites that display topographical variances from the bedrock fractures or increased nitrate concentrations from wastewater effluent recharge.

DEDICATION

I would like to dedicate this work to all of those who have loved and supported me over my entire collegiate career. Thank you to my parents Jeff and Bonnie and my sister Rebecca for always being understanding and willing to lend an ear or a word of encouragement. Thank you to my fiancé Sarah for always being there for me and her unconditional love and support.

ACKNOWLEDGMENTS

I would like to acknowledge Blake Lytle and the Clemson Center for Geospatial Technologies for their assistance in processing geospatial data. I would like to thank John Richendrfer from Penn State for his assistance with data processing and retrieval. I would like to thank the rest of the staff at the Office of the Physical Plant at Penn State University who assisted in data retrieval including Jim Loughran, Jim Baird, Dave Swisher, John Guadlip, and Ping Zhao. Professors Henry Lin, Heather Gall, and Professor Emeritus Richard Parizek where all instrumental in this collaborative research effort.

TABLE OF CONTENTS

Page

Table of Contents (Continued) Page

LIST OF TABLES

LIST OF FIGURES

List of Figures (Continued)

Figure Page

List of Figures (Continued)

CHAPTER ONE

INTRODUCTION

Pennsylvania State University has been operating a secondarily treated wastewater irrigated forested and agricultural site known as “The Living Filter” in State College, PA in some capacity since 1962 (Figure 1). The Living Filter is divided into two parcels of differing dimensions, with the Astronomy site encompassing roughly 191 hectares and the Gamelands site encompassing 517 hectares.

Prior to 1960, wastewater from the Borough of State College and the Pennsylvania State University was discharged directly into Spring Creek (Parizek et al., 1967). To mitigate this pollution, the University chose to adopt the practice of wastewater spray irrigation, but the growth of the school and surrounding environs placed Spring Creek under increased environmental stress, which was characterized by high concentrations of nitrate that caused a large fish kill due to eutrophication (Parizek et al., 1967). Even though 85-92% of the biochemical oxygen demand (BOD) was removed during the wastewater treatment process, the volume of water contributed enough mass loading to promote aquatic plant growth and reductions in dissolved oxygen for aquatic animals within Spring Creek (Pennypacker et al., 1967; Parizek et al., 1967).

As Spring creek is known as one of the state’s premier trout streams, in the spring of 1960, the Pennsylvania Department of Environmental Protection issued a cease and desist order to the wastewater treatment authority, and thus the Living Filter was

conceptualized and implemented in 1962. The Living Filter has been in continuously operation in some capacity since 1962 and was expanded in 1983 to its present size.

The use of treated wastewater for irrigation, as an alternative water resource to reduce the increasing pressures on scarce freshwater resources, is a strategic conservation measure supporting agricultural production. The result is substantial benefits from the use of nutrient-rich wastewater effluent, and the achievement of sustainable development goals in the context of the increase in the scarcity of water resources and the impacts of climate change. In arid and semi-arid regions, usually experiencing water shortages for irrigation, treated wastewater may become the main source of water and nutrients for crop production.

CHAPTER TWO

SPATIAL DISTRIBUTION AND MORPHOMETRIC ANALYSIS OF CLOSED HILLSLOPE DEPRESSIONS OVER TIME IN A WASTEWATER SPRAY IRRIGATED KARSTIC LANDSCAPE

Timothy J. Daniel[1], John Richendrfer[2], Ronald Falta[1], Lawrence Murdoch[1], Henry Lin[3], and Christophe J. G. Darnault[1*]

[1]Department of Environmental Engineering and Earth Sciences, Clemson University, Anderson, SC 29625, United States

[2]Office of the Physical Plant, The Pennsylvania State University, University Park, PA 16802, United States

[3]Department of Ecosystem Science and Management, The Pennsylvania State University, University Park, PA, 16802, United States

[*]Corresponding author: Tel: +1 864 656 1398; fax + 1 864 656 0672. E-mail address: cdarnau@clemson.edu

Abstract

Wastewater reuse, particularly via the use of spray irrigation of treated effluent, is a common practice worldwide and can help lessen the impact of the overconsumption of water resources. The increased recharge to the subsurface that enhances weathering and erosion during the irrigation application process makes it important to characterize any changes in the land surface over time. The Living Filter at Pennsylvania State University receives on average 1.5 million gallons per day (MGD) of secondary treated wastewater effluent year round. This Living Filter has been in continuous operation in some capacity for the past 55 years without any significant issues related to geomorphologic processes. The objective of this study was to identify and relate any bedrock fracture traces and surface depressions to any surficial or geomorphologic processes currently underway. The Living Filter is underlain by a massive dolomite with fractures trending near N-S that were previously documented using photogrammetry. A manual process was developed in order to determine the trend and location of several fracture traces within the Astronomy site section of the Living Filter. A semi-automated isolation scheme was next used to identify and correlate closed hillslope depressions to the location of fracture traces in the Living Filter. A predominant but slight NE-SW trend was observed among fractures at N5E in the area north of the Pennsylvania Furnace Anticline. A high occurrence of depressions was noted in the area of fractures compared

to non-fractured bedrock. The depressions in this area were found to have a net gain of 8,000 ft^2 the result of which was from the net loss of 5,000 ft^2 within the agricultural portion of the site and a net gain of 13,000 ft^2 within the forested portion of the site. Cross sections of several depressions within cropped areas indicated a lower angle slope corresponding to a V-shape while depressions within forested areas were characterized by a traditional U-shape and previously established steeper slope. These results will enhance the current understanding of the different morphologic characteristics of both forested and agricultural depressions in karst topography. The workflows implemented here can be implemented in similar sites that display topographical variances from the bedrock fractures.

Keywords: closed hillslope depressions, lineament, wastewater reuse, irrigation, karst system

1. Introduction

Pennsylvania State University has been operating a secondarily treated wastewater irrigated forested and agricultural site known as “The Living Filter” in State College, PA in some capacity since 1962 (Figure 1). The Living Filter is divided into two parcels of differing dimensions, with the Astronomy site encompassing roughly 191 hectares and the Gamelands site encompassing 517 hectares.

Prior to 1960, wastewater from the Borough of State College and the Pennsylvania State University was discharged directly into Spring Creek (Parizek et al., 1967). To mitigate this pollution, the University chose to adopt the practice of wastewater spray irrigation, but the growth of the school and surrounding environs placed Spring Creek under increased environmental stress, which was characterized by high concentrations of nitrate that caused a large fish kill due to eutrophication (Parizek et al., 1967). As Spring creek is known as one of the state's premier trout streams, in the spring of 1960, the Pennsylvania Department of Environmental Protection issued a cease and desist order to the wastewater treatment authority, and thus the Living Filter was conceptualized and implemented in 1962. The Living Filter has been in continuously operation in some capacity since 1962 and was expanded in 1983 to its present size.

One concern regarding the position of the site location of the Living Filter is that State College, PA is located in a seasonably cold climate, with soil frost depths estimated to average 10-15 inches and which is characterized by depths as far as two feet (Parizek, personal communication, 2017). The wastewater effluent is applied year round at an average rate of 1.5 MGD, even during the months of December-March where average low temperatures are below freezing, which results in a drastically altered infiltration scheme. Although localized overland flow has occurred onsite in the past, it has never been observed to flow off site, with ponding typically occurring in closed hillslope depressions. While wastewater reuse is a schemed used in cold climates such as Canada, Northern China, and the Northeastern United states, spray irrigation is not the

preferred method (Rozema et al., 2016; Griffin et al., 2017). Indeed, in several study sites, shallow wetlands are used to help denitrify groundwater runoff and ensure a focused recharge. Although several natural and man-made wetlands are within the Living Filter, a rather significant regions is required to ensure a proper period of both storage and retention. The natural wetlands that are within the Gamelands portion of the Living Filter are a result of both the differential weathering within the bedrock and enhanced infiltration from tear faults (O ’driscoll and Parizek, 2003). A study on the impact of wastewater effluent in chain wetlands found nitrate removal efficiencies in excess of 92% compared to a 34% rate of removal efficiency, which contribute to elevated nitrate levels within the Living Filter (Nemitz, 2001). As of this writing, the ranges of nitrate as nitrogen (NO_3-N) concentrations are between 1 to 8 ppm in a variety of wells underneath the Astronomy site.

Both the underlying geology and the depth of the unconfined aquifer must be considered when determining the placement of a wastewater irrigation site. Ensuring the efficacy of wastewater irrigation requires soil that is adequately permeable to ensure the infiltration of wastewater and which is also characterized by adequate periods for both denitrification and retention. Although wastewater concepts are mostly used in predominantly arid and semi-arid climates such as the Middle East and North Africa (MENA), some parts of Europe, and the western United States (Hamilton et al., 2007), regions that are characterized by delicate surface water systems are also good candidates for wastewater reuse. Indeed, the nation of Japan with the lack of

natural water bodies and retention of rainfall is a big proponent of wastewater reuse technologies (Dayanthi et al., 2006). The state of Florida is also characterized with similar difficulties in that approximately half of all rainfall occurs within a four-month period in the state, with droughts often occurring during the balance of the remaining eight months (Martinez & Clark, 2015).

Unlike traditional wastewater discharges into surface streams where the majority of water fails to replenish the aquifer, wastewater irrigation is advantageous in such regions in that groundwater can function in a nearly closed loop with the only water loss occurring through evapotranspiration. Wastewater irrigation, in addition to the contribution to the groundwater recharge, also augments the base flow into the underlying streamflow. A multitude of factors must be considered in terms of water resources in developed areas. In the United States, there is no clear archive of the percentage of wastewater that is reused between both municipal and industrial supplies ("Guidelines for Reuse", 2012). As of 2006, approximately 7-8% of the United States municipal wastewater was reclaimed, although there are no determinant amounts for industrial use (EPA, 2012; Miller, 2005). In particular areas of the world however, wastewater effluent is reused for either deep well injection or land application, an example of which is in Los Angeles, California, specifically in the Orange County groundwater basin. There, wastewater effluent is used as a seawater barrier and aquifer recharge via injection wells (Herndon and Markus, 2013). Groundwater recharge in this Orange County groundwater basin both meets and exceeds groundwater withdrawals

from the regional aquifer and is similarly cost effective as opposed to importing water to the region, thus indicating the economic viability of wastewater effluent reuse. Many methods are available to apply wastewater to the surface either through wetlands, overland flow, slow infiltration, or through fast infiltration (EPA, 2004).

Several investigations have been undertaken to elucidate the possibility of altered soil properties within the Astronomy site as a result of wastewater irrigation. The bulk densities of soil were determined to vary based on the proximity to both the sprinkler heads and the contours of the landscape (Larson, 2010; Walker and Lin, 2008). A reduced clay content was prevalent within the upper 20 cm of the soil surface within 16 m of sprinkler heads, which was likely due to the translocation of the clay. Further, a higher hydraulic conductivity was observed within the depressions, although it is unknown if this increased conductivity was a result of the preferential pathways or some other mechanism (Dadio, 1998; Walker and Lin, 2008).

Soil crop cover is a significant actor upon the amount of erosion that occurs due to the ability of plants to prevent transport and weathering through their protection of the soil from splash erosion, and through plant roots that ensure the uptake water and the binding of soil. Crop cover in 2017 varied from wheat, sorghum-sudan grass, corn, and fescue depending on the plot location (Figure 2).

Agricultural products from the Living Filter are used as cattle feed for the University's dairy cows and are not intended for human consumption. Crops such as

oranges in Florida that utilize wastewater irrigation are used for human consumption, however, as no interaction of the effluent with the edible fruit occurs (EPA, 2012).

Although no significant study has been undertaken regarding the diversity of the trees and shrubs within the forest, a study of the nearby Gamelands section of the Living Filter from 1997 to 2002 found that the irrigated forest had 200 overstory stems less per hectare than the non-irrigated forest at a population of 336 (Kelso, L.M., Bowersox, 2002). The sapling density was effected even more within the irrigated site, yielding 1008 saplings per hectare compared to 2789 stems per hectare within the non-irrigated control plot. Further, the biodiversity between trees, shrubs, and saplings was also significantly smaller within the irrigated site than that of the non-irrigated site. The irrigated site did yield a higher coverage rate of herbaceous growth compared to the non-irrigated site. It is likely that the increased herbaceous coverage is a result of ice formation on trees and saplings during the winter, preventing growth and downing larger trees due to the excess weight of the ice. Herbaceous plants are seasonal and do not respond to the negative effects of ice accumulation, as they are dormant during the winter. Also, herbaceous plants have been found to have increased yield when irrigated with treated wastewater compared to non-irrigated plants (Caldwell et al., 2007)

Wastewater effluent properties have varied throughout time within the Living Filter as a result of new technologies, population changes, and environmental concerns. In the early 1990's, nitrate within groundwater monitoring wells in and around the site exceeded the Maximum Contaminant Levels (MCLs) that were set at 10 ppm. Currently,

an activated sludge biological nitrogen removal process is employed at the wastewater treatment facility to reduce the nitrate in the effluent. Further, the values of the C:N ratio of 0.04-0.2 with a near neutral pH and nitrate concentrations of approximately 10 ppm have been reported in the effluent from the wastewater treatment facility (Sendagi et al., 2017). Indeed, the monthly averages can vary significantly due to the number of students on campus. Since 2015, the borough of State College has operated on a separate wastewater treatment system with greywater reuse slated to begin within the next several years along with wastewater treatment plant upgrades to reduce the amount of nitrate and volumetric flow received into the Living Filter. Since 1982, the range of the total nitrogen in the effluent from the wastewater treatment plant has varied from between 2-56 ppm with levels at approximately 10 ppm with the implementation of activated sludge process in 1999.

The Pennsylvania State University is currently in the process of retrofitting its campus to support greywater reuse for local irrigation projects in both its athletic fields and community gardens. Greywater is expected to take away up to 0.5 MGD per day of wastewater from the Living Filter in the immediate future with the possibility of expanded use in the future. This greywater utilized in toilets will eventually reflow again to the wastewater treatment plant, so not all of the 0.5 MGD will be completely lost to the plant, although any greywater used for irrigation will be repurposed to recharge the campus aquifer, a distance of three miles from the Living Filter. Further, although current wastewater treatment renovations are underway, neither a final design nor a

series of set treatment targets have been established that is external to the University in terms of securing a Class A (high quality) wastewater certification.

Photogrammetry, first used to capture lineaments in the Nittany Valley of Central Pennsylvania, revealed changes in vegetation, surface color, and water retention in a straight line pattern (Lattman and Parizek, 1964). Surface features in this area that are less than one mile in length are known as fractures, joints, or localized fault systems, and features over one mile in length are inferred as lineaments (Lattman, L.H., Nickelson, 1958). For the sake of this study, lineaments are inferred to manifest in relation to possible extension of bedrock fractures. However, further study is necessary to definitively determine that these lineaments are indeed the results of large scale fractures. Historical pictures of the Living Filter dating back several decades show the presence of several lineaments and depressions (Figure 3). Lattman and Parizek (1964) first noted a reduction in the transmissivity of the Gatesburg formation either along single lineaments or off lineaments in comparison to intersecting lineaments (Lattman and Parizek, 1964).

The critical nature of wastewater reuse in terms of the recharging of both aquifers and base flow to streams and to ensure sustainable agriculture, particularly in terms of the Living Filter, is of use in addressing the following two scientific questions. First, does the addition of on average 1.5 MGD of wastewater through irrigation on the Living Filter result in the increase of fracture apertures through suffusion and any mass wasting through the enlarged fractures via subsidence? Second, do the fracture traces

that indicate regions of greater weathering and permeability represent the likely occurrence of closed hillslope depressions?

In this general context, the objectives of this study are to (1) determine the correlations between the location of the lineaments and the formation of closed hillslope depressions in the cropped and forested portions of the Living Filter, and (2) examine the effects of wastewater irrigation on the spatial distribution and morphometric dynamics of the closed hillslope depression located within the cropped and forested portions of the Living Filter. We first delineated the location and orientation of fracture traces within the Mines dolomite, and then developed a suitable workflow to identify those closed hillslope depressions in both the cropped and forested portions of the Living Filter. Specifically, we designed two workflows in GIS for this study. The first GIS workflow entailed delineating the location and orientations of fracture traces within the Mines dolomite in order to determine any possible correlations between the location of fracture traces and the formation of depressions. The second GIS workflow entailed identifying the closed hillslope depressions located within the cropped and forested portions of the Living Filter to monitor their morphologic dynamics changes over time under wastewater irrigation. The results of this study will aid in the understanding of the occurrence, spatial distribution, and morphologic dynamics of depressions in both crop fields and forests over time in a wastewater spray irrigated karstic landscape. These results will also permit an evaluation of the long-term effects of wastewater reuse irrigation on soil in complex

geologic and hydrologic systems, thus demonstrating the beneficial purpose for use in water resources management, water conservation, and sustainable agriculture.

2. Geology Setting and Soils

The Astronomy site of the Living Filter is underlain by the Mines member, a largely uniform and massive coarse-grained highly bedded dolomite with intermittent sandstone and quartzite layers (Table 1). Excluding a small portion of the forested area which is underlain by the Upper Sandy member, the Mines member is the top geologic unit of the Upper Cambrian aged Gatesburg Formation and has a variable thickness of 150 to 230 feet (Caruccio, 1963). Further, most of the swales and ridges that occur in Centre county are within the common chert bedding that characterizes this Mines member (Caruccio, 1963) (Figure 4).

The geology of the valley and ridge province is predominantly a result of the Alleghenian orogeny and typically exhibits a NE-SW strike. The regional structure of the Allegheny front trends at 52° in this area are evident in the orientation of the surrounding orthoquartzite ridges (Matzke, 1961). In the area of the Living Filter, primary fracture traces exhibit a striking variance from 355° northwest to 15° northeast with secondary fractures at a near perpendicular strike. The fractures and joints in the bedrock of the Nittany valley are often inferred via swales, ridges, and localized depressions (Caruccio, 1963). The preferential flow of infiltrating water into the aquifer

system from such fractures results in a high infiltration rate that causes a subsidence of the land surface through the fracture zones, with a depressed surface extant. The factor of dissolution of the carbonate rocks within the region can also result in the formation of depressions.

While outcrops of the Mines member are absent within the Living Filter, several outcrops are present near the site with voids of 1 to 2 feet present as derived from the visible Mines outcrops solution, (Landon, 1963). Further, both vugs and microfractures in great numbers characterize this area with large surface area causing the regular occurrence of dissolution. The presence of vugs in bedrock also affects the storage coefficient (i.e., storativity) in that a solid and unfractured dolomite has a low storativity and porosity, unlike vuggy and fractured dolomite that significantly increases both of these parameters (Reep, 2009). Unlike the Mines member, the Upper Sandy member is a more granular dolomite with a high occurrence of quartzite and sandstone layers, the latter of which are known to dissolve and contribute to the large voids full of flowing sand (Lattman and Parizek, 1964).

Closed hillslope depressions are defined depressions within the immediate location of the Living Filter (Dadio, 1998). In areas where carbonate bedrock comprises the bulk of the geology, the formation of sinkholes and other karstic features are common. Central Pennsylvania is known for its formation of cover collapse and cover subsidence sinkholes, although these features have a higher likelihood to form in limestone than dolomite. In a closed depression system, hillslopes drain to a depression

in which water accumulates and eroded sediments are deposited (Norton, 1986). Closed hillslope depressions are considered an intermediate stage of hillslope subsidence in which depressions are filled with transported material at a rate near equal to the rate of the subsidence, a manifestation corroborated by Walker and Lin (2008). Also, the depth of the soil A horizon within the depressions is significantly thicker than that of the slope summits.

Depressions also present areas for the occurrence of a focused recharge due to their position within the hillslope allowing for flow accumulation. Although no storage calculations were performed on the depressions within the site, it is common for several depressions to retain water or remain heavily saturated year round. Dadio (1998) determined that a low permeability soil crust forms within the depressions at the Living Filter, which is the likely result of increased clay content and colloids within the wastewater effluent (Figures 5 and 6).

Soils in the Astronomy site are characterized as anywhere between a silt loam and a silty clay loam with varying degrees of slope angles (USDA, 1981). The study site is dominated by Hagerstown silt loam and Hagerstown silty clay loam with a partial mapping of the Hublersburg series in the same area (USDA, 1981). Although the Hublersburg series has been mapped within the study site, Walker and Lin (2008) noted the absence of a Hublersburg series due to the absence of rock fragments within the soil. The Hagerstown series consists of soils that are known to fine downward with an increased clay content at depth (Andrews et al., 2016). Both the Hublersburg series and

the Hagerstown series are soils derived from the decomposition of limestone and dolomite.

Although the depth of the overburden soil within the Astronomy site varies, the average depth of the soil throughout the Mines member is 43 feet compared to 87 feet of soil overlaying the Upper Sandy member (Caruccio, 1963). The overburden sediment above the Mines Dolomite is almost assuredly solely from the decomposition of the Mines Dolomite due to the high occurrence of both oolitic cherts and a high clay content, as the soil composing the Mines member is of a finer texture than the coarse soil of the Upper Sandy member. Caruccio (1963) estimated that the thickness of the regolith above the Upper Sandy member should be at least twice as much of that the regolith above the Mines member based on the 15% orthoquartzite content in the Upper Sandy member.

3. Fracture Trace and Depression Location Methods

The evolution of geospatial technologies has made it possible to use a variety of data processing tools to verify the visual cues of depressions and fracture traces and to detect asymptomatic fractures and depressions. The availability of high resolution Digital Terrain Models (DTM) has become more abundant in recent years with data now available for the Astronomy Site from the years 2007 and 2017. The resolution of the DTM's from 2007 and 2017 used for this study are 2×2 ft which is a high enough resolution to determine areal extent, although it has a tendency to smooth some

vertical features at this resolution. The DTM from 2007 is derived from orthoimages while the DTM from 2017 is derived from LiDAR. Both DTM's use the Pennsylvania State Plane North FIPS 3701 NAD 83 datum that are in units of feet. A higher resolution LiDAR is recommended, however, for a more in-depth analysis for volume change within depressions.

3.1. Methods of Fracture Delineation

As a variance characterizes the fracture trace orientations in this strike area from N5W to N5E based on the bedrock exposures (Matzke, 1961), the downslope faces of the fracture traces should be illuminated when a hillshade map is created perpendicularly to the strike. The lineations, which were within the Living Filter specifically were measured between 3-15° NE, served as the baseline orientations for the fracture trace identification process. A manual process was then created for the identification of fracture traces using ArcGIS 10.6.1, the outline and design of which is in Figure 7.

In order to determine the position of fracture traces in the area of the Astronomy site, the Hillshade tool within the Surface toolset was used to construct a map with an azimuth of 282° and an altitude of 45° (interpreted as sun shining from 282° with a 45° sun angle). The Aspect tool located in the Surface toolset was next used for the identification of fracture traces isolated by the Hillshade map to determine the direction of each cell within the DTM. The aspect of the cell is perpendicular to the

strike of the cell, similar to that of both the strike and dip in the structural geology. All cells with an aspect of between 273 to 285 degrees were extracted from the data at which point the Raster-to-Polygon tool in the Conversion toolset was used for their conversion to polygons (Figure 8). In order to determine the validation of the fracture trace locations based on aspect orientation, the cell aspects were isolated in groups of 12 (0-12, 12-24, 24-36, 36-48, 48-60, 60-72, 72-84, 84-96, 96-108, 108-120, 120-132, 132-144, 144-156, 156-168, 168-180) (Figure 9a, 9b, and 9c).

Once the polygons were created, the Majority Filter tool located in the Generalization toolset was used to remove polygons without five of the eight surrounding pixels of the same value. Once the Majority Filter was complete, the Boundary Clean tool within the Generalization toolset was set to descend to ensure a merging of the larger area polygons with the smaller, thus making the fracture traces easier to identify.

Finally, a polyline layer and the Editor toolbar was used to create the manually drawn fracture traces and the Zonal Geometry as Table tool located in the Zonal toolset was used to determine the fracture orientations. The length and width of fractures were not recorded for this study as the fractures often extended off site and out of the scope of our research area (Figure 10).

In order to ensure the accuracy of the results, a control site was established for the Gamelands site. The same fracture analysis as outlined above was conducted on both the forested and unforested sections of the Gamelands site in order to statistically

validate the efficacy of these methods in identifying fractures of similar orientations (Figure 11).

3.2 Methods of Closed Hillslope Depression identification

An adapted automated difference process for depression identification, as shown in Figure 12, was next used to determine the location of depressions within the Astronomy Site (Doctor, Daniel H., 2015; Jeanpert et al., 2016).

Using the Fill tool located in the Hydrology toolset, the depressions in the land were determined by isolating those cells that were lower than the surrounding counterparts, at which point they were filled to their pour point and the elevation raster smoothed. After creation, the fill raster was subtracted from the original DTM using the Raster Calculator tool located in the Map Algebra toolset to isolate areas of depression. Using the Reclass tool located in the Reclassify toolset, all depressions deeper than three inches were reclassified to a value of 1 and depressions less than three inches were classified as NoData in order to de-noise the data (Figure 13).

The Select by Attributes tool was used to select only those depressions within 50 feet of a lineament and more than five feet away from unpaved roads. Given that lineaments in this area typically average 50 feet in width, this number was used to reduce error from the created thin polylines. All depressions with an area larger than 10 ft^2 and five feet of the unpaved roads in this area, which are composed a fine grain gravel were selected and exported to create a new dataset. The purpose of this

selection was to prevent any skewing of the results of the depression formation from the high hydraulic conductivity and from the depressions within five feet of those roads, which are characterized by a flat edge that parallels them. The presence of burrows and other smaller natural features necessitated using an area above 10 ft^2 to further reduce the noise in the data. Zonal geometry was used to tabulate the orientation of the depressions for statistical comparisons between the years 2007 and 2017 (Figure 14). In order to analyze the change in areal extent, the previously described processes were performed upon DTM's from years 2007 and 2017. All selected depressions were then exported into a separate layer. The Polygon-to-Raster tool in the Conversion toolset was then used to reconvert the data into raster data that was then reclassified as "1" for depressions from the year 2007 and "2" for depressions from the year 2017.

In order to symbolize areal progression, the Raster Calculator tool located in the Map Algebra toolset was used to create a raster calculation to combine both rasters. The values of 3 indicated the presence of depressions in both the years 2007 and 2017, the values of 1 indicated their presence in only 2007, and values of 2 indicated their presence in only 2017 (Figure 15). Cross sections were created along the center line of six depressions, three in the cropped area and three in the forested area. The Profile Graph tool in the 3D Analyst toolbar was used to create these cross sections for the 2007 and 2017 depression areas via interpolation of a line along the cross section. Depressions were analyzed for both sites to consider the occurrence of various

erosional processes and the potential ecological impacts of various plant life/growth (Figure 16).

4. Results

4.1 Fracture Results

Finally, Zonal Geometry was used to trace and compare a series of fracture traces within the Astronomy site for comparison with the established results of Matzke (1961) and Parizek et al. (1967). The data in the resulting frequency graph of all determined NE-SW fractures was near identical to that developed by Matzke in 1961 (Table 2). Also photographs from the 1940's, 1980's, 1990's and early 2000's indicated the presence of visible fracture traces as evidenced by lack of vegetation and straight surface ponding areas.

4.2. Depression Results

Elongations of three depressions along a single fracture in the same direction as the original fracture trace were also observed. An analysis of the areal progression from 2007 and 2017 indicated a net positive change in area with a propagation of the area of the depressions down the hillslope and that were filled in up slope. A net positive area change of all depressions located within 50 feet of the fracture trace centers and a distance of more than five feet from all unpaved roads indicated a progression of nearly 8,000 square feet of these depressions during the period from 2007 to 2017 (Figure 17).

Finally, although the cross sections of the selected depressions during the 2007-17 period in the cropped and forested sites indicated variations in morphology, none was observed in both depth and height (Figures 18 through 23).

5. Discussion

The results of a slope aspect identification approach, which is appropriate for datasets with a fracture area width that is greater than the individual cell size, clearly elucidates the linear features in the area of the Astronomy site. The DTM that was used for slope aspect identification has a resolution of 2 $\times$ 2 feet, unlike the swales and depressions in the area that have been known to exceed 50 feet in width (Matzke, 1961). The results of the fracture traces from Table 2 are corroborated by Matzke's findings in the region of the Pennsylvania Furnace anticline. No significant lineations or depressions were identified despite a separate analysis to determine the presence of perpendicular fractures in the area. Matzke (1961) referred to the perpendicular E-W fractures as secondary in nature and less developed than those trending N-S. The regional geology of Centre County, PA and the orthoquartzite ridges that surround the Astronomy site are oriented at 52° NE which is a divergent angle from the two dominant fractures.

Matzke (1961) speculated that fractures in this area are the result of some regional event because they occur on both the hanging and foot walls of thrust faults in this area. Local joint patterns occur 45° off axis from the dominant fracture trace

direction and contradict the original postulation of Lattman and Nickelson (1958) that fractures and joints are near perpendicular in this area (Figure 24). The fracture rose diagram results from this research north of the Pennsylvania Furnace anticline and south of the Marengo syncline closely match those of Matzke (1961). The limitations of the manual correlation from the slope aspect map, however prevented an accurate characterization of both the density and numbers of fractures within the study area. A higher number fractures are evident however when using the fracture maps of Parizek et al. (1967) and Lattman and Parizek (1964) for comparison. Using a photogrammetric approach, Parizek et al. (1967) and Lattman and Parizek (1964) mapped fractures based on their surficial manifestations as linear features with discernable change in color, vegetation, and standing water. In order to avoid any sort of manual bias when mapping the fracture traces, the development of an automatic script could possibly reduce error in these regards.

When looking at all of the identified depressions, regardless of their proximity to either roads or fractures, results of the underlying hillshade map clearly indicate the presence of several elliptical features that have not been identified by the fill tool. In that the fill tool operates by creating a pour point of the lowest elevation, the manifestation of a non-detect error in the tool is possible when depressions are located on steeper hillslopes. If a pour point spills over prematurely given its location upon a slope, it will not collect water of sufficient depth for identification, and is thus eliminated during the de-noising process. The elongation of depressions in the direction

of the fracture may also obscure the detection of depressions in that they fail to create a fully enclosed ellipsoid shape. Indeed, some of these non-ellipsoid shapes may well be what Caruccio (1963) characterized as swales within the Mines Member.

The fracture traces from the Astronomy site and the Gamelands site were then statistically analyzed. A two-sample T-test of unequal variance between the two sets of measured fractures with an alpha of 0.025 corresponding to two standard deviations yields a null hypothesis that the fractures have the same orientation. A skewing of the data in one direction or another from human error is possible, however, in that these fractures were drawn by hand (Table 3).

It is unknown the extent to which the land upon which the Astronomy site currently occupies has been used for agricultural purposes, but such was the case prior to the inception of the site in 1962. Historical photos also show that much of the now forested site was clear cut and cropped as far back as 1938. The continued use of the cropped portion of the Living Filter for agricultural purposes could potentially have an effect on the extent of the depressions due to the lessened interception of precipitation and irrigation. Overland flow was a particular issue within the cropped area prior to the construction of a wetland area and drainage pipes at the bottom of the upper hillslope. The lack of interception can be correlated to a higher rate of erosion, thus depositing more fill material within the depressions and increasing the AP horizon depth as shown in Walker and Lin (2008). The Living Filter was also tilled until the mid-1990's, meaning that there were at least 35 years where the depressions could have been smoothed by

tillage. A depression change analysis was ran on the non-university owned parcel northeast of the study site were tillage is suspected to still occur and there are significantly fewer identifiable depressional features.

The lessening of the depressions within the cropped site is corroborated by the fact that the area of the depressions detected within the cropped site has been reduced by over 5,000 ft^2 since 2007. Within the forested site, the opposite of that which is occurring in the occurrence of the cropped site seems corresponds to an increase of 13,000 ft^2 of the areal extent of depressions. These findings are similar to that of Gillijns et al. (2005) study in central Belgium of closed depressions both within forested and cropped sites that were remnants of anthropogenic mining practices (Gillijns et al., 2005). They found that depressions within the cropped area had a wider areal extent, shallower depth, and a gentler relief due to the effects of tillage, splash erosion, and inter-rill/rill erosion, whereas the depressions within the forested site were characterized by a steeper relief due to the protection and interception of the forest canopy.

Cross sections taken in ArcGIS of these multiple depressions, both in the cropped site and in the forested site, do not reflect significant change in the depth of the depressions along the cross-sectional line. Although the morphology of the depressions has varied within the past 10 years as evidenced by the cross sections, the findings from the cross sections once again confirm Gillijn's analysis of the depression shapes. They noted that the depressions within the cropped land had infilled and created a v-shaped

cross section while the depressions within the forested site had preserved their original u-shaped cross sections. These classifications between both the v-shaped and u-shaped depressions are bowl (v-shaped) and saucer (u-shaped) depressions as defined by Kołodyńska-Gawrysiak and Chabudziński (2014).

A mean orientation of 10° NE and of 358° NW characterized the respective depressions within the forested and cropped sites, which further indicated large variations in their standard deviations, which were 31° and 43° of both sites respectively. The irregularity of the orientation and shapes of the depressions indicates the possible manifestations of the secondary fracture traces that skews the shape of the depressions. With the assumed substantive transmissivity of the intersecting fractures, it is possible that depressions not oriented along the primary fracture trace occur above secondary fractures, the same could be true of intercepting joint patterns.

A two-sample T-test assuming unequal variances was conducted on the orientation of the depressions in both the forested and cropped sites between the years 2007 and 2017. Using an alpha of 0.025 and a null hypothesis of the orientations of the depressions were similar to principle orientation, we accepted such a hypothesis for the 2007 and 2017 depressions identified for both the forested and the cropped sites (Table 4 and Table 5). Using those same parameters and same null hypothesis, we also accepted the null hypothesis when comparing the cropped site to the forested site (Table 6 and Table 7).

The lack of ground control points for the 2007 orthorectified DTM and the 2017 orthorectified DTM makes it impossible to determine the accuracy of the elevation from both of these models. A traditional “rule of thumb” is that the error of the model should be less than 2 pixels (4 feet) (Devos and Kay, 2005). As such, given the level of accuracy needed for a full vertical comparison of the depressions the resolution of our datasets were not suitable.

Therefore, subsequent research is recommended in order to account for any errors in the depression isolation for those depressions located in areas of steep relief due to the inability of the Fill tool to recognize these areas as pour points. Further, the limitations of the depression isolation to features that are enclosed enough to form a pour point prevents its use in identifying depressions with either a lowered edge or an incomplete elliptical shape. The possibility of intercepting joints and fractures must also be considered for the orientation distribution of depressions. Expanding the dataset to include a larger study area would likely rectify the mean orientation and standard deviation with an expanded inventory of depressions. Coring geochemical analysis similar to that of Norton (1986) should also be explored in order to determine the depth and age of transported sediment within the depressions.

A secondary area of future study may entail the combination of both the GIS technique outlined here with traditional photogrammetry practices along with advanced photogrammetry practices. Such a premise is possible given the availability of high resolution images detailing this area over multiple time periods, particularly the years

2007, 2012, 2015, and 2017. It is also possible to implement and combine a workflow that is similar to that developed by Pokharel (2017), Siart et al. (2009), and Kakavas et al. (2015) to more thoroughly elucidate fracture trace locations in areas that are characterized by skewed slope face orientation caused by the position of the landscape.

6. Conclusion

Wastewater reuse, particularly via the use of spray irrigation of treated effluent, is a common practice worldwide and can help lessen the impact of the overconsumption of water resources. The increased recharge to the subsurface that enhances weathering and erosion during the irrigation application process makes it important to characterize any changes in the land surface over time. This study identified and related any bedrock fracture traces and surface depressions to any surficial or geomorphologic processes currently underway at the site of the Living Filter. The previous measurements of fracture traces in this area undertaken by Matzke (1961), Lattman and Parizek (1964), and Parizek et al. (1967) yielded results in a near N-S orientation. The use of a manual process to estimate the primary fracture trace angles yielded results near identical to that of the aforementioned authors. Regrettably, the limitation of the work flow and the scope of the study prevented a full characterization of the length, width, and density of the fractures. A high occurrence of depressions was noted in the area of fractures compared to non-fractured bedrock. Further, a statistically significant trend was absent between the orientations of the depressions along the primary fractures within this

area, perhaps caused by a skewing of those orientations from the secondary fractures and jointing patterns also in this area. Further study is needed to determine the validity of this hypothesis, however. In the areal extent, the authors observed a dissipation of depressions within the cropped site and a growth in the depressions in the forested site. The depressions in the Living Filter were found to have a net gain of 8,000 ft^2 the result of which was from the net loss of 5,000 ft^2 within the agricultural portion of the site and a net gain of 13,000 ft^2 within the forested portion of the site. Cross sections of several depressions within cropped areas indicated a lower angle slope corresponding to a V-shape while depressions within forested areas were characterized by a traditional U-shape and previously established steeper slope. These results will enhance the current understanding of the different morphologic characteristics of both forested and agricultural depressions in karst topography. The workflows implemented here can be implemented in similar sites that display topographical variances from the bedrock fractures. However, further study of the transport of sediments within both land regimes is needed to fully characterize the extent to which these depressions are changing in terms of horizontal and vertical behavior.

Acknowledgements

We wish to convey our appreciation to Clemson University for supporting this work.

References

Andrews, D.M., Robb, T., Elliott, H., and Watson, J.E., 2016, Impact of long-term wastewater irrigation on the physicochemical properties of humid region soils: "The Living Filter" site case study: *Agricultural Water Management*, v. 178, p. 239–247.

Aschebrook-Kilfoy, B., Heltshe, S.L., Nuckols, J.R., Sabra, M.M., Shuldiner, A.R., Mitchell, B.D., Airola, M., Holford, T.R., Zhang, Y., and Ward, M.H., 2012, Modeled nitrate levels in well water supplies and prevalence of abnormal thyroid conditions among the Old Order Amish in Pennsylvania.: *Environmental health : a global access science source*, v. 11, p. 6.

Becher, A.E., 1996, GROUND-WATER RESOURCES OF CAMBRIAN AND ORDOVICIAN CARBONATE ROCKS IN THE VALLEY AND RIDGE PHYSIOGRAPHIC PROVINCE OF PENNSYLVANIA PENNSYLVANIA DEPARTMENT OF ENVIRONMENTAL PROTECTION, BUREAU OF TOPOGRAPHIC AND GEOLOGIC SURVEY:

Benjamin, N., O'Driscoll, F., Dougall, H., Duncan, C., Smith, L., Golden, M., and McKenzie, H., 1994, Stomach NO synthesis: *Nature*, v. 368, no. 6471, p. 502–502.

Brachet, F., 2004, Regional groundwater modeling for source area delineation and recharge estimation: The Pennsylvania State University.

Buda, A.R., and Dewalle, D.R., 2009, Dynamics of stream nitrate sources and flow pathways during stormflows on urban, forest and agricultural watersheds in central

Pennsylvania, USA: v. 23, p. 3292–3305.

Caldwell, H., Mancl, K., and Quigley, M.F., 2007, The Effects of Year-Round Irrigation on Landscape Plant Quality and Health in Ohio: *The Ohio Journal of Science Ohio Journal of ScienceOhio Academy of Science) Ohio Journal of Science OHIO J SCI*, v. 107, no. 1074, p. 4–76.

Caruccio, F.T., 1963, The Hydrogeology of the Sewage Disposal Experiment Area, Northwest of State College, Pennsylvania: Pennsylvania State University.

Chin, C.-V., 1996, Application and comparison of EPA wellhead protection delineation methods for karst aquifers, Centre County, Pennsylvania:

Dadio, 1998, Ponding and Runoff Dynamics of a Closed System Undergoing Irrigation with Treated Wastewater: Pennsylvania State University.

Dayanthi, W.K.C.N., Shigematsu, T., Tanaka, H., Yamashita, N., Kato, K., and de Silva, V., 2006, Utilization of Reclaimed Wastewater for Irrigation and Urban Activities in Okinawa Island, Japan: *Proceedings of the Water Environment Federation*, v. 2006, no. 12, p. 981–1005.

Devos, W., and Kay, S., 2005, Ortho-imagery: Geometric Accuracy Assessment:

Doctor, Daniel H., J.A.Y., 2015, An Evaluation of Automated GIS Tools for Delineating Karst Sinkholes and Closed Depressions From 1-Meter LiDAR-Derived Digital Elevation Data, *in* Sinkholes and the Engineering and Environmental Impacts of Karst: Proceedings of the Thirteenth Multidisciplinary Conference, p. 449–458.

EPA, 2012, 2012 Guidelines for Water Reuse.:

EPA, 2004, Primer for Municipal Wastewater Treatment Systems.:

Fan, A.M., and Steinberg, V.E., 1996, Health Implications of Nitrate and Nitrite in Drinking Water: An Update on Methemoglobinemia Occurrence and Reproductive and Developmental Toxicity: *Regulatory Toxicology and Pharmacology*, v. 23, no. 1, p. 35–43.

Fulton, J.W., Risser, D.W., Regan, R.S., Walker, J.F., Hunt, R.J., Niswonger, R.G., Hoffman, S.A., and Markstrom, S.L., 2015, Water-Budget and Recharge-Area Simulations for Spring Creek and Nittany Creek Basins and Parts of the Spruce Creek Basin, Centre and Huntingdon.:

Gannett Flemming, I., 2008, Technical memorandum ground- water flow model results proposed Grove Quarry, Marion and Spring Townships, Centre County, Pennsylvania: Yardley, Pa.:

Gatseva, P.D., and Argirova, M.D., 2008, High-nitrate levels in drinking water may be a risk factor for thyroid dysfunction in children and pregnant women living in rural Bulgarian areas: *International Journal of Hygiene and Environmental Health*, v. 211, no. 5–6, p. 555–559.

Gelhar, L.W., Welty, C., and Rehfeldt, K.R., 1992, A Critical Review of Data on Field-Scale Dispersin in Aquifers: *Water Resources Research*, v. 28, no. 7, p. 1955–1974.

Gillijns, K., Poesen, J., and Deckers, J., 2005, On the characteristics and origin of closed depressions in loess-derived soils in Europe - A case study from central Belgium: *Catena*, v. 60, no. 1, p. 43–58.

Griffin, J., Modeling, W.Q., Environmental, O., Agency, P., and Karen, M., 2017, Onsite Reuse of Reclaimed Wastewater in Winter to Determine Potential for Pollutant Runoff: v. 117, p. 74–84.

Hamilton, A.J., Stagnitti, F., Xiong, X., Kreidl, S.L., Benke, K.K., and Maher, P., 2007, Wastewater Irrigation: The State of Play: *Vadose Zone Journal*, v. 6, no. 4, p. 823.

Herndon, R., and Markus, M., 2013, Large-Scale Aquifer Replenishment and Seawater Intrusion Control Using Recycled Water in Southern California.:

Hook, J.E., and Kardos, L.T., 1978, Nitrate Leaching During Long-term Spray Irrigation for Treatment of Secondary Sewage Effluent on Woodland Sites1: *Journal of Environment Quality*, v. 7, no. 1, p. 30.

Jeanpert, J., Genthon, P., Maurizot, P., Folio, J.L., VendÃ©-Leclerc, M., SÃ©rino, J., Join, J.L., and Iseppi, M., 2016, Morphology and distribution of dolines on ultramafic rocks from airborne LiDAR data: the case of southern Grande Terre in New Caledonia (SW Pacific): *Earth Surface Processes and Landforms*, v. 41, no. 13, p. 1854–1868.

Kelso, L.M., Bowersox, T.W., 2002, Long-term Effects of Wastewater Irrigation on Forested Ecosystems at Pennsylvania State Game Lands 176- Part II:

Landon, R.A., 1963, The Geology of the Gatesburg Formation in the Bellefonte Quadrangle, Pennsylvania, and its Relationship to the General Occurence and Movement of Groundwater: Pennsylvania State University.

Larson, Z.M., 2010, Long-Term Treated Wastewater Irrigation Effects On Hydraulic

Conductivity and Soil Quality at Penn State's Living Filter: Pennsylvania State University.

Lattman, L.H., Nickelson, R.P., 1958, Photogeologic Fracture-Trace Mapping in Appalachian Plateau: *American Association of Petroleum Geologists Bulletin*, v. 42, no. 9, p. 2238–2245.

Lattman, L.H., 1958, Technique of mapping geologic fracture traces and lineaments on aerial photographs.: *Photogrammetric Engr.*, v. v. 19 no., p. 568–576.

Lattman, L.H., and Parizek, R.R., 1964, Relationship Between Fracture Traces and The Occurence of Ground Water in Carbonate Rocks: *Journal of Hydrology*, v. 2, p. 73–91.

Lindsey, B.D., Loper, C.A., and Hainly, R.A., 1997, NATIONAL WATER-QUALITY ASSESSMENT PROGRAM NITRATE IN GROUND WATER AND STREAM BASE FLOW IN THE LOWER SUSQUEHANNA RIVER BASIN, PENNSYLVANIA AND MARYLAND:

Lundberg, J.O., Feelisch, M., Björne, H., Jansson, E.Å., and Weitzberg, E., 2006, Cardioprotective effects of vegetables: Is nitrate the answer? *Nitric Oxide*, v. 15, no. 4, p. 359–362.

Martinez, C.J., and Clark, M.W., 2015, Reclaimed Water and Florida's Water Reuse Program 1:

Matzke, R.H., 1961, Fracture Trace and Joint Patterns in Western Centre County, Pennsylvania: Pennsylvania State University.

Mau, D.P., and Winter, T.C., 1997, Estimating ground-water recharge from streamflow

hydrographs for a small mountain watershed in a temperate humid climate, New Hampshire, United States: *Ground Water*, v. 35, no. 2, p. 291–304.

Miller, G.W., 2005, Integrated concepts in water reuse: managing global water needs: *Desalination G.W. Miller / Desalination*, v. 187, no. 187, p. 14–17.

Monitoring Nitrate in the Spring Creek Watershed, 2013,.

Nemitz, J.L., 2001, Nitrate Removal Efficiencies: Overland Flow Versus Wetland Systems Receiving Secondary Sewage Effluent at Penn State's Living Filter: Pennsylvania State University.

Niswonger, R.G., Panday, S., and Ibaraki, M., 2011, MODFLOW-NWT, A Newton Formulation for MODFLOW-2005.:

O 'driscoll, M.A., and Parizek, R.R., 2003, The Hydrologic Catchment Area of a Chain of Karst Wetlands in Central Pennsylvania, USA: *WETLANDS*, v. 23, no. 1, p. 171–179.

Parizek, R.R., Filley, T.H., 1982, Definitions of Aquifers and Confining Beds Within the Centre Region, Centre County, Pennsylvania: , p. 0–1.

Parizek, R.R., Siddiqui, S.H., 1970, Determining the Sustained Yields of Wells in Carbonate and Fractured Aquifers:

Parizek, R., Kardos, L., Sopper, W., Myers, E., Davis, D., Farrell, M., and Nesbitt, J., 1967, The Pennsylvania State University Studies NO. 23: Waste Water Renovation and Conservation: , no. 23.

Pennypacker, S.P., Sopper, W.E., and Kardos, L.T., 1967, Renovation of Wastewater Effluent by Irrigation of Forest Land: *Source Journal (Water Pollution Control*

Federation), v. 39, no. 2, p. 285–296.

Reep, P.J.V.A.N.D.E., 2009, Permeability of Limestone-Dolomite Composite Fracture Surfaces: The University of British Columbia.

Rozema, E., VanderZaag, A., Wood, J., Drizo, A., Zheng, Y., Madani, A., and Gordon, R., 2016, Constructed Wetlands for Agricultural Wastewater Treatment in Northeastern North America: A Review: *Water*, v. 8, no. 5, p. 173.

Sendagi, S.M., Herschel, S., and Elliott, A., 2017, Atmospheric nitrogen loss factor (f) used in determining nitrogen-based municipal wastewater effluent irrigation rates: design and nitrogen-balance estimated f values: *Nutrient Cycling in Agroecosystems*, v. 109, no. 2, p. 181–191.

Siddiqui, --I, and Parizek, R.R. Hydrogeologic Factors Influencing Well Yields in Folded and Faulted Carbonate Rocks in Central Pennsylvania:

Smith, R.E., 1966, Petrographic properties influencing porosity and permeability in the carbonate-quartz system as represented by the Gatesburg Formation: Pennsylvania State University.

Swistock, B. Nitrate in Private Water Supplies.:

Taylor, L.E., 1997, Water Budget for the Spring Creek Basin: , no. 184.

Thornthwaite, C.W., and Mather, J.R., 1957, Instructions and Tables for Computing Potential Evapotranspiration and Water Balance.: *Publ.Climatol*, v. 10, p. 185–311.

US EPA, O. National Primary Drinking Water Regulations:

USDA, 1981, Soil Survey of Centre County,Pennsylvania.:

Walker, C., and Lin, H.S., 2008, Soil property changes after four decades of wastewater: *CATENA*, v. 73, no. 1, p. 63–74.

Waltman, W.J., Ciolkosz, E.J., Mausbach, M.J., Svoboda, M.D., Miller, D.A., Kolb, P.J., Mausbach Is Director, M.J., and Kolb, P.J., 1997, Soil Climate Regimes of Pennsylvania: , no. 873.

White, P., Ruble, C.L., and Lane, M.E., 2013, The effect of changes in land use on nitrate concentration in water supply wells in southern Chester County, Pennsylvania: *Environmental Monitoring and Assessment*, v. 185, no. 1, p. 643–651.

Wood, C.R., 1980, Summary Ground-Water Resources of Centre County, Pennsylvania:

Zheng, C., Zheng, C., Wang, P.P., Zheng, C., and Wang, P.P., 1999, MT3DMS: A modular three-dimensional multi-species transport model for simulation of advection, dispersion, and chemical reactions of contaminants in ground-water systems. Documentation and user's guide: *CONTRACT REPORT SERDP-99-1, U.S. ARMY ENGINEER RESEARCH AND DEVELOPMENT*,.

List of Tables:

Stage	Name		Description	Thickness
Franconian-Trempealeauian	Gatesburg Formation	Mines Member	Massive Dolomite interbedded with thin bedded dolomite, abundant chert	76 m (250 ft)
		Upper Sandy Member	Recurring beds of coarsely crystalline dolomite, thin bedded dolomite, and orthoquartzite	198 m (650 ft)
		Ore Hill Member	Massive dolomite interbedded with thin bedded aphanitic dolomite	84 m (275 ft)
		Lower Sandy Member	Recurring beds of coarsely crystalline dolomite and orthoquartzite	122 m (400 ft)

Adapted from Caruccio, 1963

Table 1: Geologic units of the Gatesburg formation, adapted from Caruccio (1963).

Number of Fracture Traces	Fracture Orientation
1	0
1	3
4	4
3	5
1	6
2	10
2	11
2	13
1	15
2	353

1	354
1	356

Table 2: Fracture trace frequency vs. orientation.

t-Test: Two-Sample Assuming Unequal Variances

Astronomy vs. Gamelands Fracture Traces

	Gamelands	*Astronomy*
Mean	79.23644072	84.03992654
Variance	59.62212754	52.84551806
Observations	25	24
Hypothesized Mean Difference	0	
df	47	
t Stat	-2.242861612	
P(T<=t) one-tail	0.014830138	
t Critical one-tail	1.677926722	
P(T<=t) two-tail	0.029660276	
t Critical two-tail	2.011740514	

Table 3: Gamelands vs. Astronomy fracture orientations. ArcGIS uses 90° to symbolize north and 0° degrees to symbolize east.

t-Test: Two-Sample Assuming Unequal Variances

Forested Depressions

	2007	*2017*
Mean	88.85086405	80.96131306
Variance	1654.339589	1879.470274
Observations	31	63
Hypothesized Mean Difference	0	
df	63	
t Stat	0.864956239	
P(T<=t) one-tail	0.195172253	
t Critical one-tail	1.998340543	
P(T<=t) two-tail	0.390344507	
t Critical two-tail	2.296236772	

Table 4: Forested depression orientation statistics from 2007 to 2017. ArcGIS uses 90° to symbolize north and 0° degrees to symbolize east.

t-Test: Two-Sample Assuming Unequal Variances

Cropped Depressions

	2007	*2017*
Mean	85.8414144	92.42445018
Variance	1737.132674	1023.344176
Observations	21	30
Hypothesized Mean Difference	0	
df	36	
t Stat	-0.609039091	
P(T<=t) one-tail	0.273161503	
t Critical one-tail	2.028094001	
P(T<=t) two-tail	0.546323006	
t Critical two-tail	2.339060933	

Table 5: Cropped depression orientation statistics from 2007 to 2017. ArcGIS uses 90° to symbolize north and 0° degrees to symbolize east.

t-Test: Two-Sample Assuming Unequal Variances

2007 Cropped vs. Forested

	Cropped	*Forested*
Mean	85.8414144	88.85086405
Variance	1737.132674	1654.339589
Observations	21	31
Hypothesized Mean Difference	0	
df	42	
t Stat	-0.257976249	
P(T<=t) one-tail	0.39884258	
t Critical one-tail	2.018081703	
P(T<=t) two-tail	0.79768516	
t Critical two-tail	2.324620144	

Table 6: 2007 Cropped vs. Forested depression orientation. ArcGIS uses 90° to symbolize north and 0° degrees to symbolize east.

t-Test: Two-Sample Assuming Unequal Variances

2017 Cropped vs. Forested

	Cropped	*Forested*
Mean	92.42445018	80.96131306
Variance	1023.344176	1879.470274
Observations	30	63
Hypothesized Mean Difference	0	
df	75	
t Stat	1.433515699	
P(T<=t) one-tail	0.077933182	
t Critical one-tail	1.992102154	
P(T<=t) two-tail	0.155866363	
t Critical two-tail	2.287292163	

Table 7: 2017 Cropped vs Forested depression orientations. ArcGIS uses 90° to symbolize north and 0° degrees to symbolize east.

List of Figures:

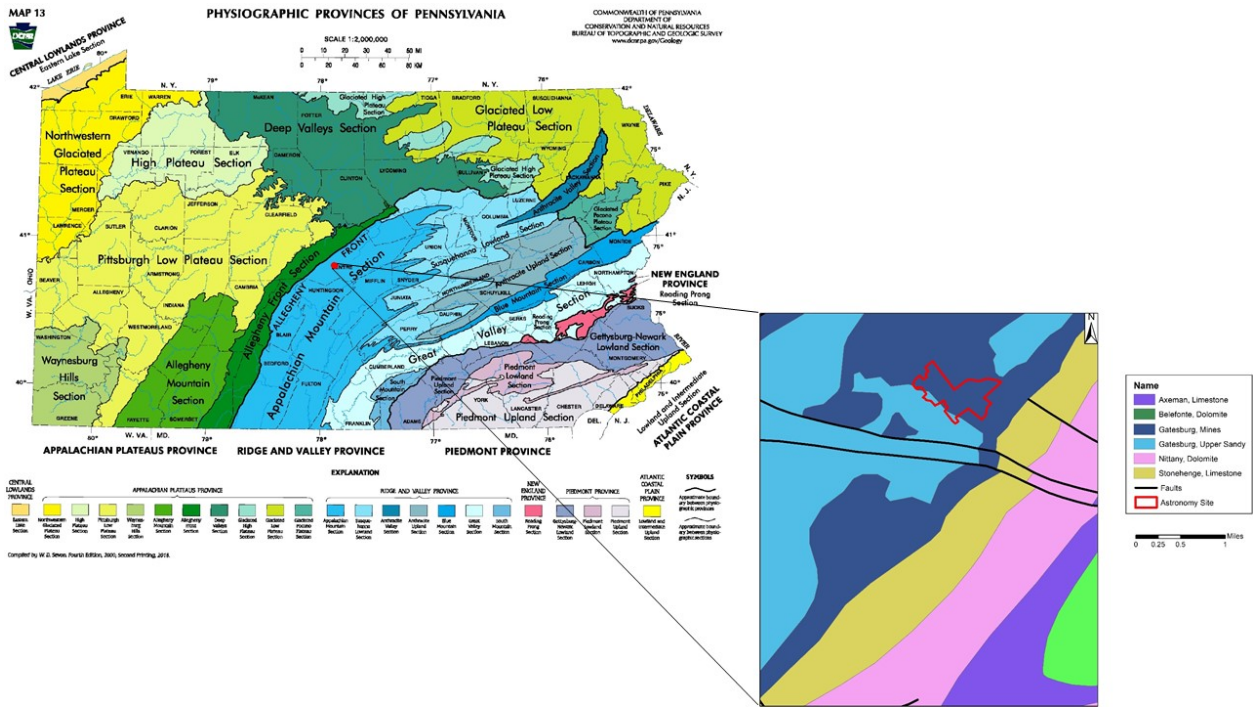

Figure 1: Outline of the Astronomy site and its location relative to the state of Pennsylvania (*PHYSIOGRAPHIC PROVINCES OF PENNSYLVANIA*)

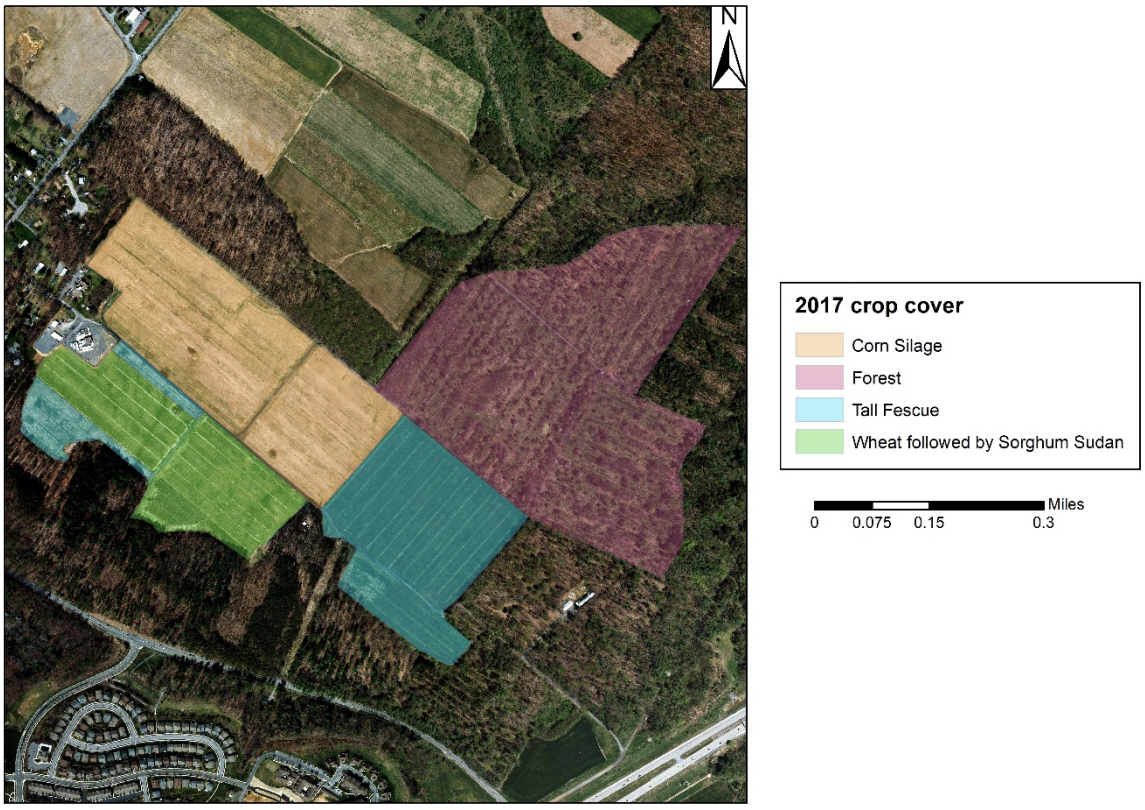

Figure 2: Crop cover during the agronomic year 2017 within the Astronomy Site.

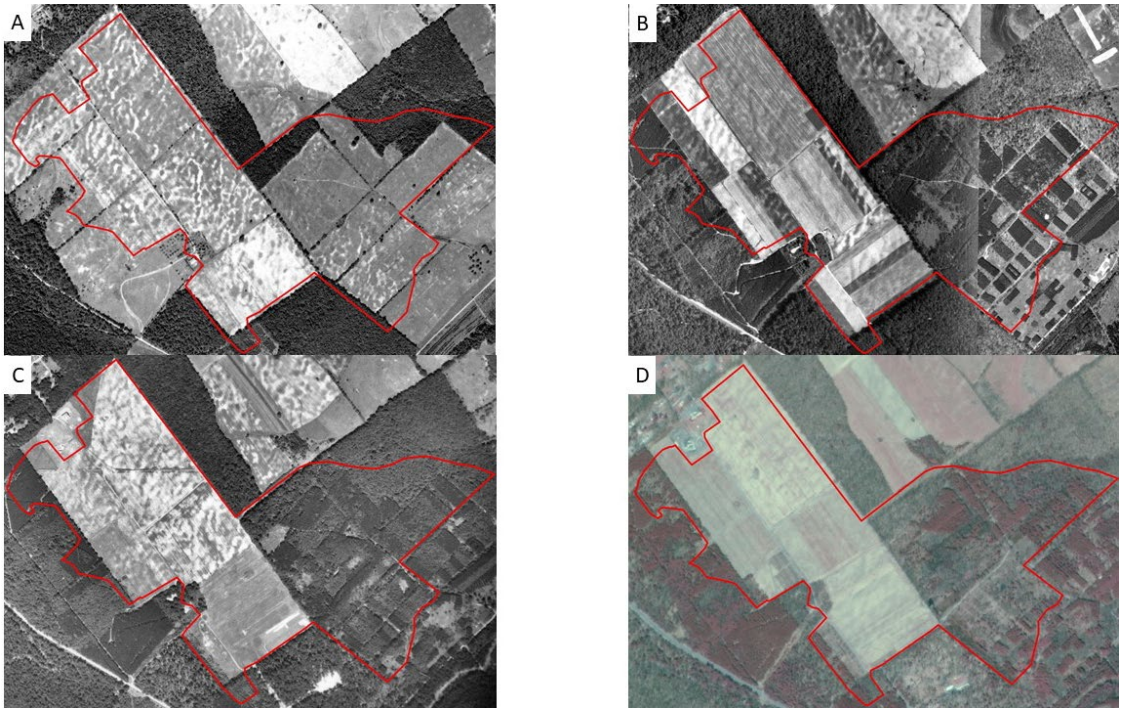

Figure 3: Areal imagery from years 1938-1983 where A) 1938 B) 1957 C) 1971 D) 1983 ("Centre County Historical Areals [air photo]. 1:20,000. Photo aqg:6II:6. Centre County, PA, 1971."; "Centre County Historical Areals [air photo]. 1:20,000. Photo aqg:7r:86. Centre County, PA, 1957."; "Centre County Historical Areals [air photo]. 1:20,000. Photo aqg:27:12. Centre County, PA, 1938."; "High Resolution NHAP CIR for Pennsylvania 1980 to 1987 [air photo]. 1:80,000. Photo HAP83_577_0027:. Centre County, PA, 1983.").

Figure 4: Photo of a swale within the Mines Member at the Astronomy site with an irrigation lateral transecting it.

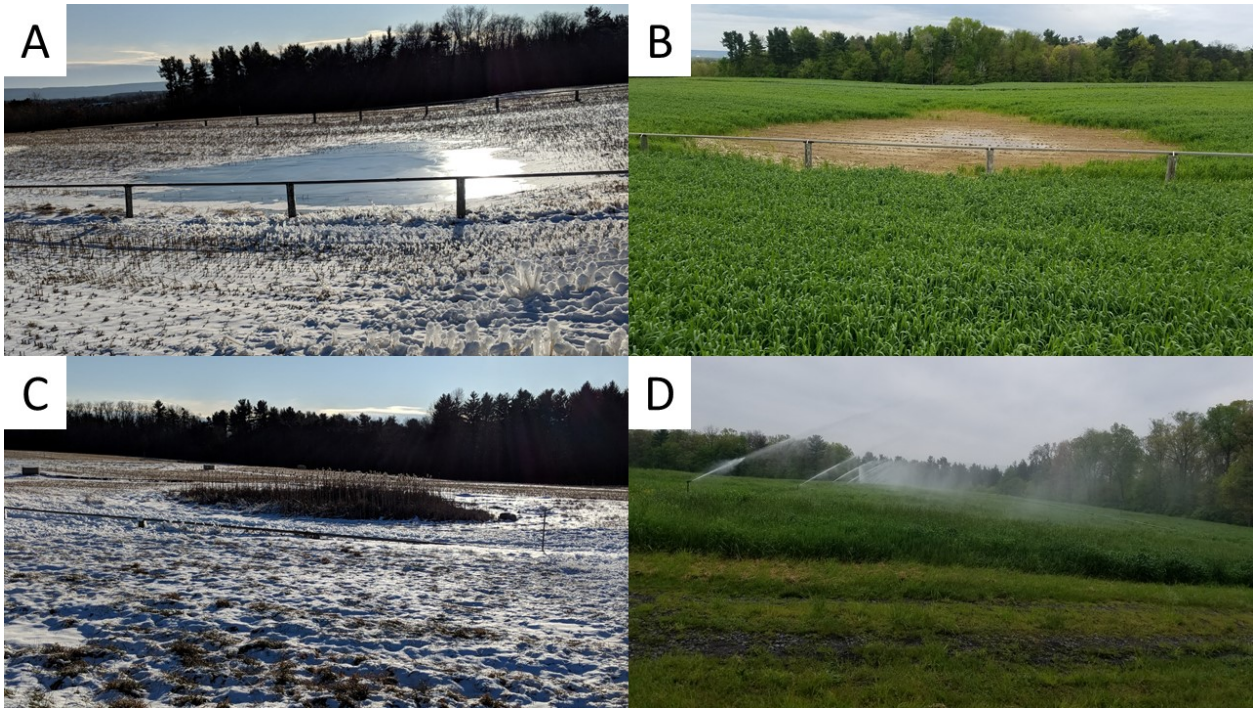

Figure 5: A) A depression within the cropped site during January. B) The same depression as image A except during the month of May. C) A depression within the cropped site with winter vegetation. D) Irrigation within the cropped site during the month of May.

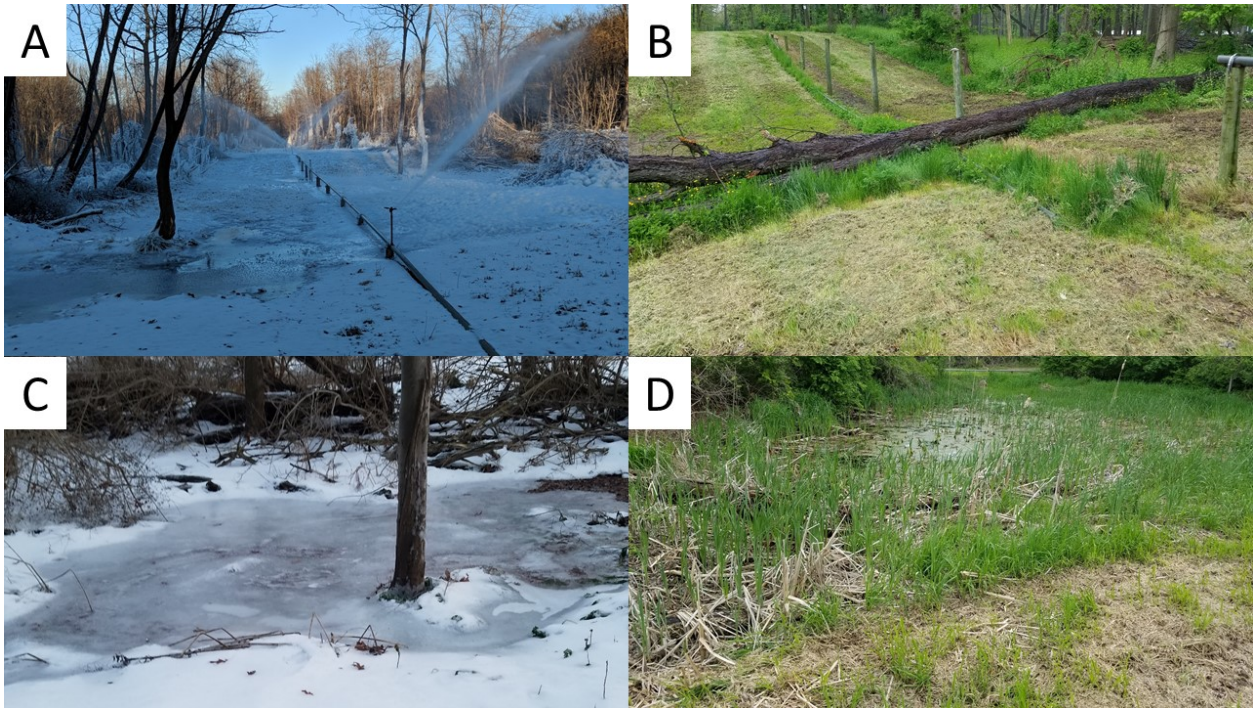

Figure 6: A) A depression under irrigation within the forested site during the month of January. B) A depression with a fallen tree in it, tree falls that take out irrigation laterals are common during the winter months. C) A small depression within the forested site. D) A large depression within the forested site occupied by wetland vegetation.

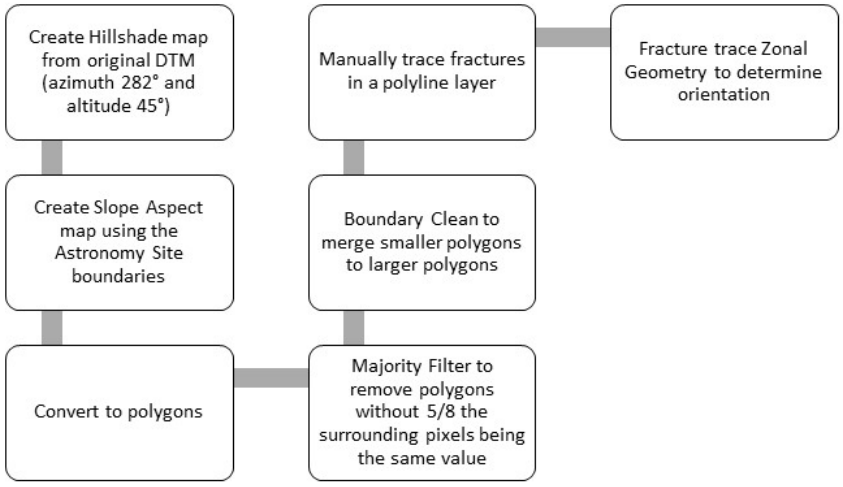

Figure 7: A workflow used to illuminate fracture trace faces.

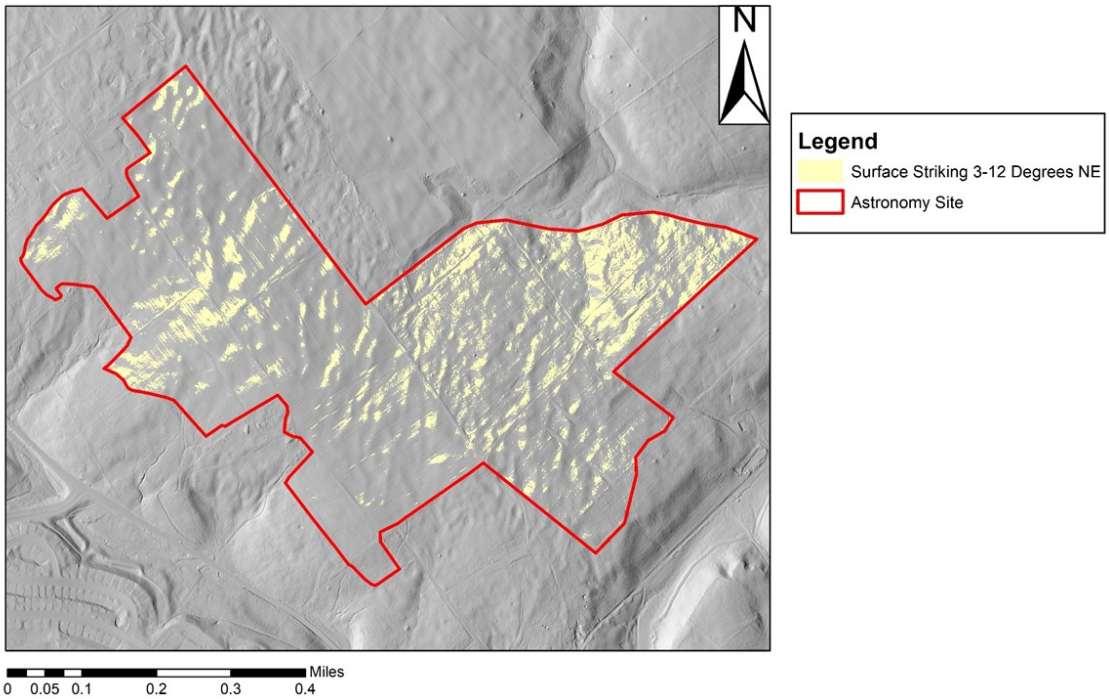

Figure 8: Isolated slope aspect ratios between 3-12 degrees NE.

Legend
0 to 12 deg.
Astronomy Site

Legend
12 to 24 deg.
Astronomy Site

Legend
24 to 36 deg.
Astronomy Site

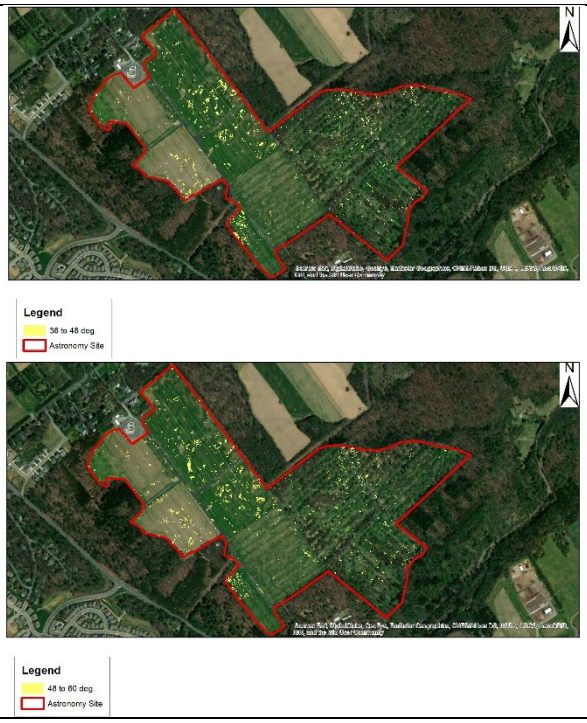

Figure 9a: Grouped cell aspects from 0-60° (including their polar opposites 180-240°).


Legend
60 to 72 deg.
Astronomy Site


Legend
72 to 84 deg.
Astronomy Site


Legend
84 to 96 deg.
Astronomy Site

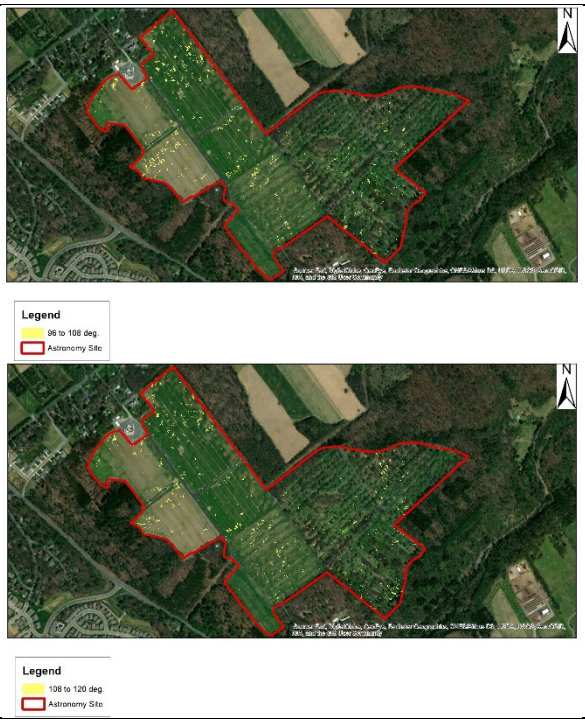

Figure 9b: Grouped cell aspects from 60-120° (including their polar opposites 240-300°).

Legend
120 to 132 deg.
Astronomy Site

Legend
132 to 144 deg.
Astronomy Site

Legend
144 to 156 deg.
Astronomy Site

Figure 9c: Grouped cell aspects from 120-180° (including their polar opposites 300-360°).

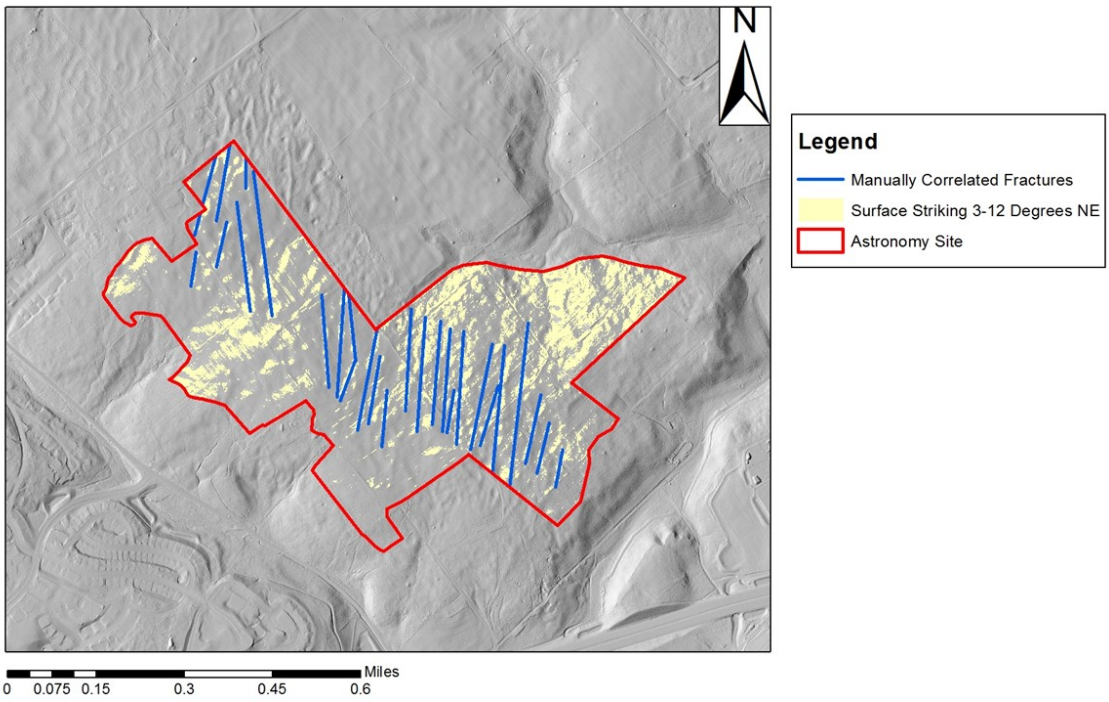

Figure 10: Manually drawn fracture traces based on slope aspect ratio.

Figure 11: Gamelands comparison fractures and aspect ratios.

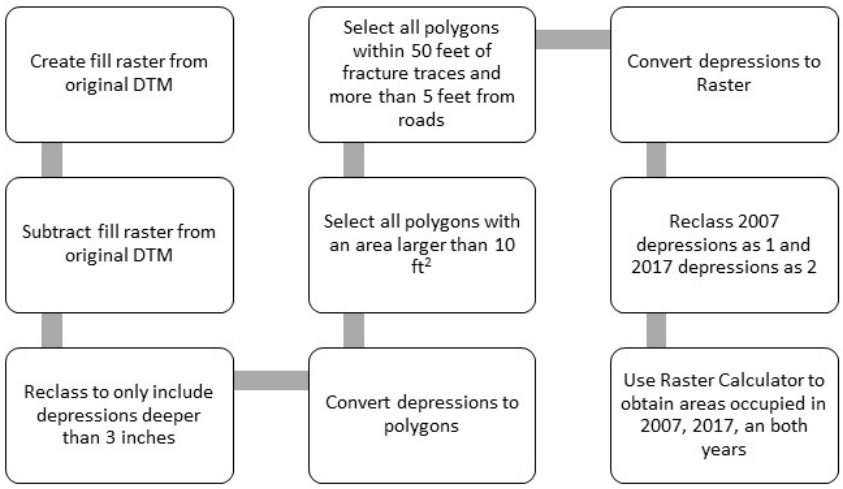

Figure 12: A workflow for depression identification.

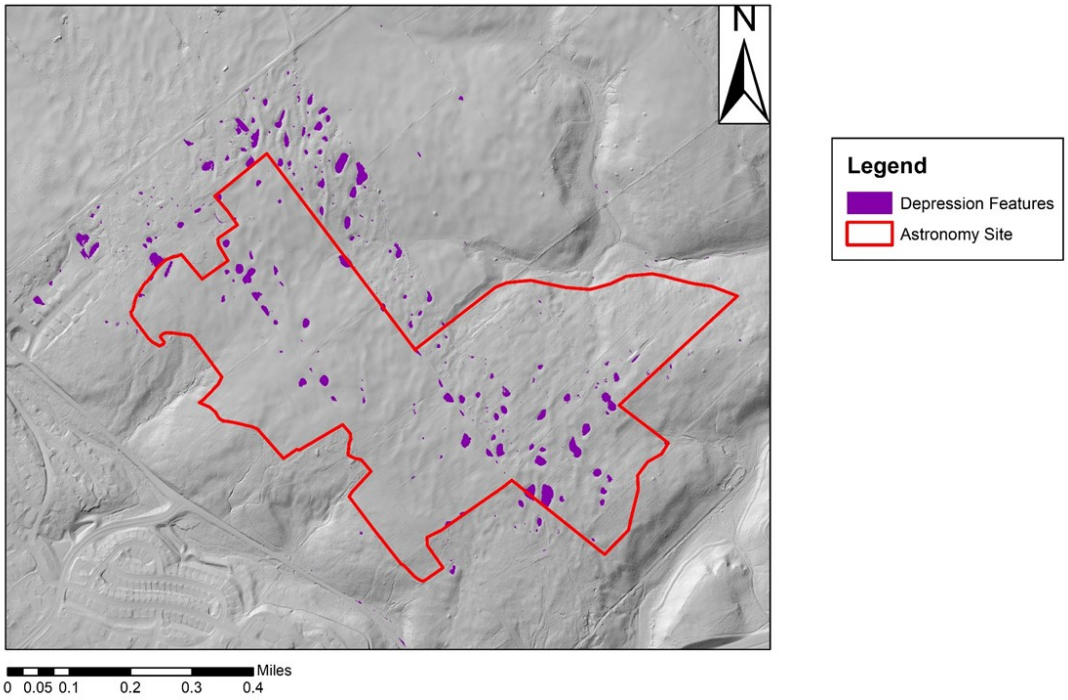

Figure 13: Depressions deeper than 3 inches and larger than 10 ft^2.\

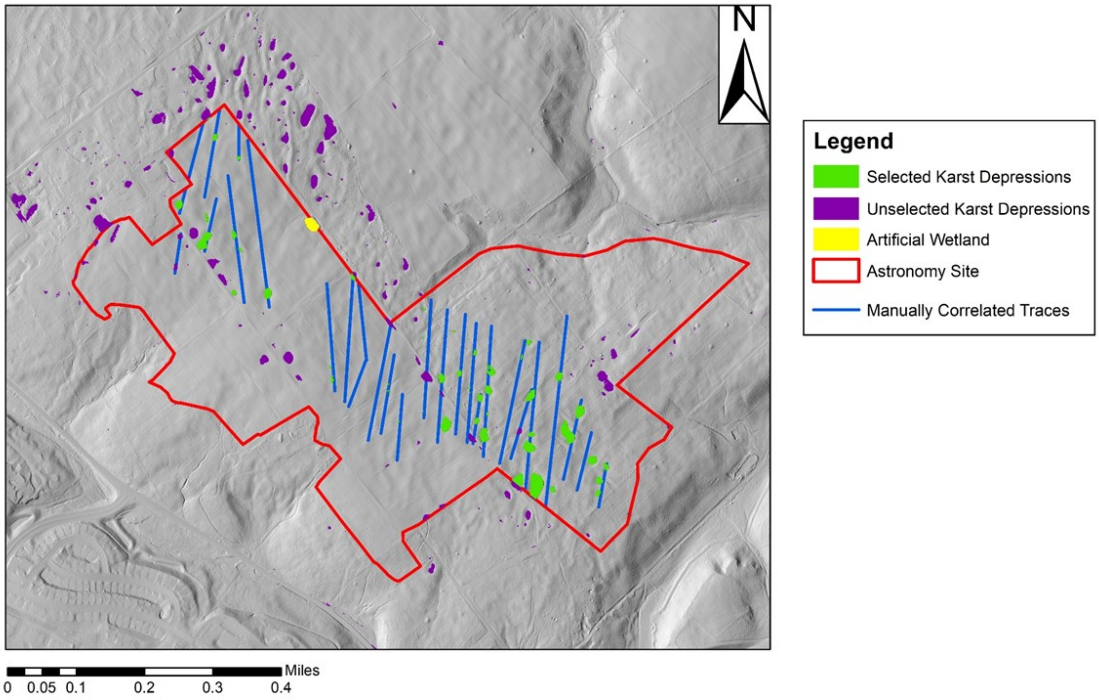

Figure 14: Selected depressions based on their proximity to road features and fracture traces.

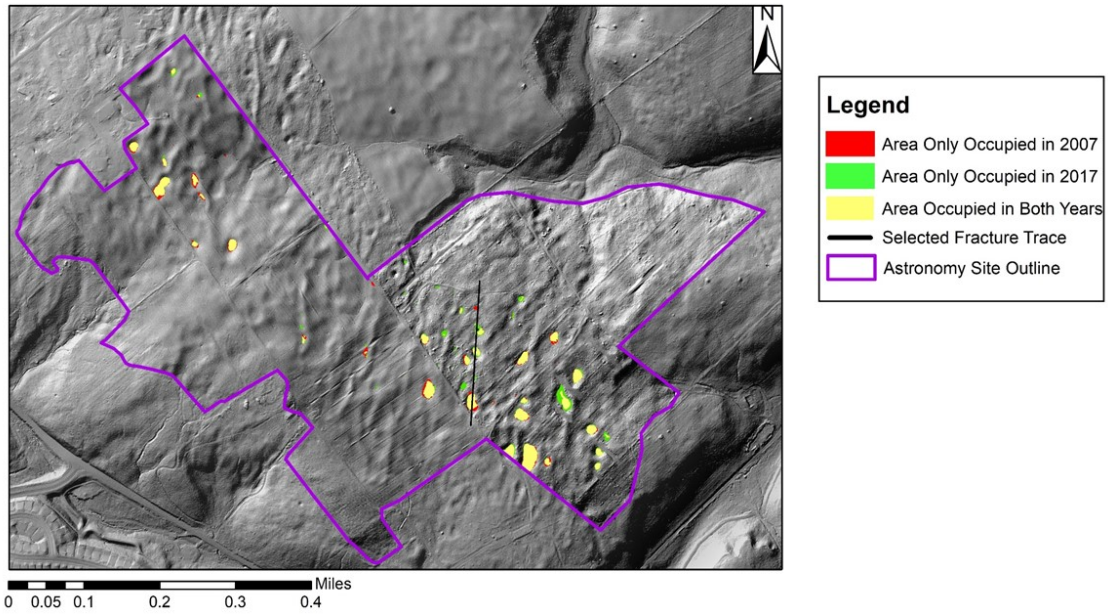

Figure 15: Areal progression of depressions from 2007-2017.

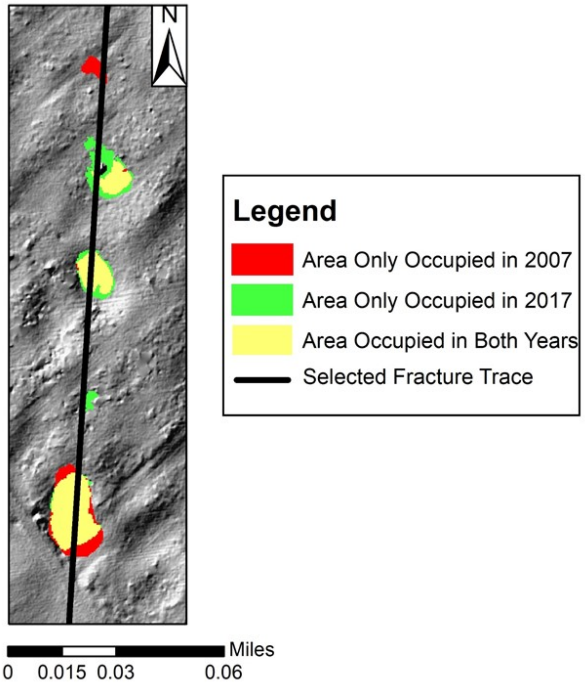

Figure 16: Areal change among 3 selected depressions within the forested site.

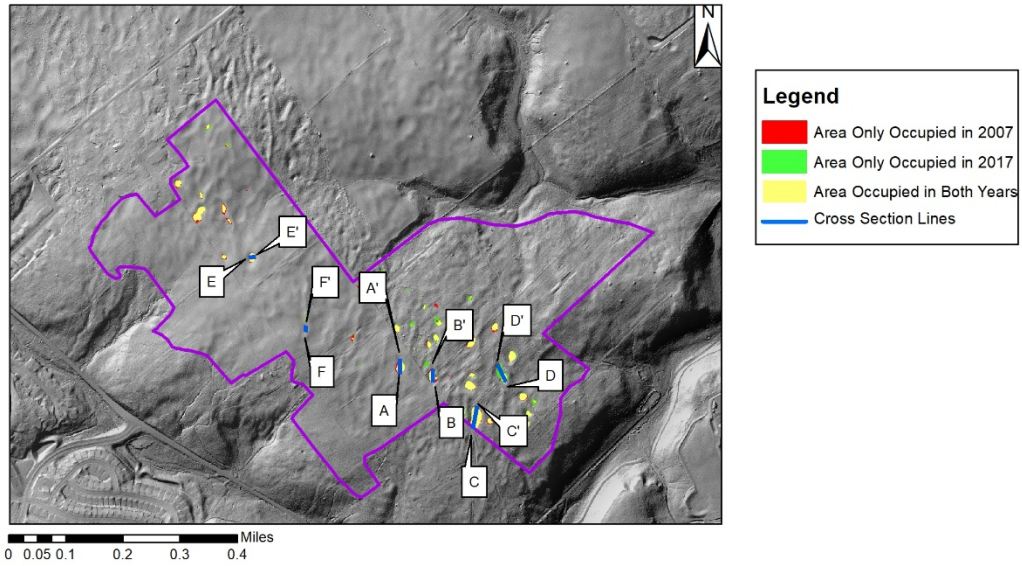

Figure 17: Locations of cross sections A-A' through E-E' relative to the entire site.

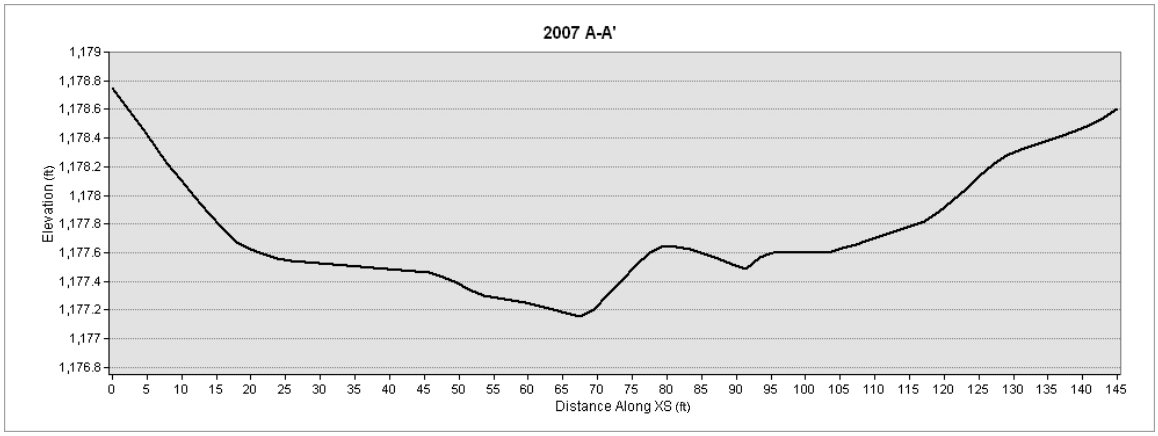
2007 A-A'
Elevation (ft)
1,179
1,178.8
1,178.6
1,178.4
1,178.2
1,178
1,177.8
1,177.6
1,177.4
1,177.2
1,177
1,176.8
0 5 10 15 20 25 30 35 40 45 50 55 60 65 70 75 80 85 90 95 100 105 110 115 120 125 130 135 140 145
Distance Along XS (ft)

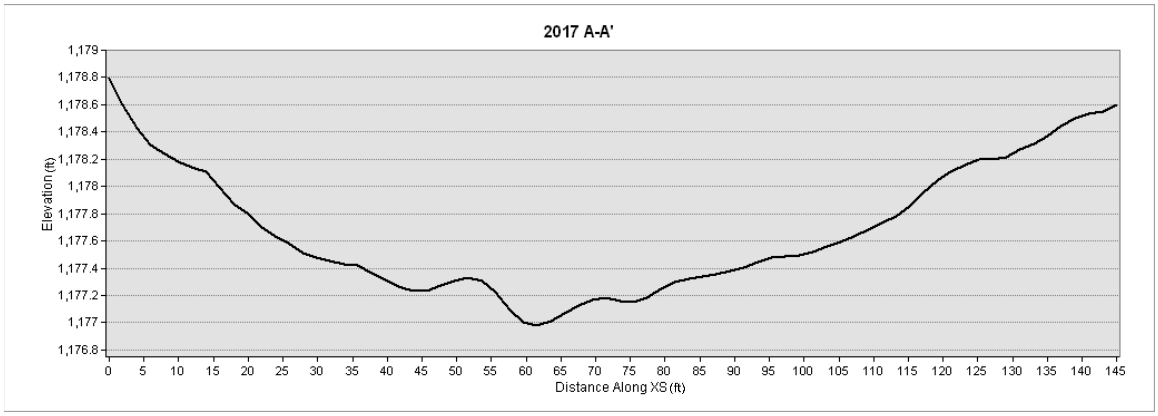
2017 A-A'
Elevation (ft)
1,179
1,178.8
1,178.6
1,178.4
1,178.2
1,178
1,177.8
1,177.6
1,177.4
1,177.2
1,177
1,176.8
0 5 10 15 20 25 30 35 40 45 50 55 60 65 70 75 80 85 90 95 100 105 110 115 120 125 130 135 140 145
Distance Along XS (ft)

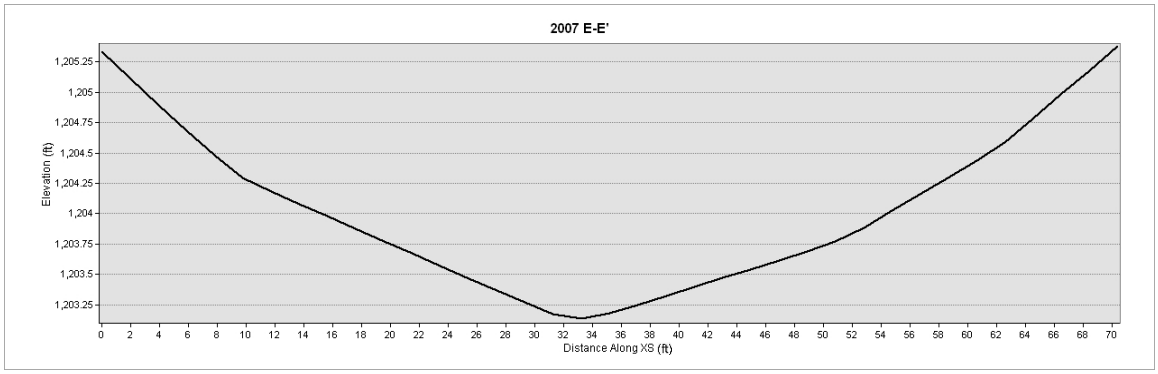
2007 E-E'
Elevation (ft)
1,205.25
1,205
1,204.75
1,204.5
1,204.25
1,204
1,203.75
1,203.5
1,203.25
0 2 4 6 8 10 12 14 16 18 20 22 24 26 28 30 32 34 36 38 40 42 44 46 48 50 52 54 56 58 60 62 64 66 68 70
Distance Along XS (ft)

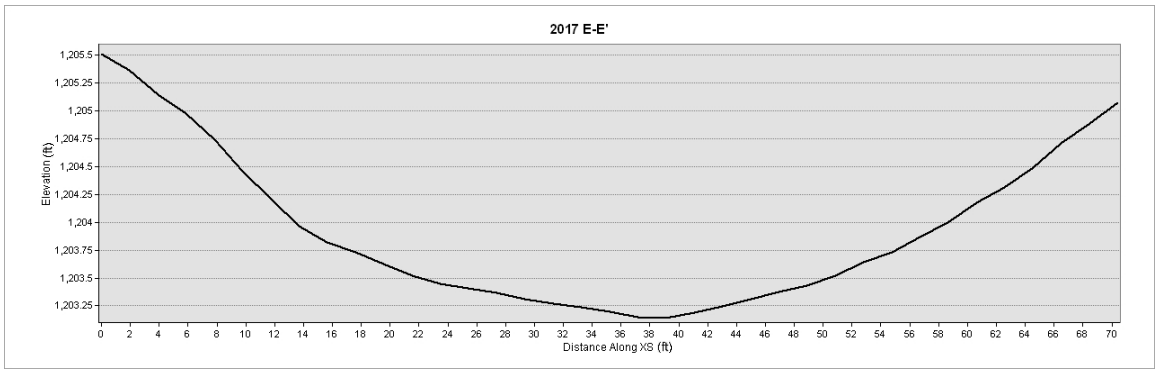
2017 E-E'
Elevation (ft)
1,205.5
1,205.25
1,205
1,204.75
1,204.5
1,204.25
1,204
1,203.75
1,203.5
1,203.25
0 2 4 6 8 10 12 14 16 18 20 22 24 26 28 30 32 34 36 38 40 42 44 46 48 50 52 54 56 58 60 62 64 66 68 70
Distance Along XS (ft)

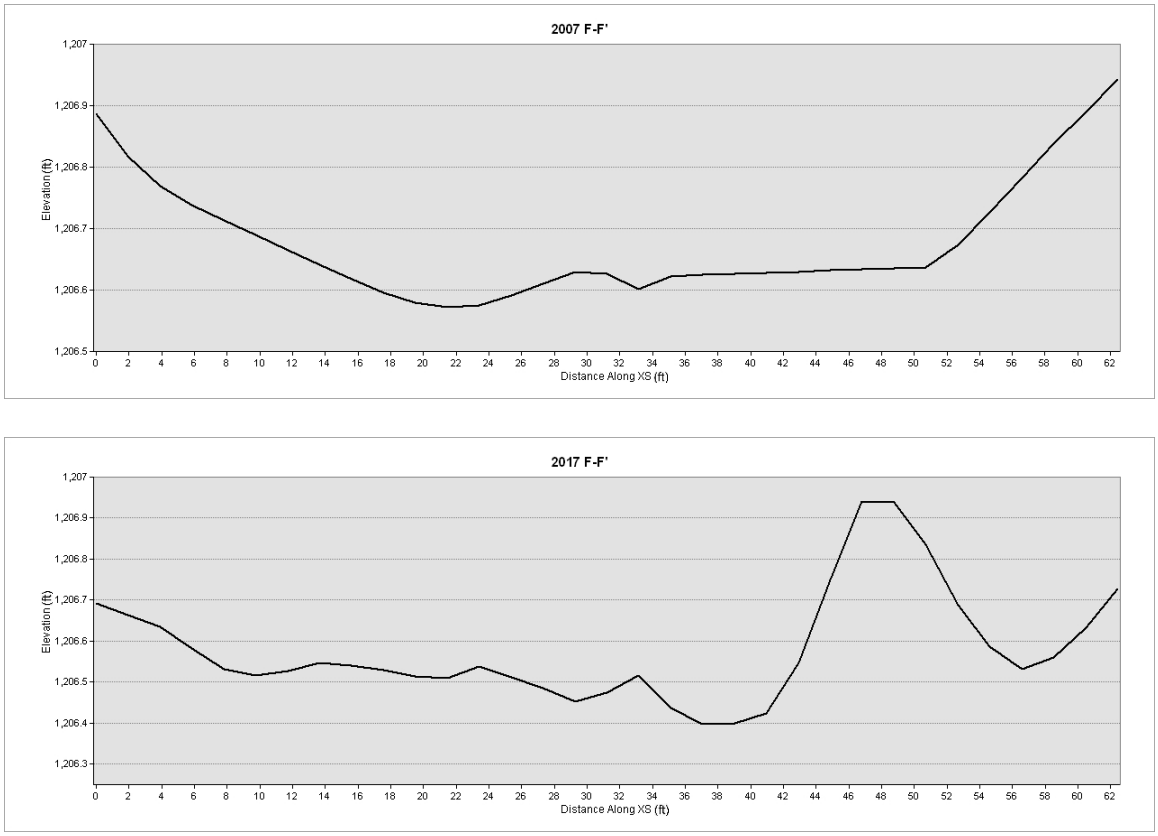

Figure 18: Cross Sections within the cropped portion of the site represented as A-A', E-E', and F-F'.

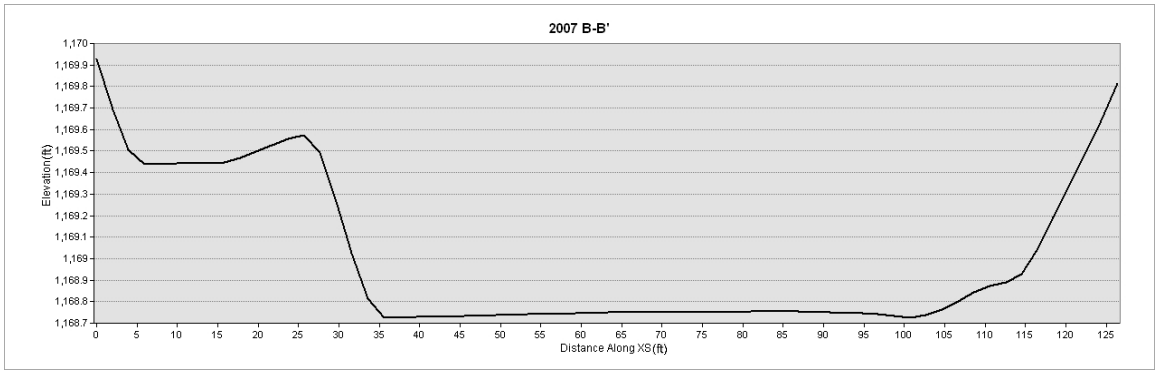
2007 B-B'
Elevation (ft)
Distance Along XS (ft)

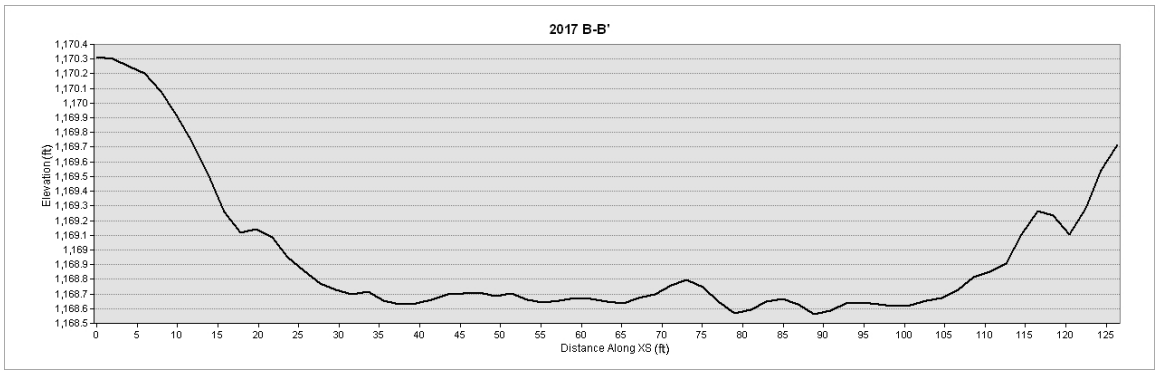
2017 B-B'
Elevation (ft)
Distance Along XS (ft)

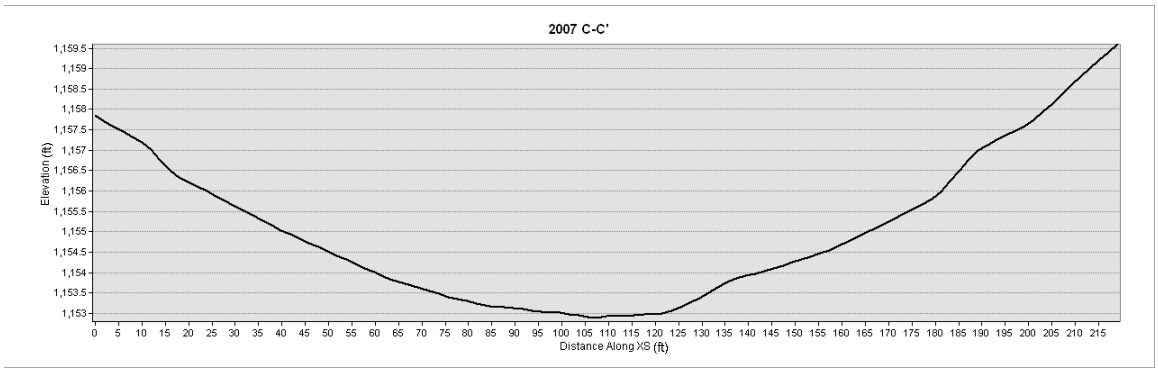
2007 C-C'
Elevation (ft)
Distance Along XS (ft)

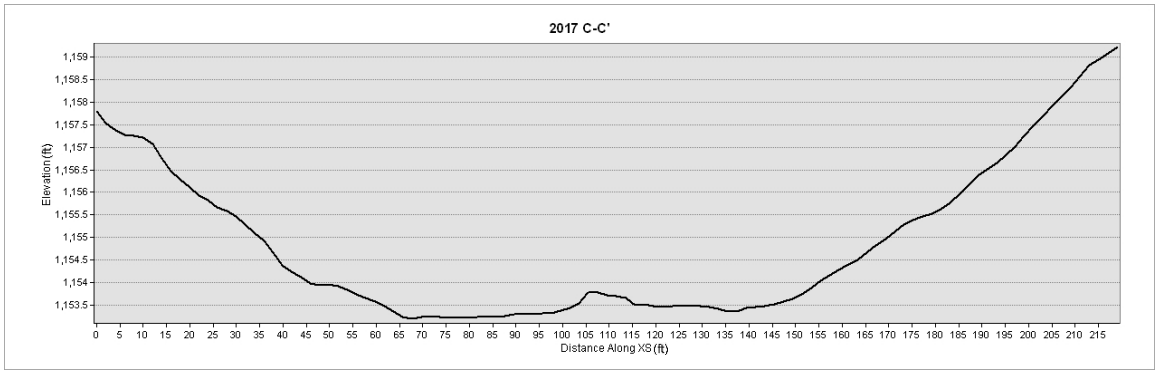
2017 C-C'
Elevation (ft)
Distance Along XS (ft)

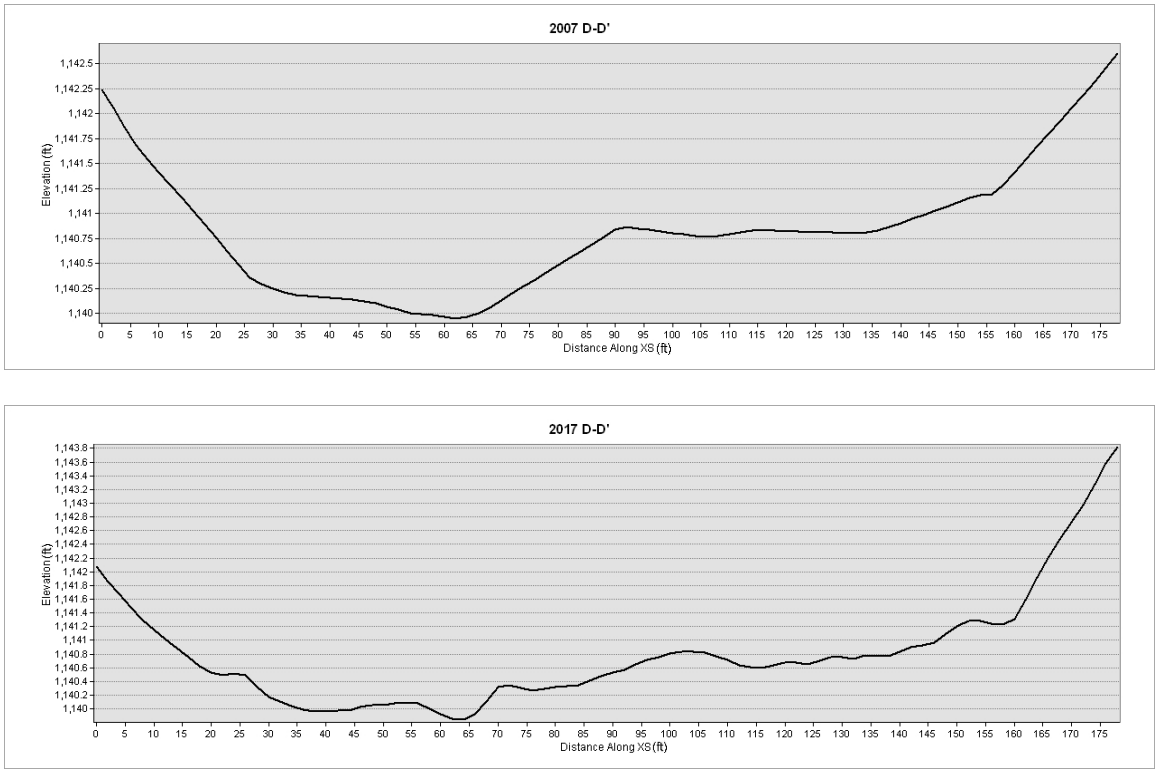

Figure 19: Cross Sections within the forested portion of the site represented as B-B', C-C', and D-D'.

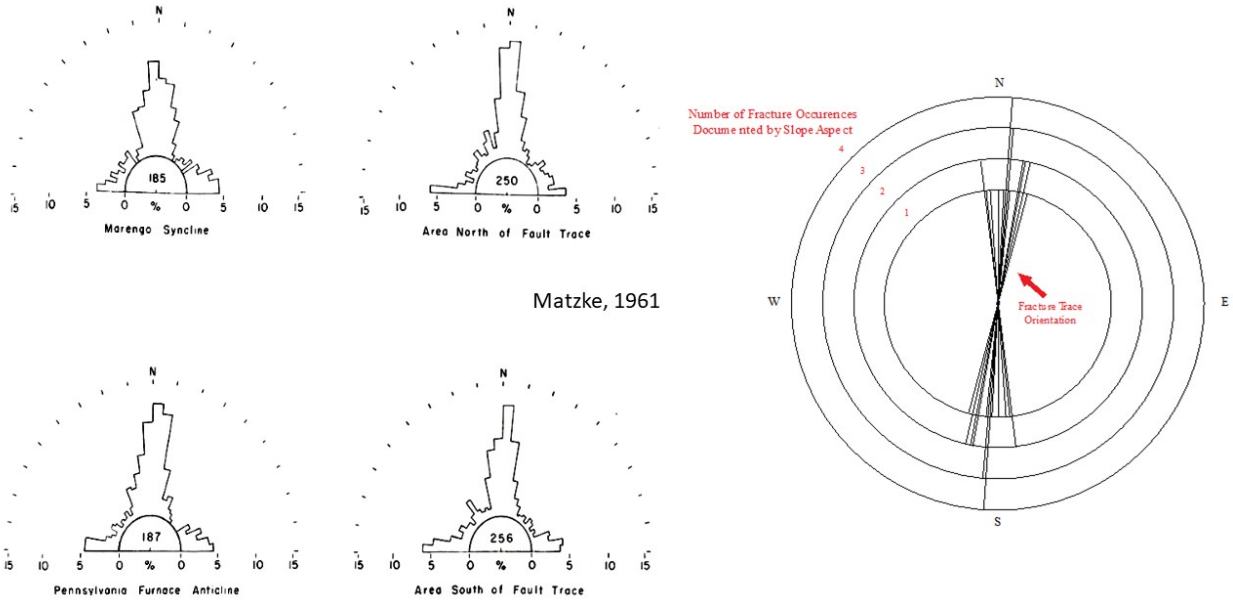

Figure 20: Fracture rose diagram comparison between Matzke and those identified within the site. The Astronomy site lies just north of the Pennsylvania Furnace Anticline and south of the Marengo Syncline.

CHAPTER THREE

MODELING GROUNDWATER FLOW AND NITRATE TRANSPORT IN KARST AQUIFER: A CASE STUDY OF THE LIVING FILTER SITE USED FOR WASTEWATER REUSE IRRIGATION IN AGRICULTURE AND FORESTRY LAND USES IN THE SPRING CREEK WATERSHED, PENNSYLVANIA

Timothy J. Daniel[1], Ronald Falta[1], Lawrence Murdoch[1], Henry Lin[2], and Christophe J. G. Darnault[1*]

[1]Department of Environmental Engineering and Earth Sciences, Clemson University, Anderson, SC 29625, United States

[2]Department of Ecosystem Science and Management, The Pennsylvania State University, University Park, PA, 16802, United States

*Corresponding author: Tel: +1 864 656 1398; fax + 1 864 656 0672. E-mail address: cdarnau@clemson.edu

Abstract

Treated wastewater reuse for irrigation is an alternative resource to meet the increasing demand for water used in the agricultural production process and to reduce the pressure on the limited existing freshwater resources. However, this reuse of treated wastewater requires the development of specific long-term management processes to mitigate both public and environmental hazards. The Pennsylvania State University has been operating a secondary treated wastewater effluent irrigation site, the "Living Filter," ever since the early 1960's with its current extent occupying 708 acres of agricultural and forested land since 1982. For over 50 years, nitrate as nitrogen (NO_3-N) concentrations in the karstic groundwater system have fluctuated with time due to variations in the application rate of the effluent and concentration within the effluent. Although nitrate concentrations previously exceeded the federal maximum contamination levels (MCL) of 10 parts per million (ppm) in groundwater monitoring wells in and around the living filter, they are now below the MCL of 10 ppm ever since the early 2000's. In this study, a framework was developed to model the impact of treated wastewater and disposal of large volumes of wastewater for irrigation in agriculture and forestry land uses on groundwater nitrate contamination in a karst landscape of the Spring Creek Watershed, central Pennsylvania, in order to understand

the long term contributions of nitrate to the unconfined karst aquifer below the "Living Filter" site. This study uses a numerical simulation model to examine groundwater flow and nitrate fate and transport in the karst landscape of the Spring Creek Watershed, central Pennsylvania, in response to aquifer recharge by wastewater irrigation of the Living Filter site. The simulation of nitrate fate and transport in the aquifer was conducted by developing a groundwater mass transport model using MODFLOW and MT3DMS. The groundwater model MODFLOW was used to simulate three-dimensional regional changes in the water table over time and constructed of the local aquifer between Buffalo Run, Slab Cabin Run, and Spring Creek in the Spring Creek watershed in central Pennsylvania. Historical and future predicted nitrate concentrations were modeled based on data provided by the Pennsylvania State University Office of the Physical Plant (OPP). The mass transport model MT3DMS was used to simulate the fate and transport of nitrate in the aquifer considering the recharge by treated wastewater irrigation with existing and long term rates of waste disposal. A number of predictive simulations for year 2015 and 2035 were carried out to evaluate the impact of treated wastewater and disposal of large volumes of wastewater for irrigation in agriculture and forestry land uses on groundwater nitrate contamination and concentrations. The calibrated groundwater model yielded a Root Mean Square Error of 5.41 for the area of irrigation and 24.67 for the entire modelled area. The results of the calibrated fate and reactive transport model show the extension of a nitrate plume over most of the study area with concentrations below 10 $mg \cdot L^{-1}$ under the current 2015 setting and the long

term 2035 scenario of increased irrigation rates. The nitrate migration was dominated by the presence of two high conductivity groundwater troughs adjacent to the study area resulting in a near steady-state total mass since the 1990's. These values are likely highly generalized due to the karstic nature of the aquifer below and the unpredictability of solution voids as transport pathways. Results of the water quality model show that the aquifer recharge by wastewater reuse irrigation does not produce nitrate levels above 10 $mg \cdot L^{-1}$ in the karstic landscape of the Spring Creek Watershed, thus meeting the regulatory standards for nitrate in groundwater. Results also demonstrated the sustainability of wastewater reuse irrigation practices for agriculture and forestry land uses.

Keywords: treated wastewater, nutrients, irrigation, groundwater model, nitrate pollution

1. Introduction

Water reuse – the use of treated wastewater – ensures the reuse of water resources. The use of treated wastewater for irrigation, as an alternative water resource to reduce the increasing pressures on scarce freshwater resources, is a strategic conservation measure supporting agricultural production. The result is substantial benefits from the use of nutrient-rich wastewater effluent, and the achievement of sustainable development goals in the context of the increase in the scarcity of water resources and

the impacts of climate change. In arid and semi-arid regions, usually experiencing water shortages for irrigation, treated wastewater may become the main source of water and nutrients for crop production.

The use of treated wastewater effluent for crop irrigation is an agricultural practice that dates to the 1500s in Germany, the 1600s in Scotland, the 1800s in France and the United States, and in the 1900s in China (Tang et al., 2004). It is now already a commonly used practice in arid and semi-arid environments throughout the Middle East and North Africa (MENA) (Jaramillo and Restrepo, 2017; Hamilton et al., 2007). By reapplying wastewater to agronomic crops, the amount of water withdrawn from an aquifer or surface water source is significantly reduced and excess water that is not evapotranspirated infiltrates and replenishes the groundwater aquifer.

Wastewater irrigation is beneficial in regions with sensitive surface water systems that would be either damaged or impaired from surficial discharge of wastewater effluent. The application of wastewater effluent to crops also reduces the amount of nutrient and pharmaceutical pollution in surface water streams (Toze, 2006). Japan is one of the largest implementers of wastewater irrigation due to its lack of natural fresh surface water resources (Dayanthi et al., 2006) and Florida also uses wastewater irrigation to mitigate the effects of seasonal droughts that can occur as the majority of its rainfall occurs only over a fourth month-period (Martinez and Clark, 2015). Further, agricultural

concerns in both arid and semi-arid regions such as the western United States and MENA that experience long periods of drought also engage in wastewater reuse (Hamilton et al., 2007).

Wastewater irrigation is advantageous over traditional wastewater discharges in that groundwater is used in a nearly closed loop with the only loss via evapotranspiration, unlike the latter in which the majority of water discharged into surface streams fails to replenish the aquifer. In the United States, there are no verified statistics on the percentage of wastewater that is reused between both municipal and industrial supplies ("Guidelines for Reuse", 2012). As of 2006 approximately 7-8% of U.S. municipal wastewater was reclaimed, although there are no estimates as to what percentage of industrial wastewater is reused (EPA, 2012; Miller, 2005). However, in some areas of the world, wastewater is used for either deep well injection or land application. There are a variety of applications used to apply wastewater to the land, either through wetlands, overland flow, and fast and slow infiltration (EPA, 2004).

Nitrate pollution and increasing nitrate levels in groundwater are a ubiquitous problem worldwide with agricultural land use being the main non-point source pollution hazard to groundwater quality (Haller et al., 2013). Nitrate is a primary polluter of groundwater with high nitrate concentrations a threat to both public health and ecosystems. The occurrence of nitrate in groundwater may result from (1) the natural fixation of nitrogen

in arid and desert regions(Barnes et al., 1992); (2) the breakdown of soil organic matter (SOM) in the lack of a nitrate sink(Faillat and Rambaud, 1991); (3) the high levels of nitrogen fertilizers use in agriculture(Dudley, 1990); (4) the disposal and decomposition of human and animal waste(Smith et al., 1999); and (5) the land treatment of municipal wastewater. Consequently, nitrogen enters the subsurface environment through the soil and is transformed in nitrate through complex processes in either the unsaturated or saturated zones, which then moves with groundwater.

The environmental and water quality damage to Spring Creek in State College PA, from wastewater discharge, and increased drought conditions and groundwater have led Pennsylvania State University (Penn State) to implement wastewater irrigation in the 1960s to reduce contamination and improve stream quality within that creek, and to recharge the regional aquifer. After wastewater effluent discharge to a local stream yielded water quality and large fish kills, Penn State began a pilot wastewater effluent irrigation site known as the “Living Filter” in 1962 (Pennypacker et al., 1967; Parizek et al., 1967). The Living Filter has been in continuous operation since 1962 where portions of State College’s treated wastewater effluent are redirected to forested and agricultural land sites. The redistribution of treated wastewater effluent was in direct response to high nutrient levels in Spring Creek as a result of wastewater discharge to one of its tributaries, Thompson Run. Even though 85-92% of the biochemical oxygen demand (BOD) was removed during the wastewater treatment process, the volume of

water contributed enough mass loading to promote aquatic plant growth and reductions in dissolved oxygen for aquatic animals within Spring Creek (Pennypacker et al., 1967; Parizek et al., 1967). In addition, wastewater discharge to streams typically has little to no effect on the amount of recharge occurring within the aquifer due to the fact that Spring Creek is a gaining stream.

The deterioration of surface water conditions within Spring Creek prompted a cease and desist order from the Pennsylvania Department of Environmental Protection (PA DEP) in 1960. Specifically, increased aquatic plant growth and CO_2 levels during the night cycle respiration, and excessive surfactants used in household cleaning practices which were not removed during the wastewater treatment process caused large fish kills and unsightly foaming of the water. After successfully reducing the contamination in streams, Penn State expanded the Living Filter in 1982 to accommodate all of the wastewater effluent from the borough of State College. The Living Filter is located in State College, PA and is situated along the edge of the Valley and Ridge physiographic province adjacent to the Allegheny front (Figure 1). The Living Filter is divided into two unequal sized portions at its current post 1982 expansion size with the Astronomy site encompassing roughly 191 acres and the Gamelands site encompassing 517 acres (Figure 2).

Wastewater irrigation on agricultural and forested land known as the “Living Filter” is a viable alternative to wastewater discharges to streams in that it recharges the underlying aquifer from which the original water was withdrawn. However, the sensitivity of the aquifer makes it urgent to understand the effects of wastewater reuse upon the water table in a karstic environment, particularly as contaminant transport occurs within fractures and solution conduits. In this general context, the objectives of this study are to (1) model groundwater flow in the karst landscape of the Spring Creek Watershed, central Pennsylvania, to examine the hydraulic response of the aquifer to the recharge by wastewater irrigation of the Living Filter site with the historic and long term application rates of treated wastewater effluent disposal, and (2) simulate the fate and transport of nitrate in the karst aquifer of the Spring Creek Watershed, central Pennsylvania, resulting from wastewater irrigation of the Living Filter site with the historic and long term application rates of treated wastewater effluent disposal to predict future nitrate concentrations and mass loading in the groundwater. A conceptual model for groundwater flow and contaminant transport of the Spring Creek Watershed in central Pennsylvania is presented in this study. A numerical simulation model is used to investigate the hydraulic response of the aquifer to the recharge from wastewater irrigation of the site known as the Living Filter, with the historic and long term rates of treated wastewater effluent disposal. The groundwater USGS MODFLOW Forward-finite difference model is used to simulate three-dimensional regional changes in the groundwater table over time. Also, a mass transport model is used to simulate the

fate and transport of nitrate in the aquifer by accounting for the recharge from wastewater irrigation of the site known as the Living Filter, with the historic and long term rates of treated wastewater effluent disposal. The Modular Transport 3-D Multi-Species (MT3DMS) model is used to simulate three-dimensional regional changes in the nitrate concentration plumes over time, and nitrate concentrations and mass loading in the groundwater. The results of the groundwater flow and contaminant transport/water quality models are used to assess the management and sustainability of aquifer recharge of the Spring Creek Watershed by wastewater irrigation of the Living Filter. These models may also be used to simulate several scenarios for aquifer recharge, irrigation, and treated wastewater effluent disposal rates and compositions, and to determine their optimal rate and schedule, depending on groundwater flow, water quality, and socio-economic constraints.

2. Study area

2.1 Geology

The geology of the study site is comprised of dolomite and limestone with some interbedding of both sandstones and oolitic cherts (Figure 3). Approximate within two miles of the site are high-relief orthoquartzite ridges with an elevation gain up to 2000 feet higher than the adjacent valley floor. While the orthoquartzite ridges operate as surface water divides, the high conductivity solution voids present in the karst systems prevents intersection of the groundwater divides in this region, with water having been

shown to flow from the north side of Bald Eagle Mountain during periods of extreme drought (Chin, 1996).

Local geologic controls in this area are characterized by thrust and tear faults along with anticlines, synclines, fracture traces, and joints. The study region itself encompasses the Marengo syncline, Gatesburg Anticline, and Pennsylvania Furnace anticline (Matzke, 1961). The anticlinal/synclinal relationship of the carbonates in the valley floor is hypothesized to have no effect upon the hydraulic conductivity of the aquifer itself (Parizek, Personal Communication). Fracture traces with a trend and 5° and 355° in their primary orientation are most predominant in the Mines member, which is also characterized by a more weakly-defined secondary fracture axis running directly E-W (Matzke, 1961). This is important as most wells installed after the 1960's are installed in fracture traces where available due to an enhanced volumetric productivity (Chin, 1996; Parizek, R.R., Filley, 1982). There are currently 13 wells monitored quarterly in and around the Living Filter, all of which are cased within fracture traces or in which primary and secondary fracture orientations intercept. Closed hillslope depressions and sinkholes have a tendency to form along the primary orientation of the fractures and can provide regions for focused recharge as evidenced by the conceptual model below (Figure 4).

2.2. Hydrogeology

Current irrigation rates average around 1.5-1.6 million gallons per day (MGD) yearly with the monthly average the highest during the active school year (mid-August through mid-December and mid-January through mid-May) and the lowest during summer and winter break (mid-May through mid-August and mid-December through mid-January). During the period in which the wells for this study were monitored, the recharge via the Living Filter was on average 2.8 MGD. Recharge from precipitation was determined via a hydrograph analysis of Bald Eagle Creek just to the north of the study site and is corroborated with values derived from Chin (1996) and Fulton et al. (2015) (Chin, 1996; Fulton et al., 2015) (Figure 5).

The Living Filter is located on a local groundwater high and discharges to two high conductivity geologic features that are exhibited as groundwater troughs, which in turn prevents over mounding of the water table (Caruccio, 1963; Parizek et al., 1967). Generalized hydraulic conductivities for each geologic unit in this area varies anywhere between 0.23 ft /d and 61 ft /d, excluding the two high conductivity features (Figure 6).

While there are many valleys throughout the Spring Creek watershed, few are occupied by perennial streams. The streams within the Spring Creek basin, excluding Spring Creek itself, are typically under drained, which is better known as a losing stream (Parizek et al., 1967). Some regions of concentrated recharge result in disappearing streams in the Upper Sandy Member and Warrior Limestone formations. The underdrainage within the

Big Hollow valley is hypothesized to be the result of high conductivity conduits within the weathered bedrock and the upper portion of the competent bedrock in this region (Parizek et al., 1967). Big Hollow serves as a groundwater trough and a collection source for water that is discharged into the living filter given its direct down-gradient proximity from the Astronomy site.

Three main perennial streams characterize the region of study (excluding conditions of severe drought): Spring Creek, Slab Cabin Run, and Buffalo Run. Buffalo Run is a traditional effluent type stream that, based on the heads within the monitoring wells to the east, is classified as a losing stream. Indeed, even during periods in which the stream bed is dry, the springs up the gradient of the Buffalo Run stream are characterized by a high flow rate, thus contradicting the observation that the portion of Buffalo Run to the northwest of the Living Filter is a losing stream. Indeed, Buffalo run is in part a combination of both a losing and gaining stream to the northwest of the Living Filter, based on upgradient spring discharges to Buffalo Run during drought conditions (Landon, 1963). In that study, Landon surmised that Buffalo Run is a gaining stream on its northwest bank and a losing stream on its southeastern bank, resulting in groundwater discharge to the water table underneath the Living Filter. Buffalo Run becomes solely a gaining stream to the northeast of the site as it moves down-gradient and nears Spring Creek, which has a significantly higher volumetric flow rate.

Slab Cabin Run, observed as losing stream in the region north of Tussey Mountain, has shown evidence of swallow-holes in regions in the past (Chin, 1996). Slab Cabin Run, composed of spring-derived water along with runoff from Tussey Mountain, is dry on occasion and characterized by high relief zones immediately adjacent to the stream that can result in difficult model simulations due to the resolution needed for accurate modeling.

Spring Creek is the main stream and the namesake of the watershed with monitoring stations towards Milesburg at the point where Slab Cabin Run and Spring Creek intercept. Spring Creek is known as a water table stream, characterized by a water table that discharges directly into the stream, which is largely a gaining stream throughout the entire reach (Parizek et al., 1967). Spring Creek, which is the recipient of several high discharge springs, has a stream routing that is surmised to be a result of joint control, especially in the northeastern edge of the site that is characterized by sharp meanders (Landon, 1963).

The Birmingham thrust fault is a low angle fault with three small fault splays south of Buffalo Run Creek and just north of the Gamelands site. The shallow dip causes the fault itself to manifest as a wide groundwater trough that underlies much of the Spring Creek basin adjacent to Buffalo Creek where it then crosses Spring creek and enters the Spruce Creek watershed. It is possible that the Birmingham thrust fault is partially responsible

for the lack of correlation between the surface water and groundwater divides in the Spring Creek watershed as the surface watershed is surmised as 22% smaller than that of the groundwater (Wood, 1980). Slickenside rock fragments have been observed from drill cuttings in the State Gamelands 176 area known as the Scotia Barrens that is approximately west of our study site. A pumping test conducted at a rate of 735 GPM from well C18 within its boundaries for three days yielded a drawdown of only 4 feet (Chin, 1996). Previously, the Birmingham thrust fault was modeled as having a conductivity of 1417 ft/day from 300-600 feet in depth (Fulton et al., 2015).

Big Hollow is a dry karst valley to the southeast of the Astronomy site in which it is hypothesized that groundwater flows directly the Astronomy site into the trough formed by that valley (Parizek et al., 1967). Transmissivity values derived from an analysis of wells drilled within fracture traces in the Big Hollow fell within a range from 100,000 to 150,000 GPD/ft while values of unfractured blocks of bedrock immediately adjacent to fractures fell within a range between 1,000 to 4,000 GPD/ft (Parizek et al., 1967). Several sinkholes are present within Big Hollow, the occurrence of which is from differential weathering at the formation contact between the Mines Dolomite and the Stonehenge Limestone due to the higher solubility of that limestone. In previous modeling undertaken by Chin (1996), a maximum conductivity of 850 ft/day was used in the region of the Big Hollow.

2.3. Water quality and nitrate contamination concerns

The Maximum Contaminant Level (MCL) for nitrate as nitrogen (NO_3-N) in groundwater is 10 parts per million (ppm) or 44 ppm as nitrate (NO_3) (US EPA, 2017). Any reference to nitrate found in this publication from this point forward will refer solely to nitrate as nitrogen (NO_3-N). Nitrate concentrations in the wastewater effluent average around 10 ppm currently while total nitrogen concentration as a result of ammonia and nitrite is significantly higher. A contributor to soil nitrate concentrations can be either the nitrification of N_2 or N_2O gas in the soil or the addition of oxygen ions to the nitrite or ammonia/ammonium molecules (Figure 7).

Fertilizer in the form of ammonium nitrate is added for rotational cropping throughout the year at an estimated rate that is representative of crop requirements. Given the lack of data on nitrate entering the aquifer in these agricultural regions, we will assume that the application of nitrate as fertilizer satisfies the agronomic demands of the crops while the application of nitrate in the wastewater effluent migrates from the Living Filter to the aquifer. The Living Filter is only one source of nitrate to the aquifer, however, in that elevated nitrate is also evident from the application of residential and commercial fertilizer in the form of ammonium nitrate or manure, and septic tank leachate.

A health risk is prevalent above the MCL of 10 ppm with the highest risk of adverse health effects occurring for pregnant women, youths, and senior citizens. Excess nitrate

in the bloodstream has been proven to contribute to thyroid enlargement and in extreme cases methemoglobinemia, better known as blue baby syndrome (Gatseva and Argirova, 2008; Fan and Steinberg, 1996). Data from several studies are characterized by contradictions in the statistical correlations of elevated nitrogen concentrations as a possible cause of increased levels of lymphoma or cancer. However, nitrogen as either nitrate or nitrite is hypothesized as beneficial to digestive and cardiovascular health along with enhanced antimicrobial properties in stomach acid (Lundberg et al., 2006; Benjamin et al., 1994).

Estimates of background nitrate concentration by land use have been conducted both in the Spring Creek watershed and beyond into other karst aquifers in Pennsylvania. The average nitrate concentration for groundwater in the entire watershed is estimated at 3.6 ppm with small variations based on the seasons (*Monitoring Nitrate in the Spring Creek Watershed*, 2013). Estimates of groundwater nitrate concentrations are higher within 100 feet of fertilized crops that in turn reduce with distance (Swistock, 2016). Significant differences in nitrate measurements in groundwater from Lancaster, Lebanon, and Chester County were observed between forested, urban, and cropped surfaces based on the 1992 National Land Cover Dataset and its effects on the Amish community (Aschebrook-Kilfoy et al., 2012). A comparison 2006 of pre- and post-development nitrate concentrations with data from the 1980's and 1990's within a subdivision in Southern Chester County found that post-development levels were on

average 0.5 ppm higher than the pre-development counterparts (White et al., 2013). In their comparison of pre- and post-storm flow groundwater chemistry from different land cover classifications in the Spring Creek watershed, Buda and Dewalle observed no significant fluctuations in nitrate concentrations in water close to agricultural areas (at 5.1ppm pre flow and 5.2 ppm post flow concentrations). (Buda and Dewalle, 2009). Nitrate values based on land use vary greatly between different physiographic provinces due to a large number of variables. In areas where sinkholes and depressions are common there is little to no interception for denitrification processes to occur, allowing for higher concentrations of nitrate to enter the groundwater. Nitrate values in soil below 120 cm are traditionally viewed as concentrations reaching the water table as little to no denitrification occurs below the root zone in the absence of anoxic conditions. Nitrate values are typically lower in regions underlying forested land due to the deeper extent of tree root systems compared to typical cover crops. Residual soils comprised from the Mines Dolomite and Upper Sandy member have been found to allow nitrate concentrations above the MCL of 10 ppm to migrate past the root zone (Hook and Kardos, 1978). Land use concentrations do not account for nitrate pools such as tree leaf litter that is not collected annually, such as that in agricultural landscapes.

In regions characterized by anoxic deep groundwater, it is possible for groundwater to be denitrified due to reducing conditions. As no data can be found on any anoxic conditions beneath the Living Filter, it is likely that these conditions do not exist.

Further, the faster transport times in karst systems mean that groundwater typically is not in the system long enough to become anoxic. Lindsey et al., (1997) found that samples that had a lower groundwater residence time retained over 90% of their initial nitrate concentrations whereas groundwater with a more tortuous path and longer residence times was significantly more denitrified. Nitrate in groundwater is generally considered as soluble and not prone to adsorption in fractured bedrock matrices.

Wastewater effluent properties have varied throughout time as a result of new technologies, population changes, and environmental issues. In the early 1990's, nitrate within groundwater monitoring wells in and around the site exceeded EPA Maximum Contaminant Level's (MCL's) of 10 ppm. Currently, activated sludge biological nitrogen removal is employed by the treatment plant to reduce nitrate in the effluent. In their 2017 study, Sendagi et al. noted a C:N ratio of 0.04-0.2 with a near neutral pH and nitrate concentrations around 10 ppm, indicating low levels of adsorption (Sendagi et al., 2017). The averages for each month can vary significantly due to the number of students on campus, compounded by the fact that since 2015 the borough of State College has operated a separate wastewater treatment system. The total nitrogen in effluent since 1982 has varied anywhere between 2-56 ppm with levels at approximately 10 ppm since the implementation of activated sludge biological nitrogen removal in 1999.

Penn State is currently in the process of retrofitting its campus to support greywater reuse for local irrigation projects on its athletic fields and community gardens. Greywater is expected to take away up to 0.5 MGD per day of wastewater from the Living Filter in the immediate future with the possibility of expanded use in the future. Greywater utilization in toilets will eventually make its way back to the wastewater treatment plant, thus preventing a total loss of the 0.5 MGD lost to the plant. Further, any greywater used for irrigation will be recharged to the aquifer on campus, over three miles distant from the Living Filter. Current wastewater treatment renovations are underway with Class A wastewater certification and the capability to process up to 3.0 MGD in order to support the sewage output from an expanding student population. Target concentrations for nitrate in class A wastewater are 10 ppm or less of total nitrogen.

3. Methods

3.1. Conceptual Model

In 1965, State College was subjected to severe drought conditions in which the water table was reduced in depth by nearly 100 feet in some regions (Parizek et al., 1967). Subsequent attempts to model transient water tables in the region have resulted in high Root Mean Square Errors (RMSE) (Fulton et al., 2015; Chin, 1996) largely due to the unpredictability of karst pathways and the lack of proper tracer tests in the region of the Living Filter. The occurrence of fluctuation of daily values can reach much as 25 feet in a

single day, especially within the dry karst valley of Big Hollow (Fulton et al., 2015; *Monitoring Nitrate in the Spring Creek Watershed*, 2013).

Soil thickness within the study area also varies in thickness, from 5 to 161 feet thick depending on proximity to topographic highs and lows (Parizek et al., 1967). The predominance of the water table within the fractured bedrock matrix obviates the use of the hydraulic conductivity of soils in this model.

Conceptually, the main sources and sinks in the extent of our study region can be reduced to several main components: recharge from precipitation, recharge from irrigation, discharge from pumping wells, loss from evapotranspiration, and discharge or recharge to streams (some stream portions recharge and some discharge are in karstic environments). Groundwater in the subsurface is assumed to be transported via both diffuse and conduit flow in karst with conduit flow occurring in bedrock fractures and solution voids created from dissolved carbonate in dolomite and limestone.

Pennsylvania is a temperate climate that receives roughly 41 inches of precipitation through rainfall and snow melt per year. The Living Filter currently receives an estimated 1.4 – 1.6 MGD of wastewater effluent during the active school year between mid-August to mid-December and mid-January to mid-May. The Living Filter occupies 708 acres between the Gamelands and Astronomy sites with some portions receiving no

irrigation. For simplicity's sake, we will assume that irrigation is evenly distributed over the entire site as irrigation application rates and locations vary daily over more than 100 irrigation laterals.

Historical nitrate concentration trends in each of the wells in the region of the Living Filter has closely followed the trend of total nitrogen contributions from wastewater effluent, therefore, the concentration at which nitrogen is applied within the model is equal to that of total nitrogen in the wastewater effluent. It is important to note that while the concentration trends are generally the same, the concentrations themselves vary considerably from well to well, likely due to not only their location in and around the Living Filter but also due to their screen elevations.

3.2 Flow and mass transport models

MODFLOW and MT3DMS models were used to simulate groundwater flow and contaminant transport in the aquifer.

3.2.1. MODFLOW model and calibration for Spring Creek watershed

In this section, the groundwater flow model for the karst aquifer is detailed. The USGS MODFLOW Forward-finite difference model was used for the groundwater low model simulations of the Spring Creek watershed in central Pennsylvania. Typical MODFLOW simulations are simulated linearly and do not account for the wetting and drying of cells

in the standard unaltered MODFLOW-2005 version. A Newtonian solver (UZF) was developed based on the MODFLOW-2005 approach known as MODFLOW-NWT (Niswonger et al., 2011). The partial differential solution in MODFLOW is expressed in equation 1 below:

$$\frac{\partial}{\partial x}\left[K_{xx}\frac{\partial h}{\partial x}\right] + \frac{\partial}{\partial y}\left[K_{yy}\frac{\partial h}{\partial y}\right] + \frac{\partial}{\partial z}\left[K_{zz}\frac{\partial h}{\partial z}\right] + W = S_s\frac{\partial h}{\partial t} \qquad \text{(Eq. 1)}$$

where W is the model sources and sinks (recharge, pumping, discharge to streams, discharge from streams); K_{ii} is the hydraulic conductivity in the x, y, and z direction; H is the potentiometric head; T is the time; and S_s is the specific storage. Since the analysis implemented here is steady state, the variables S_s and t are unused.

MODFLOW-NWT accounts for the wetting and drying of cells and is more suitable for use in higher relief study sites such as the high ridges and valleys within the Spring Creek Basin. Although the majority of the water table resides in the bedrock, NWT is still preferable as the top of the bedrock is heavily weathered indicating the location of the saturated/unsaturated transition zone in this region. Should a transient analysis be implemented in this area, MODFLOW-NWT is preferable to the extreme seasonal water table variations associated with karst systems. A Workflow for model creation and calibration was created and followed as a base principal for any simulations (Figure 8).

The model grid was initially created with a rectangular grid comprised of 500 × 500 foot grid cells in the X and Y directions. The grid is oriented 52° along the X axis to the northeast to ensure alignment with the principle hydraulic conductivity and the slope of the water table along with the ridges to the north and south of the model. The model created by Chin (1996) (Chin, 1996) extends just past the University Park airport and occupies 31 mi^2 of the watershed. The model created by Fulton et al. (2015) (Fulton et al., 2015) occupies 229 mi^2 of the Spring Creek and Nittany basins along with the headwaters of the Spruce Creek basin. The full extent of the model in this study encompasses 94.4 mi^2 although the focus area of the study is only 46.1 mi^2 within the area encompassed by the Slab Cabin Run, Buffalo Run, and Spring Creek. Our modeled region of study extends beyond our region of interest to prevent the manifestation of errors from the close proximity of the model boundaries. The model extends to the base of the ridges formed by Bald Eagle Mountain, Tussey Mountain, and Nittany Mountain. Previous attempts to include the high relief ridges resulted in a significant overestimation of the water table due to the starting heads on the base map that followed closely to the ridge relief (Taylor 1997). It is more likely that heads lack contouring as closely spaced as that of Taylor's water table map, supported by the evident flow of water from under Bald Eagle Mountain during periods of severe drought (Parizek et al., 1967).

The model grid is comprised of 9 layers in the Z direction from depths of 0-600 feet below the land surface. To ensure a higher resolution of nitrate migration within the upper portion of the aquifer, layers 1-5 are each 40 feet in thickness and layers 6-9 are each 100 feet thick and uniform with the land surface above. An aquifer thickness of 600 feet is likely an overestimation in some regions although Fulton previously modelled the aquifer thickness to 900 feet below the land surface by reducing the hydraulic conductivity by 96% between depths of 600-900.

The base 500 $\times$ 500 foot XY grid was manually refined based on regions with unrealistic heads after the initial run. The high relief and large base cell size resulted in an overexaggeration of the surface elevation in several regions as the height represented by each cell is an average of elevation for that entire cell. In regions of both high topographic relief and in which streams had sharp meanders, extra refinement is needed to derive the proper cell elevation. If a cell designated to a specific head has a higher average elevation than the rest of surrounding specified cell heads, then it is represented as an unrealistic head change in the stream.

The model was first run with this baseline refinement and monitored for any abnormalities within the water table. The high relief along the streams in several regions of the site made it necessary to refine the grid along much of the stream portions. Further, the 10 m resolution of the base DEM meant that some small portions of the

stream elevation were not mapped properly within tight valleys and close meanders in the northeastern section of the model. Stream traces used in the model were obtained directly from the Pennsylvania State Department of Agriculture geospatial database with some adjustments required to follow the lowest elevation. The main streams of Buffalo Run, Slab Cabin Run, and Spring Creek were simulated as constant head boundaries while other stream valleys were not simulated given that they are dry the majority of the year (Figure 9).

Hydraulic conductivities were tested via trial-and-error based on values from previous studies (Becher, 1996; Gannett Flemming, 2008; Brachet, 2004; Parizek, R.R., Filley, 1982; Fulton et al., 2015) and hand drawn conductivity zones used to closely reflect that of Chin (1996) and the water table of Taylor (1997). Over 100 iterations of the model were used to obtain the results of our groundwater flow model with the assumption that the diffuse flow is the dominant flow regime in the overall geologic unit even though likely areas of turbulent conduit flow within the karstic units exist. Anisotropy was set to a constant 10:1 ratio between the horizontal and vertical in each geologic layer using established measurements (Chin 1996). Porosity within the Gatesburg formation ranges between 2-25%, so a constant value of 5% was implemented throughout the entire study area (Smith, 1966). Longitudinal dispersivity of 50 feet with a vertical ratio of 0.01 and a horizontal ratio of 0.1 was assigned to each unit based on values representative of dolomite (Gelhar et al., 1992).

Two high conductivity zones were implemented adjacent to the Living Filter to simulate the Birmingham thrust fault and the trough associated with Big Hollow. The Living Filter is located between two groundwater troughs which permits no extra surface to groundwater discharges and over-saturated conditions immediately under the site. A high hydraulic conductivity zone of 2500 ft/day was simulated between 400-600 feet in depth in the assumed proximity of the Birmingham thrust fault. Since there is no surface manifestation of the fault, its extent is estimated by slickenside fragments, high productivity wells, and high productivity springs. The Birmingham thrust fault is also hypothesized as controlling Buffalo Run. A high hydraulic conductivity of 2250 ft /day was estimated for the trough associated with Big Hollow between 0-400 feet in depth which accounts for open sinkholes and theorized enhanced solution conduits within the geologic formation.

The hydraulic head from 78 wells (Chin, 1996) taken in October 1994 were used for calibration. Although Chin recorded elevations for more than 95 wells within the scope of the model, several wells were omitted due to suspect elevations or their proximity to the model boundaries resulting in overestimation in some regions. The starting heads for the model were based upon those of Taylor (1997) as the water table mapped in Chin (1996) did not extend to the edge of our study site (Figure 10).

The premise that no water escapes the Living Filter via runoff and that which is not evapotranspirated reaches the groundwater directly as recharge served as the basis for calculating the evapotranspiration for the Living Filter. The Thornthwaite analysis (Thornthwaite and Mather, 1957) and average sunlight and temperature data for State College was used to calculate the potential evapotranspiration, and determine the precipitation minus potential evapotranspiration analysis. During the summer months (June, July, and August), the potential evapotranspiration only exceeded average precipitation for years 2007-2018. During those months where potential evapotranspiration exceeded precipitation, the difference was subtracted from the recharge provided by the Living Filter.

The basin wide average recharge was calculated using a stream hydrograph and a basin recharge analysis originally developed by Mau and Winter (1997). The analysis implemented here accounts for recharge based on precipitation and stream gauge from April 2007-March 2018. Precipitation data was obtained from the National Oceanic and Atmospheric Administration for the city of State College. The stream gauge data was obtained from the USGS station 01547100 on Spring Creek stationed just beyond the confluence of Spring Creek with Buffalo Run, thus serving as an accurate representation of basin wide recharge. The hydrograph analysis was used to derive a recharge rate of 0.88 ft/year (10.5 inches/year) which is similar to the 10 inches/year recharge rate used by (Chin) 1996). The potential evapotranspiration rate, calculated via hydrograph

analysis was 2.39 ft /year; the evapotranspiration rate, calculated via the Thornthwaite equation was 2.18 ft /year; and the previous evapotranspiration rate, calculated via the modified Thornthwaite approach was 2.13 ft/year (Waltman et al., 1997) (Figure 11).

3.2.2. MT3DMS model and calibration for Spring Creek Watershed

The model used for the nitrate reactive transport in an aquifer is detailed here. First, the MT3DMS (Modular Transport 3-D Multi-Species), based on a mass balance from cell-to-cell using the flow velocities from MODFLOW, was used for the simulations (Zheng et al., 1999). The equation associated with MT3DMS is expressed below as:

$$\frac{\partial(\theta C)}{\partial t} = \frac{\partial}{\partial x_i}\left(\theta D_{ij}\frac{\partial C}{\partial x_j}\right) - \frac{\partial}{\partial x_i}(\theta v_i C) + q_s C_s + \sum R_n \qquad \text{(Eq. 2)}$$

where C is the concentration of the dissolved species (M L^{-3}); θ is the porosity (dimensionless)

t is the time (T); x_i is the distance on the respective Cartesian axis (L); D_{ij} is the hydrodynamic dispersion coefficient (L^2 T^{-1}); $v_i$is the linear pore velocity (L T^{-1}); q_i is the volumetric flow rate per unit volume of aquifer representing fluid sources and sinks (T^{-1}); $C_s$is the concentration of the source or sink flux (M L^{-3}); and $\sum R_n$ is the chemical reactions (M L^{-3} T^{-1})

The absence of reactions in this simulation sets the chemical reaction term to 0 which is ignored. In order to run in steady state, MT3DMS requires the estimated porosity, the longitudinal dispersivity, the horizontal and vertical dispersivities, and hydraulic conductivity along with any recharge or sources and sinks of the contaminant. MT3DMS is compatible with most versions of MODFLOW excluding MODFLOW-USG. Mass loading was accomplished by implementing a recharge value in the irrigation coverage using the transient total nitrate values from 1982 through 2015 provided by the Pennsylvania State Office of the Physical Plant.

Nitrate is applied to the Living Filter via (1) nitrate in wastewater effluent, and (2) ammonium-nitrate used as fertilizer. Our analysis uses a generalized nitrate application rate instead of any separation based on crop cover as both the crop cover and application rate varies from year to year. While the goal is to provide just enough nitrate for agronomic demand that is typically not the case as previous nitrate measurements in groundwater below the Living Filter have shown otherwise and previous applications have resulted in excess nitrate accumulation in the soil (Loughran, Personal Communication).

The rate at which nitrate is applied in the model is directly related to the amount of total nitrate applied to the Living Filter in the form of wastewater effluent. A transient application rate was used in the model using actual concentrations in effluent with the

assumption that any future effluent application rate would be at a rate of 10 ppm of total nitrogen (Figures 12 and 13). In order to simulate the Living Filters contribution to nitrate dynamics in the aquifer, no background nitrate values were used in the simulations and no mass loading from rainwater was considered. Simulations were run for a total of 23 and 53 years to reflect concentrations in 2015 and predicted concentrations for 2035. The length at which the transient model was run was necessary to achieve a steady-state due to some low conductivities in the geologic units surrounding the Mines Dolomite and Upper Sandy member.

4. Results and Discussion

Results for the groundwater modeling portion of our analysis were on par with previous models by Chin, 1996 and Fulton et al. (2015) (Chin, 1996; Fulton et al., 2015) in terms of both the shape and consistency of the model (Figures 14-16).

It is important to remember that a comparison of models with different parameters will yield different results. The model created by Fulton of the entire Spring Creek watershed uses 656 $\times$ 656 ft grid blocks and is not refined enough to appropriately model the groundwater trough associated with Big Hollow. While Chin does not state the size of the grid blocks used in his model, it can be assumed that the grid blocks are of a similar size to Fulton's, excluding refinement in the area of the living filter. The Root

Mean Standard Error was computed for both models using equation 3 below based on the observed well values from the fall of 1994.

$$\text{RMSE}=\sqrt{\frac{\sum_{i=1}^{n}\left(h_{cal_i}-h_{m_i}\right)^2}{n}} \qquad \text{(Eq. 3)}$$

where h_{cal_i} is the calculated head at a node; h_{m_i} is the measured head at a node; n is the number of comparison points; and i is the subscript defining comparison point between 1 and n

The 13 wells within the extent of the Living Filter model had a combined RMSE of 6.03 feet while the RMSE for the entire model was 24.76 feet. A model RMSE can be further used to determine the accuracy of a model by dividing the RMSE by the total head change of the model. Typically a normalized RMSE value of less than 10% is the target for acceptable error within a model (Rumbaugh and Rumbaugh, 2017; Johnson, 2010).

The normalized RMSE for heads in the region of the Living Filter was 6.0%, given 101 feet of observed head change between the lowest well (P-1) and the highest well (W-3). Computed heads for wells in the southeastern portion of the Living Filter (P-2, P-3, P-4, and P-5) were generally underestimated excluding well P-1 (Figure 17). The three wells in the southeastern portion of the Gamelands portion of the Living Filter (W-3, W-1, and

W-5) were also underestimated while wells in the northwestern corner of the Gamelands site (W-2, W-6, W-7, G-10, and G-12) were overestimated. These computer values compare favorably to the observation wells measured in 1994. While more current water levels for the Living Filter are available for the purpose of this study, they were omitted due to the lack of basin wide values. Calibrating the model to both current water levels for the Living Filter along with basin wide water levels from 1994 would result in an erroneous model.

The normalized RMSE for the model basin wide, assuming 700 feet of head change from Taylor (1997), is 3.5%. The lack of observed head data within the orthoquartzite ridges of Tussey and Bald Eagle mountains also indicate the lack of data needed to calibrate the model in these regions. Also, the nitrate contribution simulated within the model which is directly from the Living Filter obviates the need to model outside of the stream boundaries as the streams are constant head boundaries.

Several factors inform the error in the groundwater model outside of the Living Filter. First, the dataset is old from October 1994, and has no changes to the water table from the past 24 years that could arise from additional pumping from residential use. The starting heads and groundwater contours for the model are from Taylor (1997) while the observed heads to calibrate the model are from Chin, (1996) which introduces error

based on the fact that no two groundwater maps will be the same when hand drawn and using values from different times.

The model itself uses wells that currently are in use and pumping data rate from 2017-2018, both of which have greatly changed since 1996. Most of the university wells are located within the highly productive Big Hollow so their drawdown has a relatively minimal effect. No estimated drawdown from wells used in 1996 was in excess of 9 feet when all wells were pumped continuously in the steady state model from (Chin, 1996). Also, the pumping rates down gradient of the Living Filter at the eastern edge were not known at the time of this study and their effect is suspected to be minimal.

Using their previously developed model, Fulton et al. (2015) (Fulton et al., 2015) failed to model the trough created by Big Hollow although this failure is attributable to the size of the individual grid blocks at 656 $\times$ 656 ft. Unlike our model, the Fulton model also modeled a significantly larger region than the extent of our modeled land, and as a result had a higher margin of error. The model previously developed by Chin (1996) (Chin, 1996) followed the shape of the interpreted water table map more closely although that is likely due to the difference in how hydraulic conductivity was mapped within the model. That model was created using zones of hydraulic conductivity that took over 150 model iterations to perfect.

Well drillers logs for the 13 continuously monitored wells were not available for this study for use in analyzing the depths at which the screens were installed and where previous nitrate samples were taken from each. As such, our partial understanding of the transport relationship to each well from the karst system and the concentration that actually migrates past 120 cm in depth prevents a precise match of our scenario results with the actual results.

Although the actual calculated concentrations varied, the nitrate trajectories for the 2015 model were similar to that of the measured data obtained through groundwater well monitoring. Nitrate concentrations within wells P3, P4, P5, W1, W2, W3, W7, and G10 were within 3.6 ppm (the level of background nitrate for the Spring Creek watershed) of the actual concentrations from 2015 while the concentrations of wells P1, P2, W5, W6, and G12 were simulated within 7.2 ppm of the actual concentrations (Figures 18 and 19). Although likely due in some part to the lack of differentiation between the agronomic uptake of nitrate based on different plant species near each well, the main contribution to the simulation errors is likely from the unpredictable transport properties of karst pathways. One such example is well P1 which is the closest to Big Hollow. Note that although the hydraulic heads in the Living Filter wells have consistently dropped over the past 10 years, the head in P1 has not. The well logs of P1 show that it is located within solution conduit which likely suppresses hydraulic head in

the well due to its assumed high hydraulic conductivity, which has varied little despite changes in irrigation rates (Lattman and Parizek, 1964).

Nitrate concentrations have been known to vary by season in this region based on nitrate observed in Spring Creek, the concentrations of which near Milesburg between 1999 and 2013 show a median fluctuation between winter and fall seasons of 0.4 ppm (*Monitoring Nitrate in the Spring Creek Watershed*, 2013). The background nitrate concentrations near corn fields in the Spruce Creek basin have an average concentration of 6.0 ppm so the values currently observed at the Living Filter appear to be within reason (Swistock, 2016). The basin wide nitrate averages of 3.6 ppm are prevalent in the Spring Creek basin while the average nitrate concentrations for agricultural fields are 5.1 ppm pre-flow and 5.2 ppm post-flow from rainfall events (Buda and Dewalle, 2009). The nitrate values within the Living Filter as of 2015 did not exceed 8 ppm in the 13 wells that are continuously monitored within the site (Figure 20).

Nitrate concentrations for the extended model through 2035 are very similar to that of the concentrations in the 2015 version of the model (Figures 21 and 22). This scenario largely demonstrates that if the total nitrogen contribution to the aquifer remains at the 10 ppm Class A wastewater threshold, then the concentrations within the groundwater should closely reflect current values, assuming no significant change in the volumetric rate of the effluent application (Figure 23).

The lack of screened elevations for each monitoring well necessitated including a degree of uncertainty in the model. Without assigning a screen elevation to the wells MODFLOW automatically assumes that the wells are set to intersect the top of the water table. In the event that these are deep screened wells or the wells are set within fractures with confined head, an accurate nitrate concentration might be skewed in that although the well reflects the true potentiometric head, the water from within the well may be at a much deeper level. As nitrate is considered a conservative tracer and flows without hinderance in groundwater, it is possible that nitrate concentrations would be higher closest to the potentiometric surface as the horizontal velocity of the flow transports more nitrate than does the vertical. This difference in velocity is also evident within cross-sections of the model in which the nitrate concentration reduces significantly with depth (Figures 24 and 25).

It is likely that our simulation of nitrate contribution from the Living Filter is a highly generalized scenario due to the unpredictably of future mass loading from nitrate concentration and the volume of effluent. The highly altered nature of the bedrock underlying the Living Filter makes it difficult to establish the location of the preferential pathways created by solution voids. One method of utilizing wells in the region of Living Filter to represent one form of high conductivity pathways entails installing wells within single and double fracture traces. Wells located on fracture traces are 40-100 times

more hydraulically productive in this region and can approximate the aquifers response rate to external factors. Fractures are denoted on the surface via dark lineaments and have been heavily mapped in the region of the Living Filter (Matzke, 1961; Lattman, 1958; Parizek, R.R., Siddiqui, 1970; Siddiqui and Parizek). All monitoring wells within the site are located along fracture traces or at fracture trace intersections indicating that each well is a true characterization of the water table elevation.

Only one tracer test was evident near the site where a tracer dye was introduced to well F-2 which is nearly 1000 feet from pumping well U-14. Pumping well U-14 was subsequently pumped at a rate of 370 GPM for 10 days without any observance of the tracer from F-2. The well logs of F-2 show that F-2 intercepts several sand filled solution conduits that contribute to the phenomena of “flowing sand” (Lattman and Parizek, 1964; Parizek et al., 1967; Wood, 1980). It is possible that the presence of sand and silt in the solution conduits can reduce the hydraulic conductivity and restrict groundwater movement. The presence of flowing sand as a result of suffusion of soil through fracture traces is also possible given that it is ubiquitous along fracture traces (Lattman and Parizek, 1964). Another possible explanation for the presence of flowing sand is the dissolution of the cement holding the sand and silt sized particles in the Gatesburg formation. If the movement of water is enough to dissolve the cement but not enough to transport the sand and silt, then it is possible for downward settling and infilling of solution cavities to occur (Caruccio, 1963).

5. Conclusion

Wastewater irrigation is a viable alternative to wastewater discharges to streams in that it recharges the underlying aquifer from which the original water was withdrawn. The sensitivity of the aquifer makes it urgent to understand the effects of wastewater reuse upon the water table in a karstic environment, particularly as contaminant transport occurs within fractures and solution conduits. Accurate estimates of nitrogen loadings in soils and nitrate leaching to groundwater is essential for developing models to predict the fate and transport of nitrate in groundwater to assess public health risk and impacts on ecosystems, and develop sustainable irrigation practices with treated wastewater. In this study, a framework was developed to model the effect of treated wastewater and the use of large volumes of that water in agricultural irrigation/forest use and to determine groundwater nitrate contamination in a karst landscape of the Spring Creek Watershed, in central Pennsylvania. MODFLOW and MT3DMS models used to simulate groundwater flow and contaminant transport in the aquifer were in agreement with previous models. The 13 wells within the extent of the Living Filter model had a combined RMSE of 6.03 feet while the RMSE for the entire model was 24.76 feet. Although nitrate concentrations in groundwater were highly variable across the watershed and seasons, they were correlated to agriculture activities, i.e., irrigation with treated wastewater. The 2015 model for nitrate compared reasonably well with measured nitrate concentration in groundwater wells, with differences between

observed and modeled nitrate concentrations in the aquifer attributed to the heterogeneity of the subsurface environment due to the unpredictable karst terrain with high conductivity solution conduits present leading to non-uniform flow and nitrate transport. Although a reduction in the mounding of the water table was evident given the decline in flows by more than half of that previously, wastewater irrigation is a major contributor to the nitrate dynamics of the aquifer. Nitrate concentrations were further simulated for the year 2035 under a specific land use scenario, which was of nitrogen fertilizer application and irrigation with treated wastewater. These 2035 modeled nitrate concentrations were similar that of the 2015 model, demonstrating that if total nitrogen contribution to the aquifer remains at the 10 ppm Class A wastewater threshold, then the concentrations within the groundwater should closely reflect current values, assuming no significant change in the volumetric rate of the effluent application.

Results of the 2035 model also demonstrated the sustainability of irrigation practices of agriculture and forestry land uses with treated wastewater for the Living Filter site and ultimately for the Spring Creek Watershed, central Pennsylvania. The qualitative and quantitative data on the sustainability of wastewater reuse derived here is also of use to local government and policy makers in formulating long-term management and sustainable development land use plans via the use of treated wastewater for irrigation to optimize agricultural management practices and reduce groundwater contamination

from nitrate. The modeling framework developed here to simulate the spatial and temporal variability of nitrate concentrations, is applicable to similar aquifers in a karst watershed system, characterized by high permeability materials and high conductivity solution conduits, in which water resources are vulnerable to agricultural activities.

Acknowledgements

We wish to convey our appreciation to Clemson University and the Pennsylvania State University for supporting this research.

References

Aschebrook-Kilfoy, B., Heltshe, S.L., Nuckols, J.R., Sabra, M.M., Shuldiner, A.R., Mitchell, B.D., Airola, M., Holford, T.R., Zhang, Y., and Ward, M.H., 2012, Modeled nitrate levels in well water supplies and prevalence of abnormal thyroid conditions among the Old Order Amish in Pennsylvania.: *Environmental health : a global access science source*, v. 11, p. 6.

Barnes, D., and Bliss, P.J. (Peter J., 1983, Biological control of nitrogen in wastewater treatment: E. & F.N. Spon.

Barnes, C.J., Jacobson, G., and Smith, G.D., 1992, The origin of high-nitrate ground waters in the Australian arid zone: *Journal of Hydrology*, v. 137, no. 1–4, p. 181–197.

Becher, A.E., 1996, GROUND-WATER RESOURCES OF CAMBRIAN AND ORDOVICIAN CARBONATE ROCKS IN THE VALLEY AND RIDGE PHYSIOGRAPHIC PROVINCE OF PENNSYLVANIA PENNSYLVANIA DEPARTMENT OF ENVIRONMENTAL PROTECTION, BUREAU OF TOPOGRAPHIC AND GEOLOGIC SURVEY:

Benjamin, N., O'Driscoll, F., Dougall, H., Duncan, C., Smith, L., Golden, M., and McKenzie, H., 1994, Stomach NO synthesis: *Nature*, v. 368, no. 6471, p. 502–502.

Brachet, F., 2004, Regional groundwater modeling for source area delineation and recharge estimation: The Pennsylvania State University.

Buda, A.R., and Dewalle, D.R., 2009, Dynamics of stream nitrate sources and flow pathways during stormflows on urban, forest and agricultural watersheds in central Pennsylvania, USA: v. 23, p. 3292–3305.

Caruccio, F.T., 1963, The Hydrogeology of the Sewage Disposal Experiment Area, Northwest of State College, Pennsylvania: Pennsylvania State University.

Chin, C.-V., 1996, Application and comparison of EPA wellhead protection delineation methods for karst aquifers, Centre County, Pennsylvania:

Dayanthi, W.K.C.N., Shigematsu, T., Tanaka, H., Yamashita, N., Kato, K., and de Silva, V., 2006, Utilization of Reclaimed Wastewater for Irrigation and Urban Activities in Okinawa Island, Japan: *Proceedings of the Water Environment Federation*, v. 2006, no. 12, p. 981–1005.

Dudley, N., 1990, Nitrates: the threat to food and water.: *Nitrates: the threat to food and water.*,.

EPA, 2012, 2012 Guidelines for Water Reuse.:

EPA, 2004, Primer for Municipal Wastewater Treatment Systems.:

Faillat, J.P., and Rambaud, A., 1991, Deforestation and leaching of nitrogen as nitrates into underground water in intertropical zones: The example of Côte d'Ivoire: *Environmental Geology and Water Sciences*, v. 17, no. 2, p. 133–140.

Fan, A.M., and Steinberg, V.E., 1996, Health Implications of Nitrate and Nitrite in Drinking Water: An Update on Methemoglobinemia Occurrence and Reproductive and Developmental Toxicity: *Regulatory Toxicology and Pharmacology*, v. 23, no. 1, p. 35–43.

Fulton, J.W., Risser, D.W., Regan, R.S., Walker, J.F., Hunt, R.J., Niswonger, R.G., Hoffman, S.A., and Markstrom, S.L., 2015, Water-Budget and Recharge-Area Simulations for Spring Creek and Nittany Creek Basins and Parts of the Spruce Creek Basin, Centre and Huntingdon.:

Gannett Flemming, I., 2008, Technical memorandum ground- water flow model results proposed Grove Quarry, Marion and Spring Townships, Centre County, Pennsylvania: Yardley, Pa.:

Gatseva, P.D., and Argirova, M.D., 2008, High-nitrate levels in drinking water may be a risk factor for thyroid dysfunction in children and pregnant women living in rural Bulgarian areas: *International Journal of Hygiene and Environmental Health*, v. 211, no. 5–6, p. 555–559.

Gelhar, L.W., Welty, C., and Rehfeldt, K.R., 1992, A Critical Review of Data on Field-Scale Dispersin in Aquifers: *Water Resources Research*, v. 28, no. 7, p. 1955–1974.

Haller, L., McCarthy, P., O'Brien, T., Riehle, J., and Stuhldreher, T., 2013, NITRATE POLLUTION OF GROUNDWATER.:

Hamilton, A.J., Stagnitti, F., Xiong, X., Kreidl, S.L., Benke, K.K., and Maher, P., 2007, Wastewater Irrigation: The State of Play: *Vadose Zone Journal*, v. 6, no. 4, p. 823.

Hook, J.E., and Kardos, L.T., 1978, Nitrate Leaching During Long-term Spray Irrigation for Treatment of Secondary Sewage Effluent on Woodland Sites1: *Journal of Environment Quality*, v. 7, no. 1, p. 30.

Jaramillo, M.F., and Restrepo, I., 2017, Wastewater reuse in agriculture: A review about its limitations and benefits: *Sustainability (Switzerland)*, v. 9, no. 10.

Johnson, J., 2010, Framework to Effectively Quantify and Communicate Groundwater Model Uncertainty to Management and Clients.:

Landon, R.A., 1963, The Geology of the Gatesburg Formation in the Bellefonte Quadrangle,

Pennsylvania, and its Relationship to the General Occurence and Movement of Groundwater: Pennsylvania State University.

Lattman, L.H., 1958, Technique of mapping geologic fracture traces and lineaments on aerial photographs.: *Photogrammetric Engr.*, v. v. 19 no., p. 568–576.

Lattman, L.H., and Parizek, R.R., 1964, Relationship Between Fracture Traces and The Occurence of Ground Water in Carbonate Rocks: *Journal of Hydrology*, v. 2, p. 73–91.

Lindsey, B.D., Loper, C.A., and Hainly, R.A., 1997, NATIONAL WATER-QUALITY ASSESSMENT PROGRAM NITRATE IN GROUND WATER AND STREAM BASE FLOW IN THE LOWER SUSQUEHANNA RIVER BASIN, PENNSYLVANIA AND MARYLAND:

Lundberg, J.O., Feelisch, M., Björne, H., Jansson, E.Å., and Weitzberg, E., 2006, Cardioprotective effects of vegetables: Is nitrate the answer? *Nitric Oxide*, v. 15, no. 4, p. 359–362.

Martinez, C.J., and Clark, M.W., 2015, Reclaimed Water and Florida's Water Reuse Program 1:

Matzke, R.H., 1961, Fracture Trace and Joint Patterns in Western Centre County, Pennsylvania: Pennsylvania State University.

Mau, D.P., and Winter, T.C., 1997, Estimating ground-water recharge from streamflow hydrographs for a small mountain watershed in a temperate humid climate, New Hampshire, United States: *Ground Water*, v. 35, no. 2, p. 291–304.

Miller, G.W., 2005, Integrated concepts in water reuse: managing global water needs: *Desalination G.W. Miller / Desalination*, v. 187, no. 187, p. 14–17.

Monitoring Nitrate in the Spring Creek Watershed, 2013,.

Niswonger, R.G., Panday, S., and Ibaraki, M., 2011, MODFLOW-NWT, A Newton Formulation for MODFLOW-2005.:

Parizek, R.R., Filley, T.H., 1982, Definitions of Aquifers and Confining Beds Within the Centre Region, Centre County, Pennsylvania: , p. 0–1.

Parizek, R.R., Siddiqui, S.H., 1970, Determining the Sustained Yields of Wells in Carbonate and Fractured Aquifers:

Parizek, R., Kardos, L., Sopper, W., Myers, E., Davis, D., Farrell, M., and Nesbitt, J., 1967, The Pennsylvania State University Studies NO. 23: Waste Water Renovation and Conservation: , no. 23.

Pennypacker, S.P., Sopper, W.E., and Kardos, L.T., 1967, Renovation of Wastewater Effluent by

Irrigation of Forest Land: *Source Journal (Water Pollution Control Federation)*, v. 39, no. 2, p. 285–296.

Rumbaugh, J.O., and Rumbaugh, D.B., 2017, Guide to Using Groundwater Vistas: , p. 435.

Sendagi, S.M., Herschel, S., and Elliott, A., 2017, Atmospheric nitrogen loss factor (f) used in determining nitrogen-based municipal wastewater effluent irrigation rates: design and nitrogen-balance estimated f values: *Nutrient Cycling in Agroecosystems*, v. 109, no. 2, p. 181–191.

Siddiqui, --I, and Parizek, R.R. Hydrogeologic Factors Influencing Well Yields in Folded and Faulted Carbonate Rocks in Central Pennsylvania:

Smith, R.E., 1966, Petrographic properties influencing porosity and permeability in the carbonate-quartz system as represented by the Gatesburg Formation: Pennsylvania State University.

Smith, G.D., Wetselaar, R., Fox, J.J., van de Graaff, R.H.M., Moeljohardjo, D., Sarwono, J., Wiranto, Asj'ari, S.R., Tjojudo, S., and Basuki, 1999, The origin and distribution of nitrate in groundwater from village wells in Kotagede, Yogyakarta, Indonesia: *Hydrogeology Journal*, v. 7, no. 6, p. 576–589.

Swistock, B., 2016, Nitrate in Private Water Supplies.:

Tang, C., Chen, J., Shindo, S., Sakura, Y., Zhang, W., and Shen, Y., 2004, Assessment of groundwater contamination by nitrates associated with wastewater irrigation: A case study in Shijiazhuang region, China: *Hydrological Processes*, v. 18, no. 12, p. 2303–2312.

Taylor, L.E., 1997, Water Budget for the Spring Creek Basin: , no. 184.

Thornthwaite, C.W., and Mather, J.R., 1957, Instructions and Tables for Computing Potential Evapotranspiration and Water Balance.: *Publ.Climatol*, v. 10, p. 185–311.

Toze, S., 2006, Reuse of effluent water—benefits and risks: *Agricultural Water Management*, v. 80, no. 1–3, p. 147–159.

US EPA, O. National Primary Drinking Water Regulations:

Waltman, W.J., Ciolkosz, E.J., Mausbach, M.J., Svoboda, M.D., Miller, D.A., Kolb, Philip J, Mausbach Is Director, M.J., and Kolb, Phlip J, 1997, Soil Climate Regimes of Pennsylvania: , no. 873.

White, P., Ruble, C.L., and Lane, M.E., 2013, The effect of changes in land use on nitrate

concentration in water supply wells in southern Chester County, Pennsylvania: *Environmental Monitoring and Assessment*, v. 185, no. 1, p. 643–651.

Wood, C.R., 1980, Summary Ground-Water Resources of Centre County, Pennsylvania:

Zheng, C., Zheng, C., Wang, P.P., Zheng, C., and Wang, P.P., 1999, MT3DMS: A modular three-dimensional multi-species transport model for simulation of advection, dispersion, and chemical reactions of contaminants in ground-water systems. Documentation and user's guide: *CONTRACT REPORT SERDP-99-1, U.S. ARMY ENGINEER RESEARCH AND DEVELOPMENT*,.

Figures

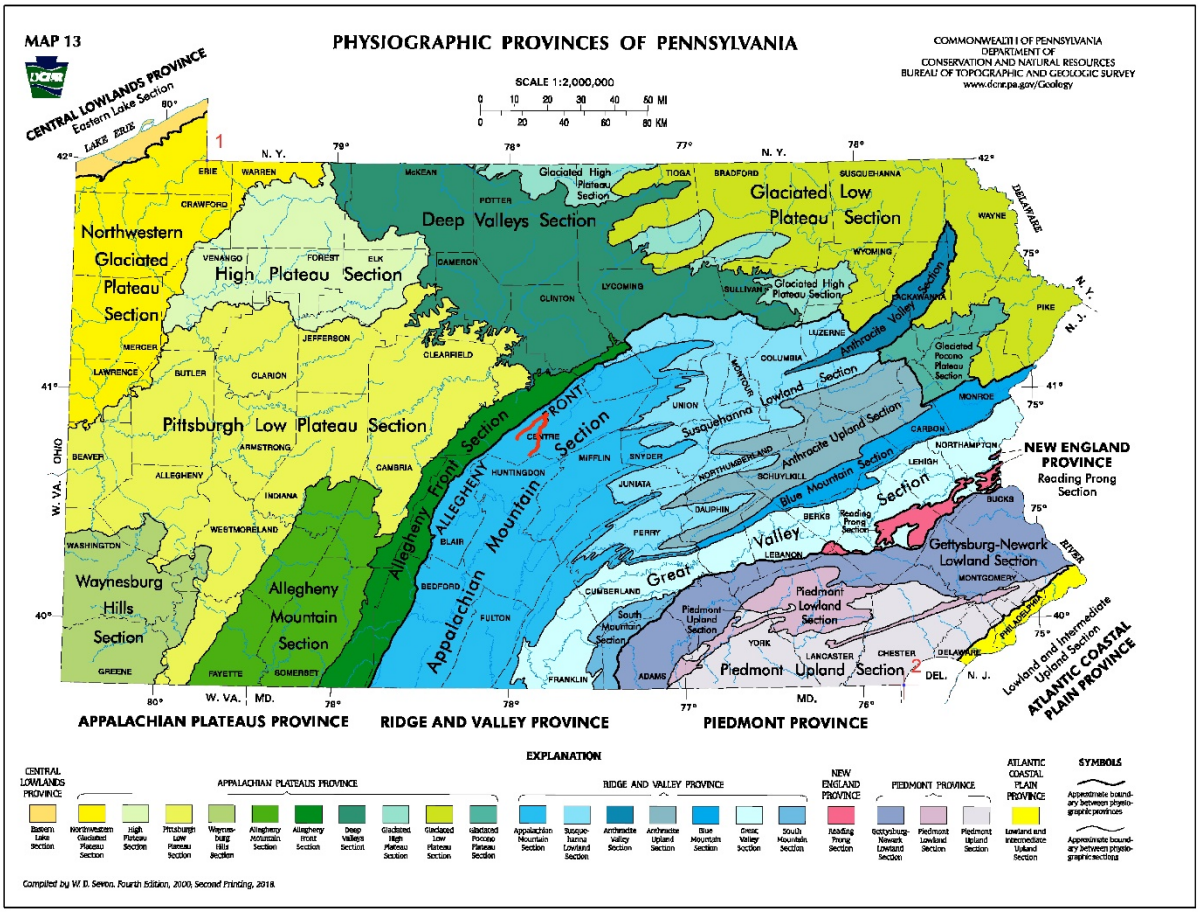

Figure 1. Focus area shown in red in relation to physiographic provinces of Pennsylvania. Adapted from W.D. Sevon. Fourth Edition, 2000.

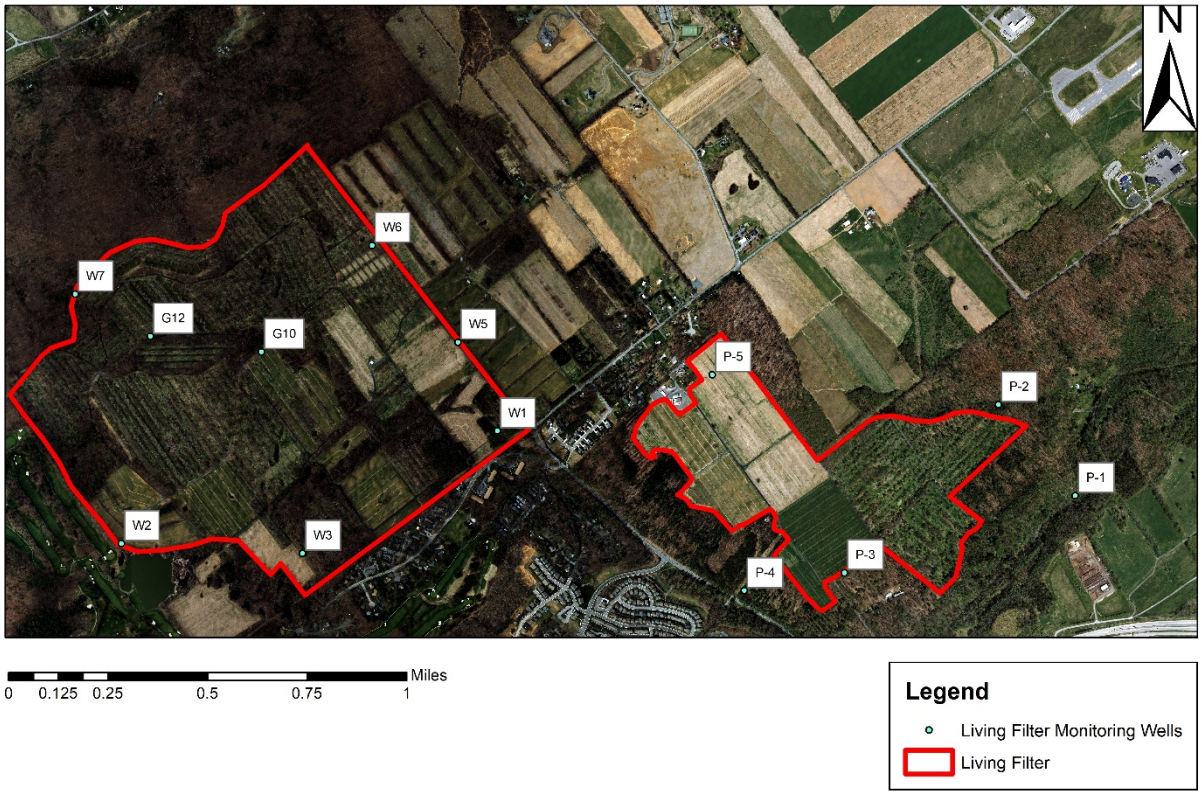

Figure 2. Living Filter outline and well locations overlain on 2017 areal imagery.

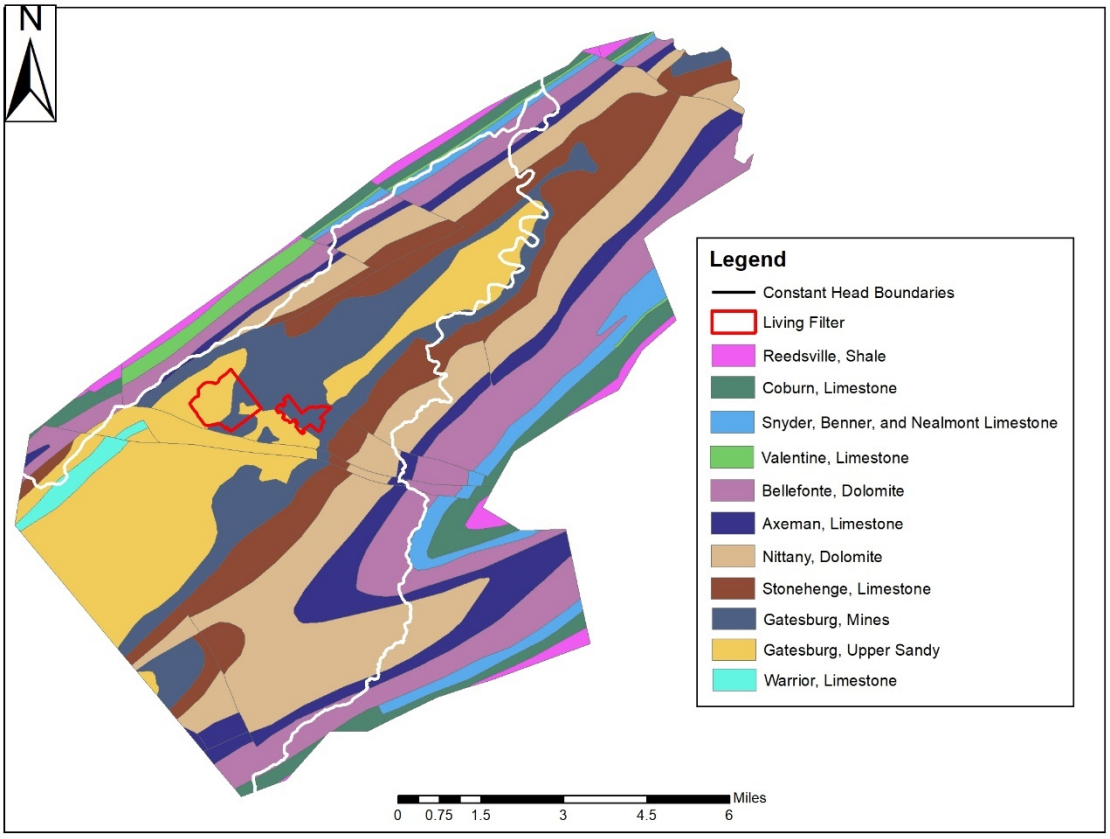

Figure 3. Geology of modeled area with outlines of the Focus Area and Living Filter.

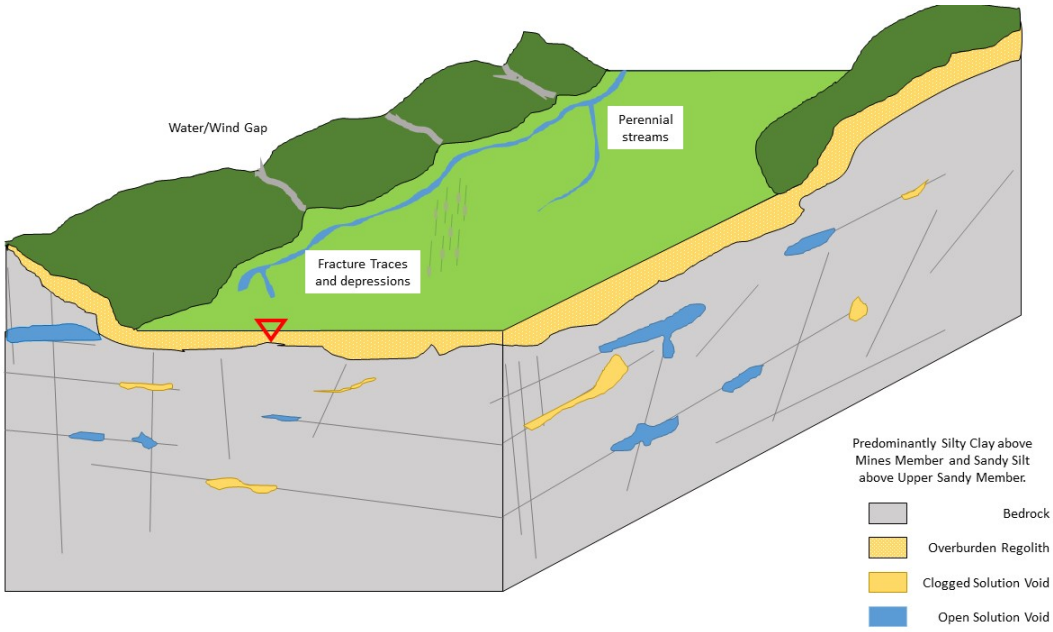

Figure 4. Conceptual model of the Spring Creek Watershed.

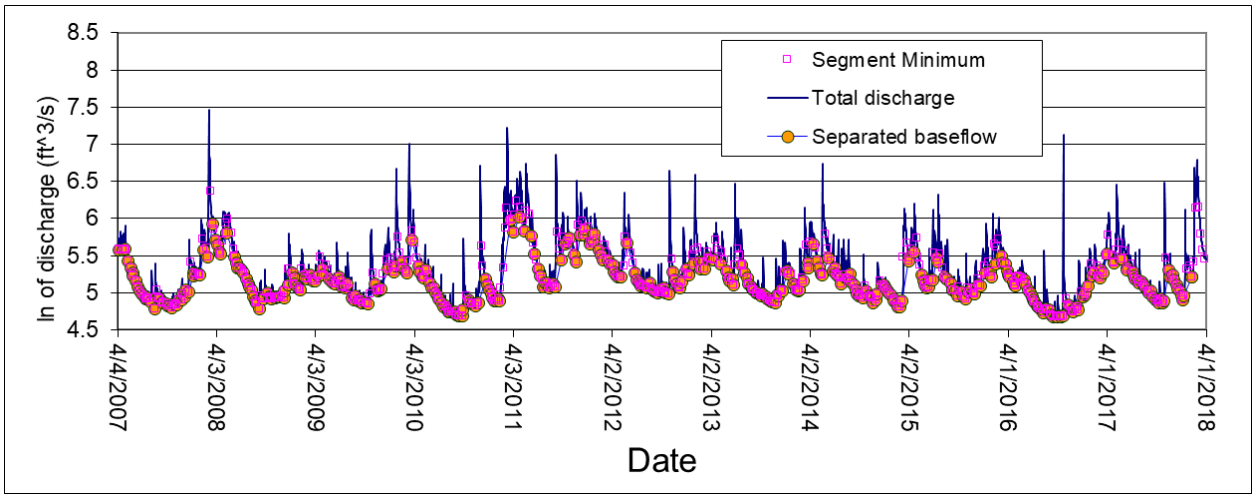

Figure 5. Natural log of stream flow (cfs) with separated baseflow and segment minimums according to Mau and Winter. Baseflow is separated using several factors ranging from watershed area, stream flow, average precipitation data, and the slope of the average baseflow recession.

System	Geologic Unit	Estimated Thickness	Composition	Aquifer Type
Ordovician	**Reedsville Formation**	900-1400	Shale; somewhat calcaroues near base; sandy near top	Fracture dominated siliciclastic
	Coburn Formation	300	Thin bedded limestone with some shale interbeds	Conduit dominated carbonate
	Salona Formation	180-300	Thin bedded limestone with shale partings	Conduit dominated carbonate
	Nealmont Formation	70	Thin to thick impure limestone	Conduit dominated carbonate
	Benner Formation	150	Dark-gray laminated, thick to thin bedded limestone	Conduit dominated carbonate
	Valentine Member		Dark-gray laminated, thick to thin bedded limestone	Conduit dominated carbonate
	Snyder Formation	80	Medium bedded limestone and dolomite	Conduit dominated carbonate
	Hatter Formation	75	Medium bedded limestone and laminated, argillaceous and arenaceous dolomite	Conduit dominated carbonate
	Loysburg Formation	50-450	Laminated, medium to thin bedded limestone and dolomite	Conduit dominated carbonate

	Belefonte Formation	1400	Light gray, thick bedded dolomite; some chert; sandstone bed in upper part	Fracture dominated carbonate
	Axemann Formation	400-700	Blue, thin bedded limestone; some dolomite layers	Conduit dominated carbonate
	Nittany Formation	1200	Blue, thick bedded, coarsely crystalline dolomite	Fracture dominated carbonate
	Stonehenge Formation	250-600	Blue, thin bedded limestone; some dolomite	Conduit dominated carbonate
Cambrian	**Gatesburg Formation**	1800		Conduit dominated carbonate
	Mines Member		Dark gray, coarse grained dolomite and subordinate light gray fine grained dolomite; abundant oolitic chert	Fracture dominated carbonate
	Upper Sandy Member		Dolomite and interbedded orthoquartzite and sandy dolomite	Diffuse flow dominated carbonate
	Ore Hill Member		Dark gray dolomite	Diffuse flow dominated carbonate
	Lower Sandy Member		Dolomite and interbedded orthoquartzite and sandy dolomite	Diffuse flow dominated carbonate
	Warrior Formation	1300	Blue, impure limestone and dolomite; thin sandy partings	Fracture dominated carbonate

Figure 6. Stratigraphy of the region and their respective conductivity's.

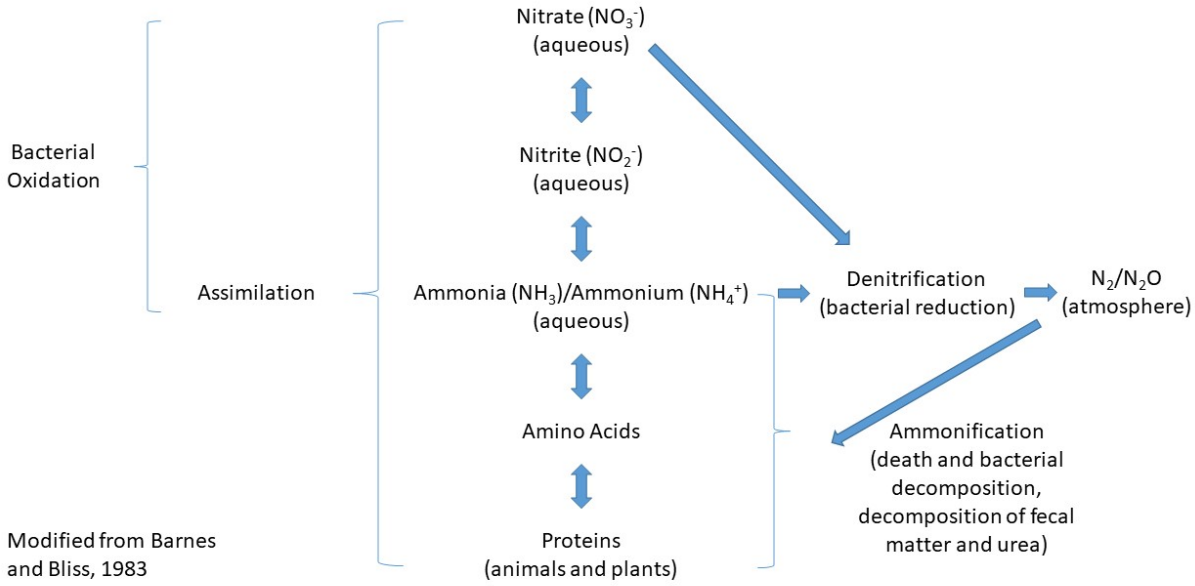

Figure 7. Nitrogen cycle in wastewater systems according to Barnes and Bliss (1983).

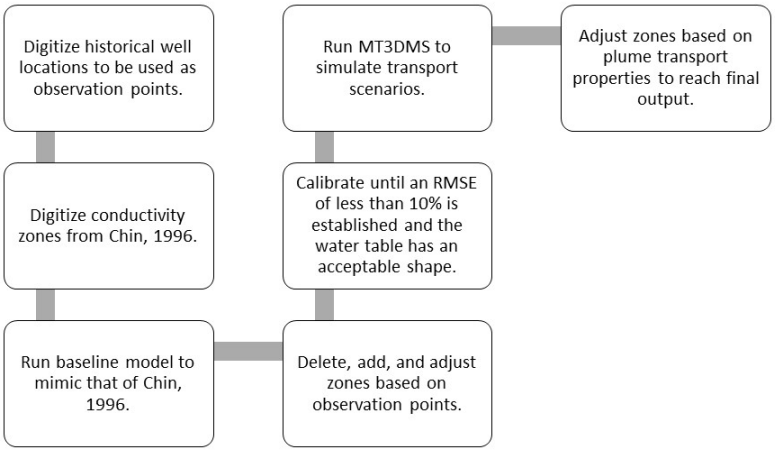

Figure 8. Model creation and calibration workflow.

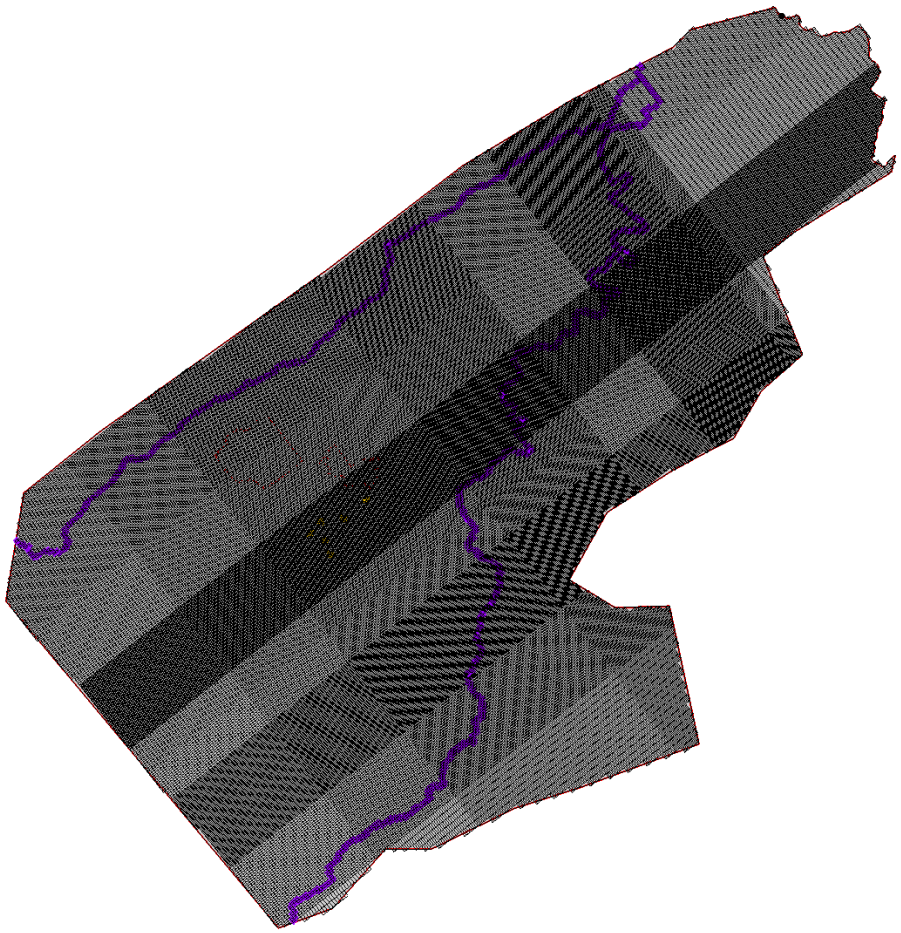

Figure 9. Activated and refined cells in model grid. A total of 1035846 cells are active in the grid.

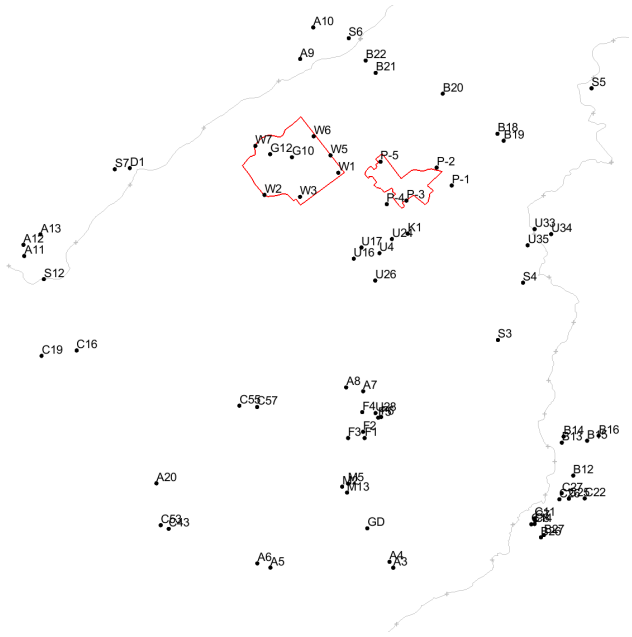

Figure 10. Locations of the 83 monitoring wells used in the study from Chin.

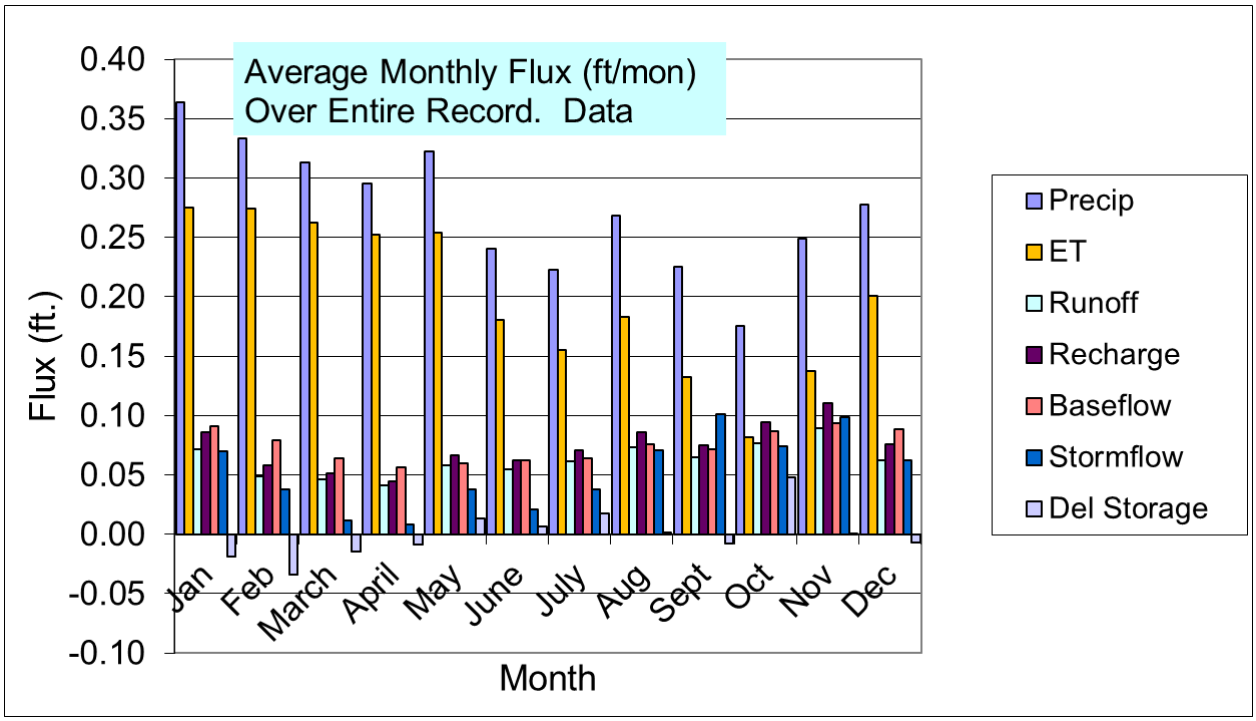

Figure 11. Water balance using the Mau and Winter, (1997) hydrograph approach.

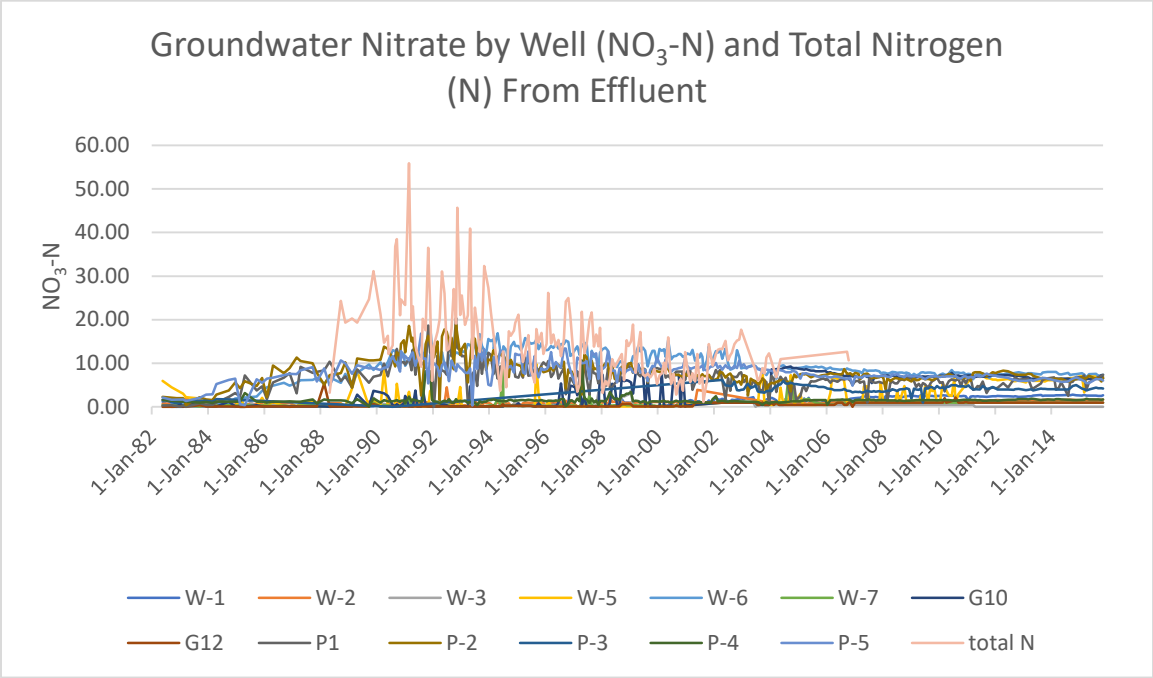

Figure 12. Nitrate concentration for each well post 1990 along with total nitrogen in wastewater effluent.

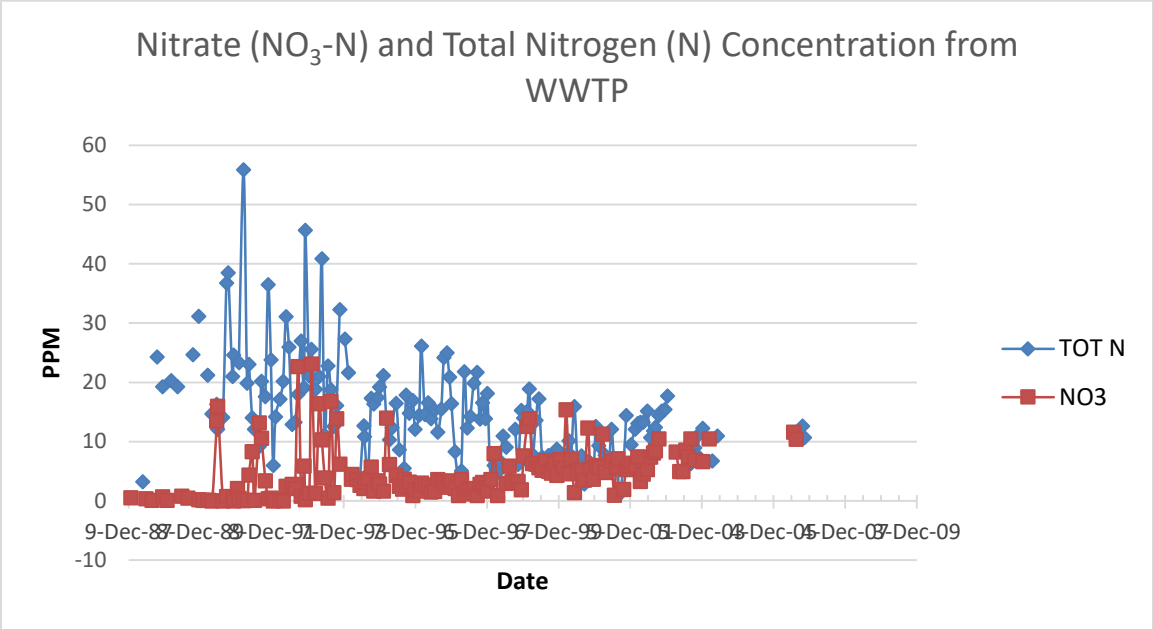

Figure 13. Total Nitrogen and nitrate in wastewater effluent. Data was only provided until 2006 from the Office of the Physical Plant (OPP) at Penn State.

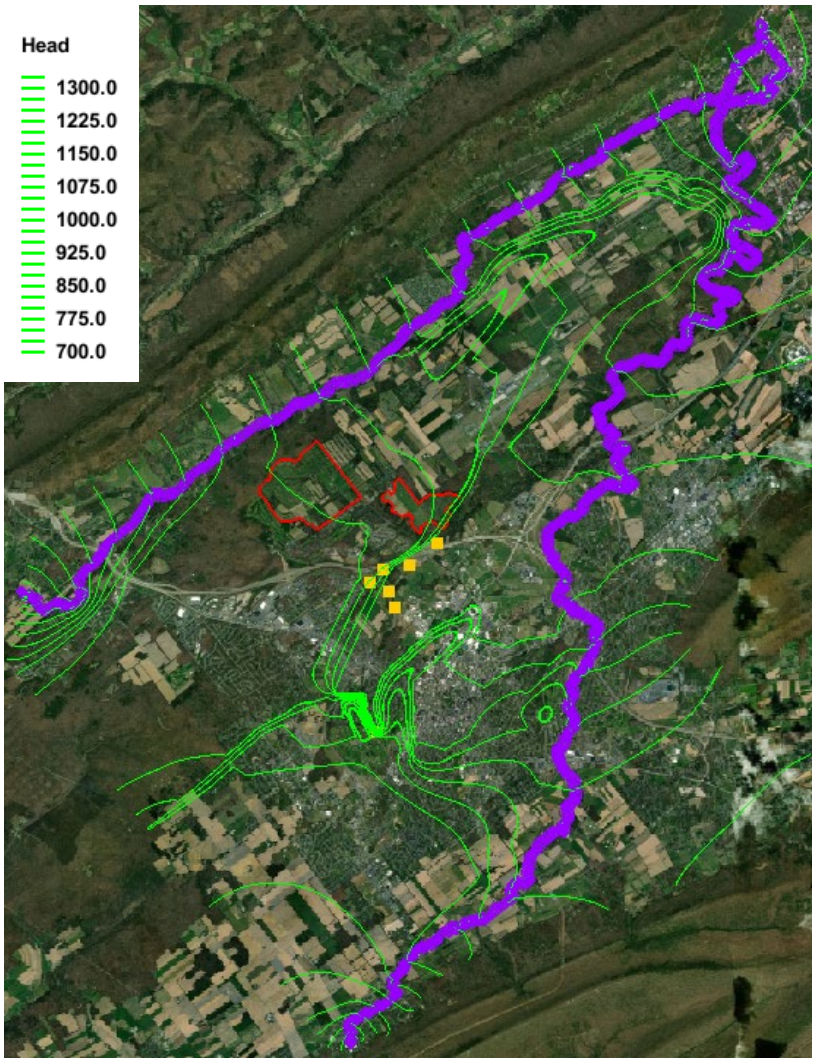

Figure 14. Groundwater 25 ft. contours for the model overlain on aerial imagery of State College.

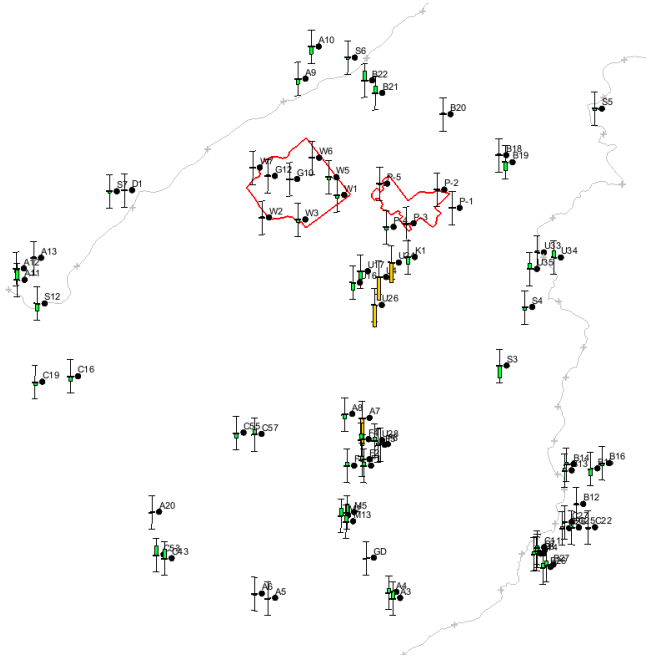

Figure 15. Corresponding observation well values for the groundwater model using a 60 ft. interval.

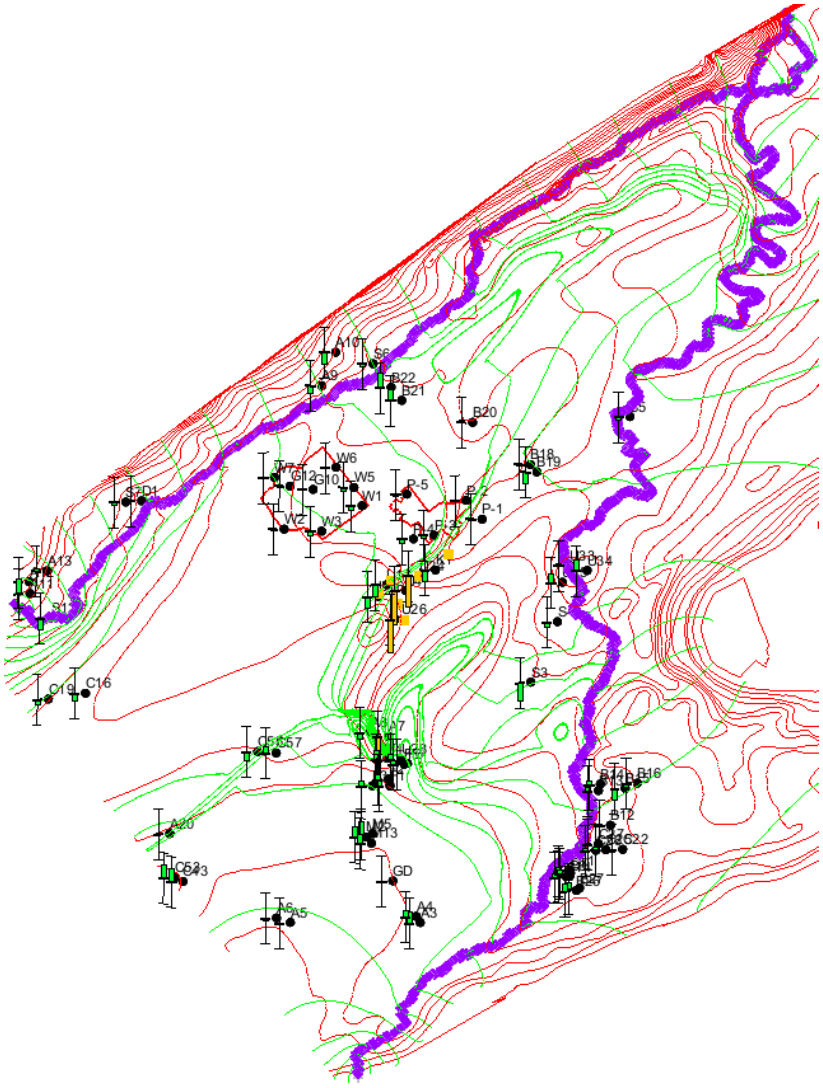

Figure 16. Taylor 1997 (red) vs modelled water levels (green). Only the area between Spring Creek, Buffalo Run, and Slab Cabin Run were calibrated due to the effects of the high relief orthoquartzite ridges.

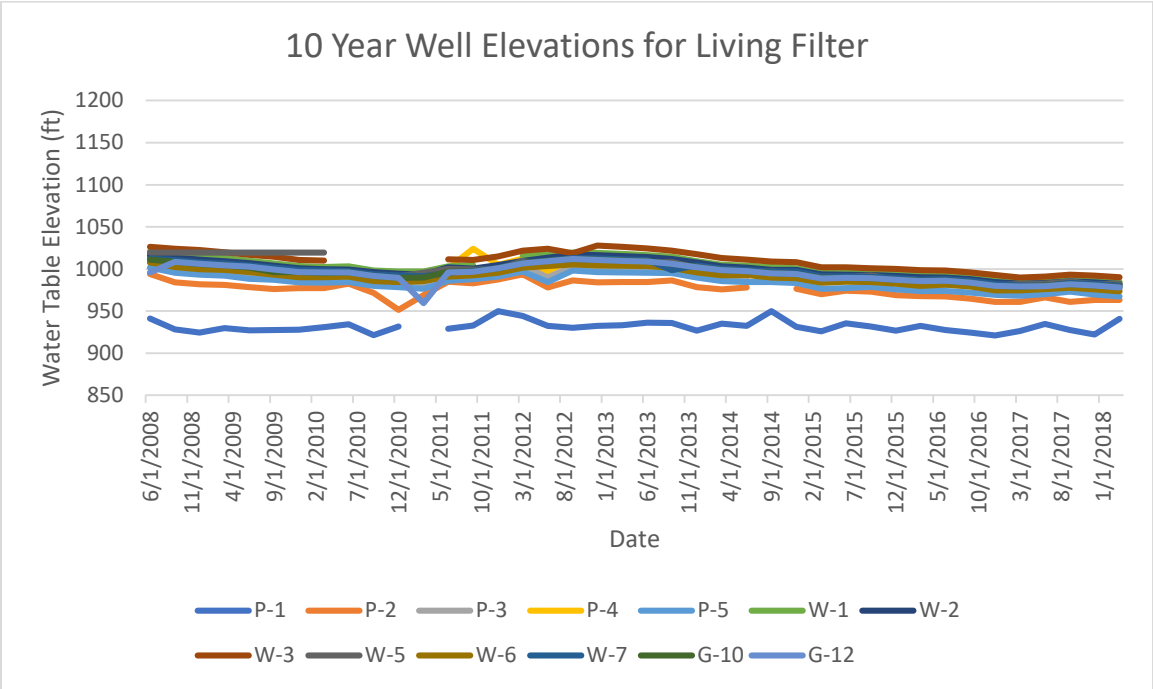

Figure 17. Water table elevations in the Living Filter Monitoring wells over the past 10 years. Overall water table elevations have decreased except for t hose in P1.

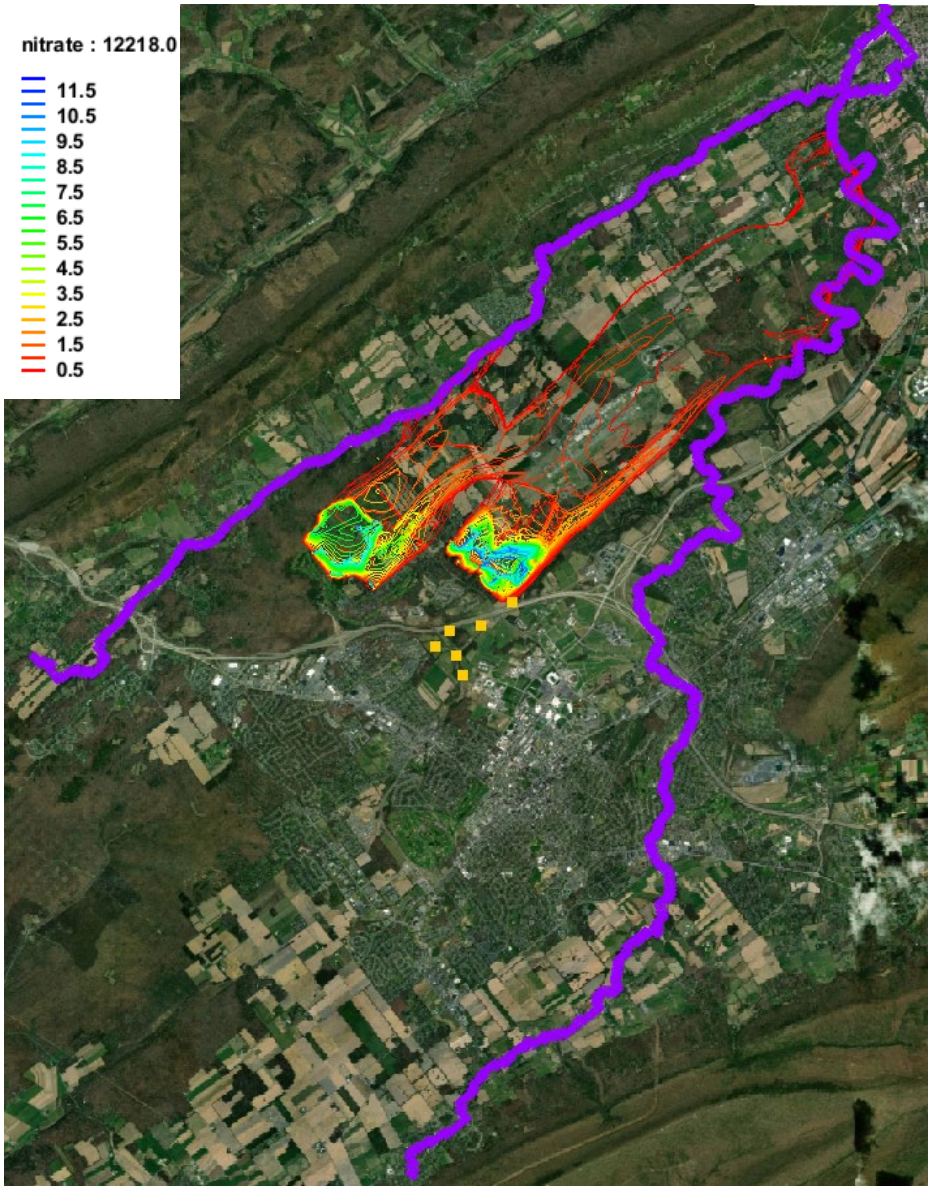

Figure 18. Modelled nitrate concentrations in 2015 after 33 years of irrigation.

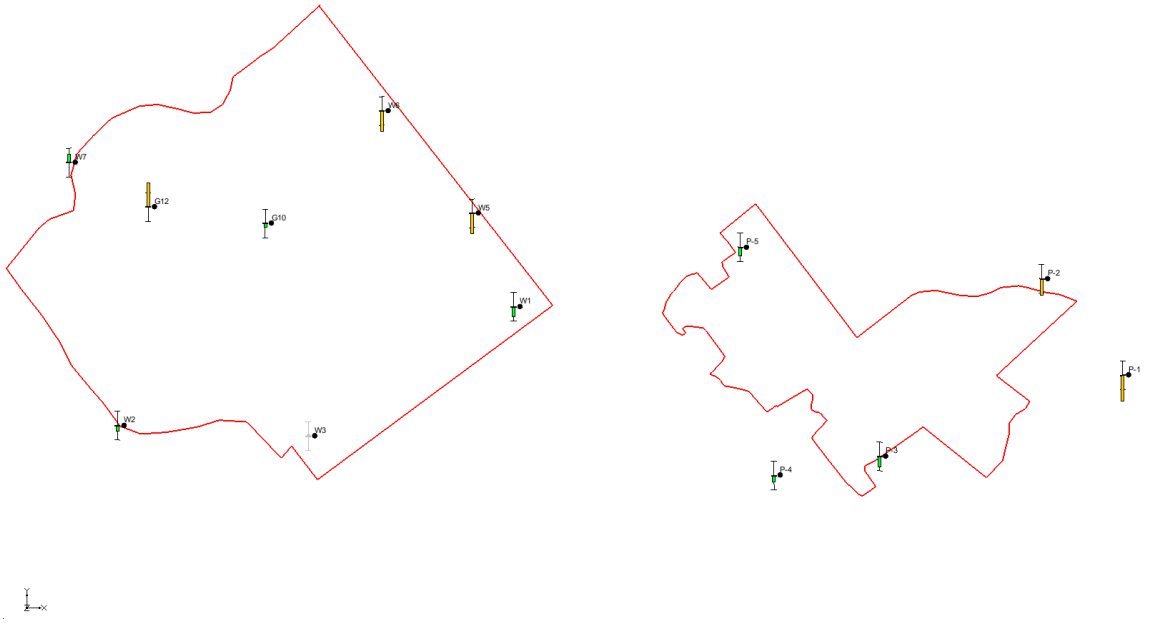

Figure 19. Observed nitrate concentrations vs. modelled for 2015. Error bars are based on a 3.6 ppm standard deviation based on the estimated background nitrate concentration in the Spring Creek watershed.

Simulated vs. Observed Nitrate Concentrations in November, 2015			
Well ID	**Average Simulated Concentration for Cell (mg/L)**	**Observed Concentration (mg/L)**	**Difference Between Simulated and Observed**
W1	0.02	2.67	-2.65
W2	0.26	1.61	-1.35
W3	0.35	-	N/A
W5	1.95	6.92	-4.97
W6	2.25	7.36	-5.11
W7	3.08	1.00	2.08
G10	5.55	6.54	-0.99
G12	7.02	1.00	6.02
P1	0.38	7.35	-6.97
P2	2.34	6.63	-4.29
P3	1.35	4.20	-2.85
P4	0.00	1.68	-1.68
P5	3.86	6.06	-2.20

Figure 20. Simulated vs. observed nitrate values for each well. Values were generally undersimulated, likely due to any lack to background nitrate in the model.

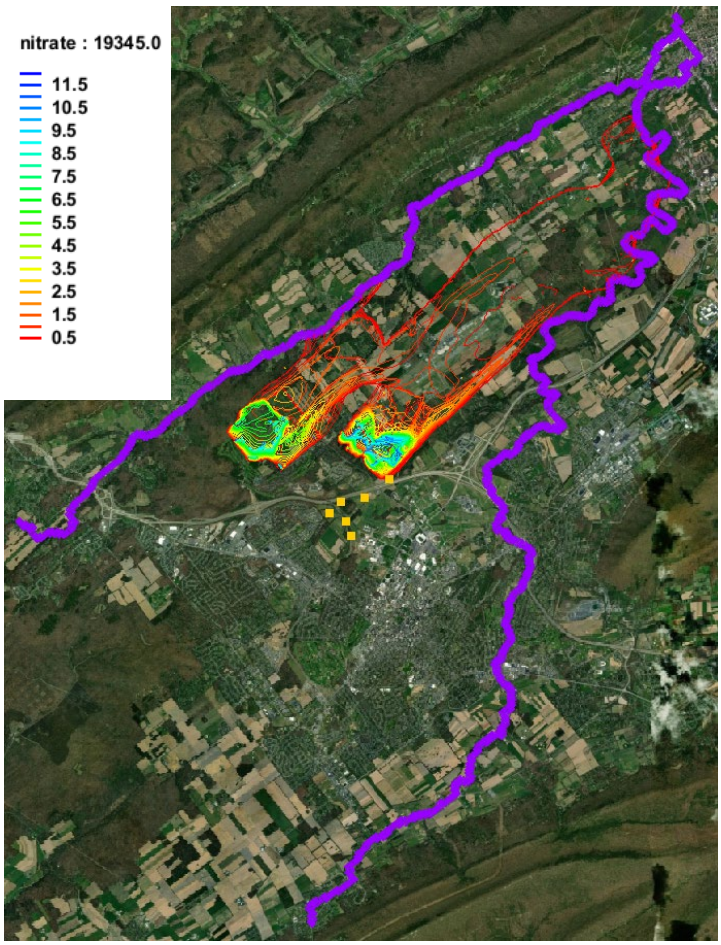

Figure 21. Modelled nitrate concentrations in 2035 after 53 years of irrigation.

Simulated vs. Observed Nitrate Concentrations in November, 2015	
Well ID	**Average Simulated Concentration for Cell (mg/L)**
W1	0.03
W2	0.03
W3	0.35
W5	1.95
W6	2.25
W7	3.08
G10	5.55
G12	7.02
P1	0.38
P2	2.36
P3	1.35
P4	0.00
P5	3.86

Figure 22. Simulated nitrate Values for each well in 2035 after 53 years of irrigation.

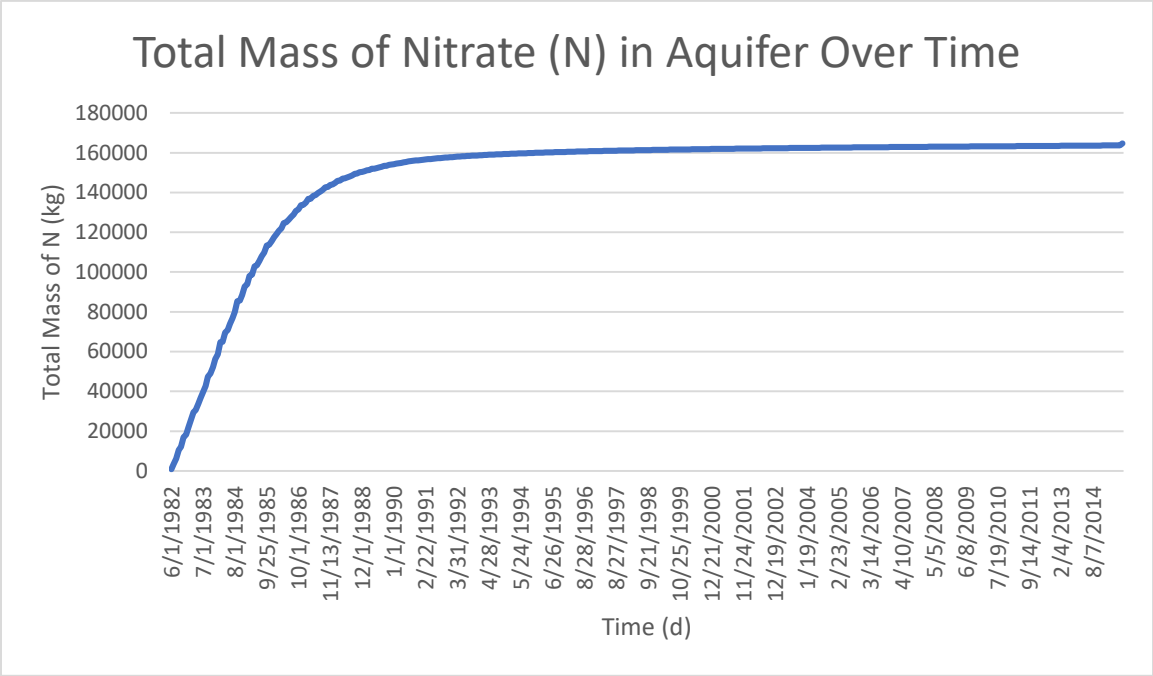

Figure 23. Total modelled mass of nitrate stored in the aquifer as a result of wastewater effluent irrigation.

a)

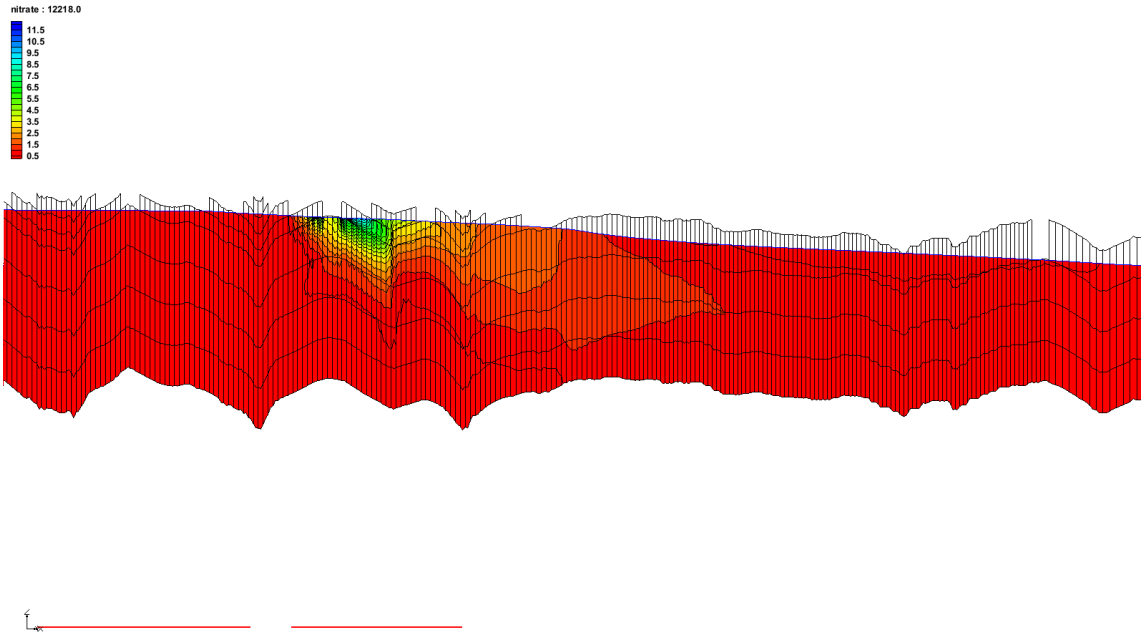

b)

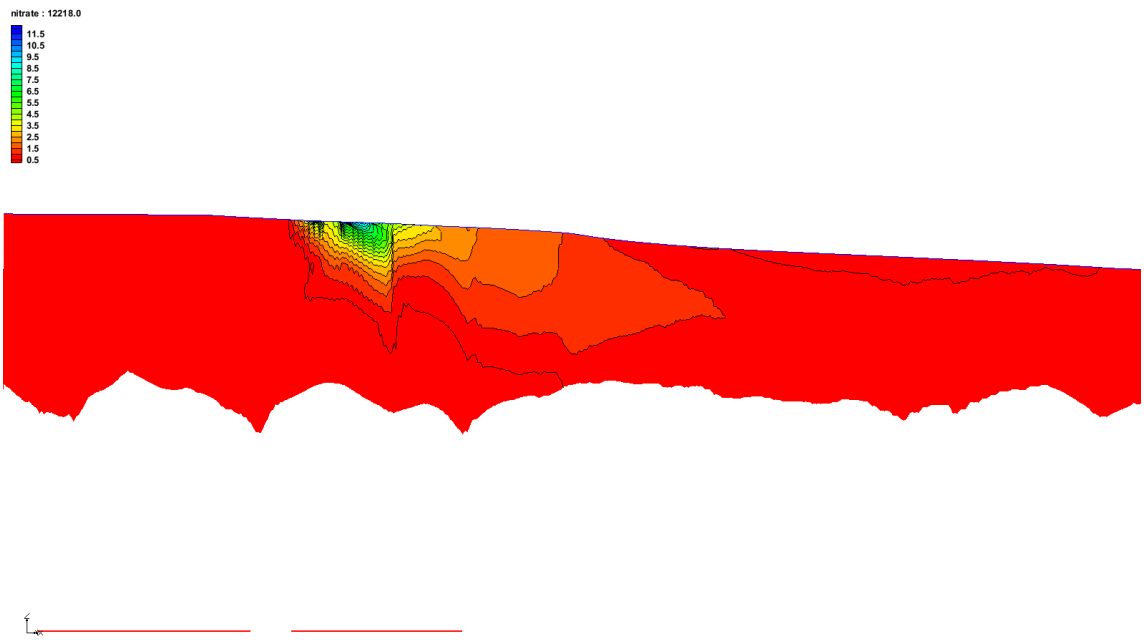

Figure 24. Nitrate concentrations in row i:115 in the year 2015.
a) Concentration including the mapped grid layers in which it is simulated.
b) Concentration without the corresponding grid layers for enhanced visibility.

a)

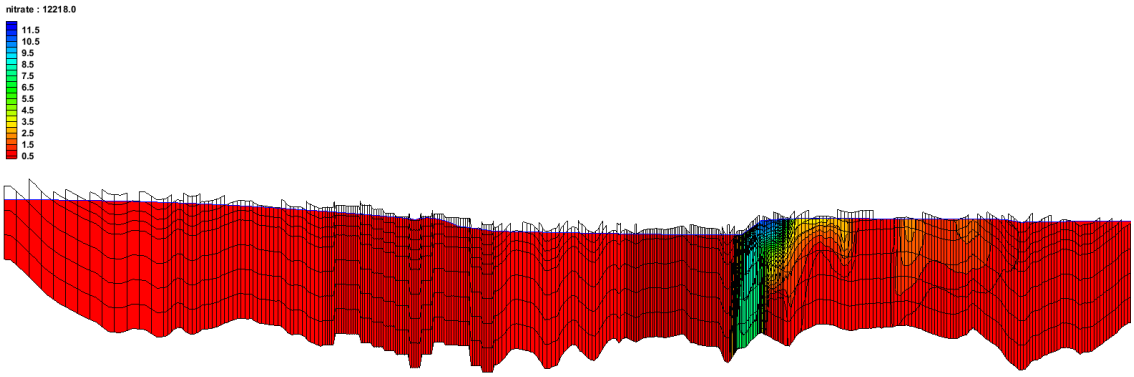

b)

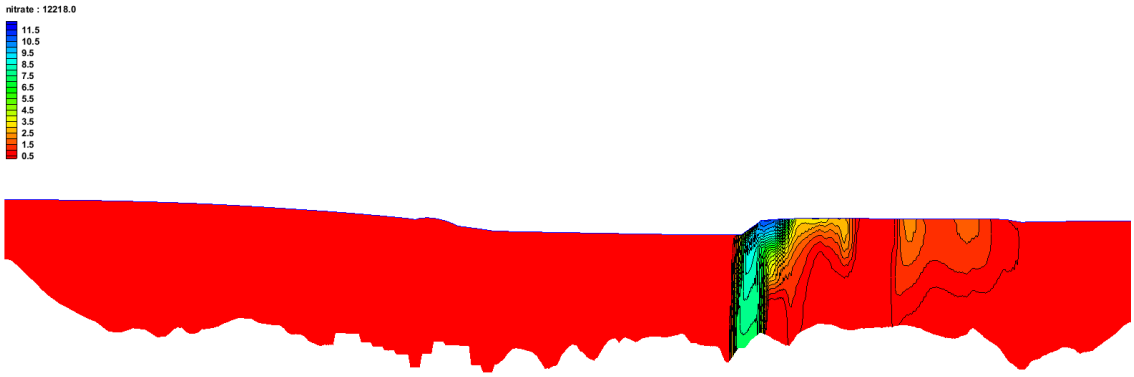

Figure 25. Nitrate concentrations in row j:228 in the year 2015.
a) Concentration including the mapped grid layers in which it is simulated
b) Concentration without the corresponding grid layers for enhanced visibility.

CHAPTER FOUR

CONCLUSIONS

Wastewater reuse, particularly via the use of spray irrigation of treated effluent, is a common practice worldwide and can help lessen the impact of the overconsumption of water resources. The increased recharge to the subsurface that enhances weathering and erosion during the irrigation application process makes it important to characterize any changes in the land surface over time. Wastewater irrigation is a viable alternative to wastewater discharges to streams in that it recharges the underlying aquifer from which the original water was withdrawn. The sensitivity of the aquifer makes it urgent to understand the effects of wastewater reuse upon the water table in a karstic environment, particularly as contaminant transport occurs within fractures and solution conduits.

Chapter Two of this study identified and related any bedrock fracture traces and surface depressions to any surficial or geomorphologic processes currently underway at the site of the Living Filter. The previous measurements of fracture traces in this area undertaken by Matzke (1961), Lattman and Parizek (1964), and Parizek et al. (1967) yielded results in a near N-S orientation. The use of a manual process to estimate the primary fracture trace angles yielded results near identical to that of the aforementioned authors. A high occurrence of depressions was noted in the area of fractures compared to non-fractured bedrock. Further, a statistically significant trend was absent between the orientations of the depressions along the primary fractures

within this area, perhaps caused by a skewing of those orientations from the secondary fractures and jointing patterns also in this area. Further study is needed to determine the validity of this hypothesis, however. Cross sections of several depressions within cropped areas indicated a lower angle slope corresponding to a V-shape while depressions within forested areas were characterized by a traditional U-shape and previously established steeper slope.

In Chapter Three of this study, a framework was developed to model the effect of treated wastewater and the use of large volumes of that water in agricultural irrigation/forest use and to determine groundwater nitrate contamination in a karst landscape of the Spring Creek Watershed, in central Pennsylvania. MODFLOW and MT3DMS models used to simulate groundwater flow and contaminant transport in the aquifer were in agreement with previous models. The 13 wells within the extent of the Living Filter model had a combined RMSE of 6.03 feet while the RMSE for the entire model was 24.76 feet. Although nitrate concentrations in groundwater were highly variable across the watershed and seasons, they were correlated to agriculture activities, i.e., irrigation with treated wastewater. The 2015 model for nitrate compared reasonably well with measured nitrate concentration in groundwater wells, with differences between observed and modeled nitrate concentrations in the aquifer attributed to the heterogeneity of the subsurface environment due to the unpredictable karst terrain with high conductivity solution conduits present leading to non-uniform flow and nitrate transport. Nitrate concentrations were further simulated for the year

2035, these 2035 modeled nitrate concentrations were similar that of the 2015 model. This demonstrates that if total nitrogen contribution to the aquifer remains at the 10 ppm Class A wastewater threshold, then the concentrations within the groundwater should closely reflect current values, assuming no significant change in the volumetric rate of the effluent application.

The workflows implemented here can be implemented in similar sites that display topographical variances from the bedrock fractures. The groundwater modeling framework developed here to simulate the spatial and temporal variability of nitrate concentrations, is applicable to similar aquifers in a karst watershed system, characterized by high permeability materials and high conductivity solution conduits, in which water resources are vulnerable to agricultural activities.

APPENDICES

Appendix A
Thornthwaite Calculations

Month	Temp C°	Temp F°	Heat Index	PET (mm)	PET (ft)
January	0.00	27.00	0.00	0.00	0.00
February	0.00	30.00	0.00	0.00	0.00
March	2.78	37.00	0.41	8.53	0.03
April	9.72	49.50	2.74	39.59	0.13
May	15.28	59.50	5.43	68.89	0.23
June	20.28	68.50	8.33	97.48	0.32
July	22.50	72.50	9.75	110.73	0.36
August	21.39	70.50	9.03	104.06	0.34
September	16.94	62.50	6.35	78.22	0.26
October	10.83	51.50	3.22	45.21	0.15
November	5.56	42.00	1.17	19.94	0.07
December	0.00	31.50	0.00	0.00	0.00
Sum			46.42	572.64	1.88
Alpha		1.23			

Figure A-1. Basic Thornthwaite Calculation

Month	Avg. Temp (°C)	Avg. Temp (°F)	Heat Index	PET (mm)	PET (ft)	Sunlight (hrs)	Days in month	Corrected PET (ft)	Average Precipitation 07-17 (ft)	P-PE (ft)	Irrigation 1.5 MGD (ft/month)	PI+1.5MGD-PE (ft)	1.5 MGD-PE (ft)
January	0.000	27.0	0.000	0.000	0.000	9.7	31	0.000	0.193	0.193	0.205	0.398	0.205
February	0.000	30.0	0.000	0.000	0.000	10.7	28	0.000	0.220	0.220	0.185	0.405	0.185
March	2.778	37.0	0.411	8.526	0.028	12.0	31	0.029	0.242	0.213	0.205	0.418	0.205
April	9.722	49.5	2.737	39.591	0.130	13.3	30	0.144	0.281	0.137	0.198	0.335	0.198
May	15.278	59.5	5.425	68.895	0.226	14.5	31	0.282	0.351	0.068	0.205	0.273	0.205
June	20.278	68.5	8.329	97.476	0.320	15.0	30	0.400	0.337	-0.063	0.198	0.135	0.135
July	22.500	72.5	9.749	110.726	0.364	14.8	31	0.462	0.342	-0.119	0.205	0.085	0.085
August	21.389	70.5	9.030	104.062	0.342	13.8	31	0.405	0.350	-0.055	0.205	0.150	0.150
September	16.944	62.5	6.346	78.217	0.257	12.4	30	0.265	0.275	0.010	0.198	0.208	0.198
October	10.833	51.5	3.224	45.206	0.148	11.1	31	0.142	0.332	0.190	0.205	0.395	0.205
November	5.556	42.0	1.173	19.939	0.065	9.9	30	0.054	0.171	0.117	0.198	0.315	0.198
December	0.000	31.5	0.000	0.000	0.000	9.3	31	0.000	0.303	0.303	0.205	0.507	0.205
Sum			46.423	572.638	1.880			2.183	3.397	1.214	2.409	3.623	2.172
											Daily Irrigation rate (ft)		0.006
Alpha	1.225667794												
											Percent of original irrigation recharged to groundwater		90.14%

Figure A-2. Modified Thornthwaite calculations and irrigation totals.

Appendix B
Observed and Computed Well Elevations

Name	Observed Head (ft)	Observed Head Interval (ft)	Computed Head (ft)	Residual Head (ft)
A3	1110	60	1132.720215	-22.72021484
A4	1123	60	1132.966675	-9.9666748
A5	1157	60	1146.787476	10.21252441
A6	1157	60	1145.584351	11.41564941
S5	915	60	909.4041138	5.59588623
B19	953	60	924.9642334	28.0357666
B18	920	60	924.9072876	-4.907287598
B20	977	60	985.2958374	-8.295837402
B21	966	60	994.7001953	-28.70019531
B22	959	60	994.7926025	-35.79260254
S6	980	60	974.9603882	5.039611816
A10	1013	60	987.177063	25.82293701
A9	1017	60	998.7250977	18.27490234
D1	1101	60	1103.074341	-2.07434082
S7	1115	60	1110.20166	4.79833984
U16	1014	60	992.5904541	21.4095459
U17	1025	60	1002.15155	22.84844971
U24	1008	60	938.0240479	69.97595215
K1	961	60	936.0189209	24.9810791
U4	1018	60	940.8909912	77.10900879
U26	1015	60	938.1306152	76.86938477
U33	936	60	941.9488525	-5.948852539
U34	917	60	943.4447632	-26.44476318
U35	922	60	943.5446167	-21.5446167
S4	956	60	945.7597046	10.24029541
S3	1015	60	973.1925049	41.80749512
C25	1057	60	1064.012085	-7.01208496
C27	1059	60	1061.879761	-2.87976074
C26	1058	60	1063.680298	-5.68029785
C22	1071	60	1065.097046	5.9029541
B12	1053	60	1057.611206	-4.61120605
B27	1056	60	1070.138672	-14.13867188
B26	1055	60	1070.415649	-15.41564941
C8	1060	60	1067.719116	-7.71911621
C14	1059	60	1067.619141	-8.61914062
C11	1059	60	1066.563721	-7.5637207
C7	1059	60	1067.146362	-8.1463623

B13	1036	60	1044.850586	-8.85058594
B14	1036	60	1043.085938	-7.0859375
B15	1074	60	1048.710327	25.28967285
B16	1058	60	1049.14563	8.85437012
C57	1089	60	1044.878174	44.12182617
C55	1083	60	1040.825195	42.17480469
A20	1103	60	1094.140015	8.85998535
C53	1114	60	1138.286377	-24.28637695
C43	1114	60	1138.334595	-24.33459473
M5	1110	60	1135.251221	-25.2512207
M2	1114	60	1135.382935	-21.38293457
M13	1119	60	1135.230713	-16.23071289
GD	1141	60	1134.335327	6.66467285
A7	1090	60	990.0768433	99.92315674
A8	1095	60	1062.16626	32.83374023
A13	1174	60	1179.825684	-5.82568359
A12	1216	60	1201.692749	14.30725098
A11	1180	60	1215.630859	-35.63085938
S12	1230	60	1203.661499	26.33850098
C16	1060	60	1043.292358	16.7076416
C19	1061	60	1047.941162	13.05883789
F4	1095	60	1105.201904	-10.2019043
U28	1095	60	1099.981079	-4.9810791
F6	1099	60	1095.547852	3.45214844
F5	1098	60	1099.813599	-1.81359863
F1	1103	60	1110.1427	-7.1427002
F2	1104	60	1108.527588	-4.52758789
F3	1111	60	1114.858276	-3.85827637
W1	1030	60	1023.409058	6.59094238
W2	1022	60	1029.16626	-7.16625977
W3	1036	60	1028.508179	7.49182129
W5	1023	60	1019.101501	3.89849854
W6	1014	60	1018.710815	-4.71081543
W7	1022	60	1027.682495	-5.68249512
G12	1020	60	1027.408325	-7.4083252
G10	1021	60	1026.623169	-5.62316895
P-1	929	60	931.7875977	-2.787597656
P-2	991	60	990.4318848	0.568115234
P-3	1007	60	1004.339233	2.6607666
P-4	1022	60	1013.992249	8.00775146
P-5	1011	60	1010.242554	0.75744629

Appendix C

Pumping Rates

RECORD OF GROUND-WATER PUMPAGE FOR REMAINING WELLS

Project Name: Penn State University-19890106
Well ID[1]: Wells 2, 14, 16, 17, 24, and 26
Report Period: 04/17-03/18

Date	Well 2		Well 14		Well 16		Well 17		Well 24		Well 26	
	1,000's	Actual	1,000's	Actual	1,000's	Actual	1,000's	Actual	1,000's	Actual	1,000's	Actual
4/1/2017	0	0	0	0	242.2	242,241	442.7	442,696	315.1	315,058	262.8	262,762
4/2/2017	0	0	0	0	240.3	240,309	443.2	443,219	315.2	315,223	0.0	0
4/3/2017	0	0	0	0	238.6	238,551	442.7	442,691	313.7	313,711	0.0	0
4/4/2017	0	0	0	0	239.5	239,509	443.9	443,859	314.6	314,646	0.0	0
4/5/2017	0	0	0	0	149.4	149,439	397.9	397,856	322.7	322,682	78.1	78,076
4/6/2017	0	0	0	0	151.9	151,916	414.1	414,128	320.6	320,565	85.4	85,404
4/7/2017	0	0	0	0	205.5	205,482	409.7	409,701	318.9	318,938	92.0	91,998
4/8/2017	0	0	0	0	220.6	220,575	447.2	447,162	315.8	315,810	0.0	0
4/9/2017	0	0	0	0	244.6	244,613	447.0	447,030	315.9	315,879	0.0	0
4/10/2017	0	0	0	0	198.2	198,245	412.7	412,701	319.8	319,844	91.3	91,291
4/11/2017	0	0	0	0	200.8	200,770	390.1	390,140	318.9	318,856	90.9	90,883
4/12/2017	0	0	0	0	176.6	176,580	403.6	403,560	322.0	321,977	99.8	99,754
4/13/2017	0	0	0	0	159.4	159,414	403.7	403,697	321.4	321,387	77.3	77,292
4/14/2017	0	0	0	0	189.0	189,000	438.9	438,938	275.6	275,627	0.0	0
4/15/2017	0	0	0	0	247.7	247,716	449.5	449,471	255.5	255,457	0.0	0
4/16/2017	0	0	0	0	243.5	243,516	447.0	446,952	288.4	288,376	0.0	0
4/17/2017	0	0	0	0	240.9	240,901	445.1	445,099	316.1	316,074	0.0	0
4/18/2017	0	0	0	0	217.3	217,320	442.0	441,959	275.1	275,081	0.0	0
4/19/2017	0	0	0	0	194.1	194,055	440.1	440,142	314.8	314,799	0.0	0
4/20/2017	0	0	0	0	183.9	183,878	442.2	442,237	313.4	313,351	0.0	0
4/21/2017	0	0	0	0	185.9	185,925	445.3	445,271	315.4	315,404	92.9	92,940
4/22/2017	0	0	0	0	201.6	201,574	444.5	444,549	315.8	315,800	0.0	0
4/23/2017	0	0	0	0	216.0	215,958	443.6	443,584	315.6	315,608	0.0	0
4/24/2017	0	0	0	0	127.7	127,700	231.6	231,600	191.1	191,100	109.8	109,758
4/25/2017	0	0	0	0	81.1	81,130	157.3	157,254	115.6	115,605	273.6	273,637
4/26/2017	0	0	0	0	60.8	60,845	344.1	344,052	257.7	257,740	531.3	531,251
4/27/2017	0	0	0	0	0.0	0	429.4	429,410	339.5	339,539	772.0	771,954
4/28/2017	261	260,703	243	242,901	157.3	157,307	375.4	375,387	323.6	323,647	704.6	704,553
4/29/2017	176	176,002	220	219,781	121.7	121,732	176.2	176,194	149.4	149,389	232.2	232,235
4/30/2017	193	192,914	238	238,338	131.3	131,257	192.9	192,890	162.6	162,588	253.1	253,073
5/1/2017	123.3	123,296	151.7	151,691	0.0	0	122.3	122,278	102.9	102,910	180.7	180,661

RECORD OF GROUND-WATER PUMPAGE FOR REMAINING WELLS

Project Name: Penn State University-19890106
Well ID[1]: Wells 2, 14, 16, 17, 24, and 26
Report Period: 04/17-03/18

Date	Well 2		Well 14		Well 16		Well 17		Well 24		Well 26	
	1,000's	Actual	1,000's	Actual	1,000's	Actual	1,000's	Actual	1,000's	Actual	1,000's	Actual
5/2/2017	355.8	355,810	202.1	202,110	143.1	143,149	176.5	176,462	263.4	263,425	509.2	509,154
5/3/2017	135.0	135,041	97.8	97,794	0.0	0	0.0	0	190.1	190,131	420.5	420,451
5/4/2017	188.2	188,219	92.5	92,503	0.0	0	0.0	0	155.5	155,504	348.2	348,199
5/5/2017	205.5	205,538	172.0	172,027	0.0	0	0.0	0	82.1	82,085	390.5	390,546
5/6/2017	126.5	126,529	222.8	222,812	0.0	0	0.0	0	105.2	105,175	230.7	230,729
5/7/2017	130.7	130,747	230.4	230,372	0.0	0	0.0	0	113.8	113,758	238.5	238,454
5/8/2017	211.6	211,592	369.5	369,450	0.0	0	0.0	0	171.6	171,632	384.3	384,250
5/9/2017	154.8	154,777	283.3	283,316	0.0	0	0.0	0	142.3	142,330	284.6	284,646
5/10/2017	184.0	183,981	294.6	294,598	0.0	0	0.0	0	61.2	61,212	313.6	313,628
5/11/2017	167.6	167,614	277.8	277,804	0.0	0	0.0	0	108.3	108,279	293.9	293,874
5/12/2017	157.2	157,207	286.7	286,693	0.0	0	0.0	0	138.6	138,627	292.1	292,100
5/13/2017	74.4	74,365	126.2	126,189	0.0	0	0.0	0	47.0	47,015	130.6	130,565
5/14/2017	98.5	98,510	213.7	213,729	0.0	0	0.0	0	83.0	83,049	229.9	229,853
5/15/2017	68.7	68,701	355.5	355,467	0.0	0	0.0	0	215.0	214,977	381.4	381,402
5/16/2017	173.6	173,623	348.5	348,504	0.0	0	0.0	0	178.6	178,603	359.2	359,196
5/17/2017	71.6	71,631	350.1	350,051	0.0	0	0.0	0	203.3	203,273	373.5	373,477
5/18/2017	162.4	162,432	406.1	406,070	0.0	0	0.0	0	195.0	194,979	401.1	401,106
5/19/2017	179.4	179,353	401.6	401,645	0.0	0	0.0	0	184.1	184,114	392.1	392,145
5/20/2017	22.7	22,733	289.2	289,158	0.0	0	0.0	0	134.3	134,334	279.6	279,554
5/21/2017	40.0	39,999	238.6	238,644	0.0	0	0.0	0	110.7	110,685	229.9	229,870
5/22/2017	131.2	131,156	293.7	293,688	26.5	26,475	0.0	0	104.8	104,771	328.4	328,435
5/23/2017	220.2	220,208	143.7	143,685	0.0	0	0.0	0	67.6	67,558	313.1	313,064
5/24/2017	171.6	171,570	303.3	303,264	65.7	65,681	0.0	0	0.0	0	278.8	278,805
5/25/2017	126.6	126,569	0.0	0	74.6	74,562	74.4	74,411	0.0	0	323.0	323,002
5/26/2017	149.2	149,188	62.1	62,052	76.2	76,233	63.7	63,742	30.6	30,644	276.3	276,297
5/27/2017	158.1	158,074	148.1	148,076	0.0	0	0.0	0	72.6	72,613	236.3	236,336
5/28/2017	175.5	175,476	242.9	242,915	0.0	0	0.0	0	45.0	44,972	287.3	287,344
5/29/2017	178.4	178,448	216.4	216,358	0.0	0	0.0	0	0.0	0	214.3	214,339
5/30/2017	247.7	247,654	186.9	186,861	0.0	0	8.9	8,926	0.0	0	392.8	392,810
5/31/2017	100.2	100,199	180.9	180,901	48.9	48,880	44.8	44,753	34.8	34,778	348.3	348,301
6/1/2017	115.5	115,463	115.5	115,524	65.0	64,956	41.7	41,652	105.5	105,526	382.6	382,596

RECORD OF GROUND-WATER PUMPAGE FOR REMAINING WELLS

Project Name: Penn State University-19890106

Well ID[1]: Wells 2, 14, 16, 17, 24, and 26

Report Period: 04/17-03/18

Date	Well 2		Well 14		Well 16		Well 17		Well 24		Well 26	
	1,000's	Actual	1,000's	Actual	1,000's	Actual	1,000's	Actual	1,000's	Actual	1,000's	Actual
6/2/2017	127.1	127,143	0.0	0	161.5	161,496	161.2	161,200	0.0	0	435.1	435,146
6/3/2017	132.1	132,065	59.2	59,209	84.4	84,418	157.6	157,605	2.7	0	292.8	292,850
6/4/2017	97.0	96,988	165.2	165,202	30.1	30,121	172.3	172,308	2.6	0	272.2	272,210
6/5/2017	243.6	243,580	24.6	24,595	34.4	34,387	74.8	74,779	5.8	0	349.5	349,457
6/6/2017	239.9	239,896	0.0	0	108.4	108,412	213.6	213,610	96.5	96,511	432.1	432,138
6/7/2017	130.9	130,889	0.0	0	52.0	52,038	97.9	97,913	116.3	116,253	238.9	238,907
6/8/2017	139.9	139,922	0.0	0	0.0	0	229.0	229,035	111.7	111,714	395.6	395,565
6/9/2017	208.6	208,639	0.0	0	29.2	29,187	100.3	100,303	96.7	96,748	324.3	324,334
6/10/2017	224.4	224,353	0.0	0	59.4	59,363	171.8	171,795	115.8	115,783	384.9	384,940
6/11/2017	242.8	242,810	0.0	0	71.9	71,921	129.5	129,541	104.0	104,001	373.5	373,475
6/12/2017	301.5	301,459	0.0	0	162.7	162,707	301.5	301,515	239.4	239,404	496.8	496,767
6/13/2017	131.9	131,867	0.0	0	23.5	23,527	45.1	45,075	172.8	172,760	451.4	451,418
6/14/2017	128.2	128,200	0.0	0	117.8	117,848	360.5	360,462	186.0	185,991	606.0	606,033
6/15/2017	100.0	100,000	0.0	0	102.4	102,366	317.9	317,876	139.4	139,426	529.0	529,043
6/16/2017	141.8	141,800	0.0	0	85.9	85,903	251.9	251,890	167.6	167,577	440.6	440,636
6/17/2017	68.2	68,200	0.0	0	24.7	24,670	189.5	189,522	42.7	42,686	286.8	286,777
6/18/2017	132.8	132,800	0.0	0	136.6	136,628	254.7	254,737	187.6	187,585	495.1	495,104
6/19/2017	114.0	114,000	0.0	0	43.6	43,554	97.3	97,292	180.2	180,190	382.3	382,284
6/20/2017	0.0	0	100.7	100,677	104.5	104,510	275.4	275,419	99.2	99,195	454.1	454,125
6/21/2017	0.0	0	207.3	207,322	79.3	79,281	274.3	274,331	0.0	0	415.6	415,573
6/22/2017	0.0	0	206.7	206,671	33.5	33,516	278.5	278,452	0.0	0	384.3	384,309
6/23/2017	55.9	55,914	191.9	191,884	0.0	0	0.0	0	0.0	0	366.7	366,653
6/24/2017	141.6	141,586	94.7	94,737	0.0	0	67.9	67,886	0.1	0	255.1	255,145
6/25/2017	175.4	175,430	150.7	150,732	51.9	51,910	76.9	76,923	0.1	0	304.3	304,330
6/26/2017	72.9	72,899	173.2	173,187	0.0	0	150.8	150,817	51.8	51,783	383.7	383,653
6/27/2017	100.7	100,699	192.5	192,495	51.7	51,674	123.7	123,659	97.7	97,678	314.0	313,961
6/28/2017	234.7	234,688	84.7	84,655	0.0	0	0.0	0	45.4	45,438	346.4	346,445
6/29/2017	256.7	256,737	376.4	376,359	0.0	0	0.0	0	151.7	151,676	498.3	498,296
6/30/2017	274.8	274,824	178.4	178,423	77.8	77,780	140.3	140,348	145.8	145,794	505.7	505,684
7/1/2017	55.7	55,716	6.2	6,218	53.7	53,670	60.6	60,623	146.2	146,247	345.0	345,038
7/2/2017	86.7	86,677	285.9	285,885	63.1	63,080	143.4	143,361	0.0	0	300.8	300,756
7/3/2017	260.8	260,815	350.0	350,014	0.0	2	0.0	0	0.0	34	424.0	424,033
7/4/2017	260.0	259,986	219.8	219,772	0.0	2	0.0	0	0.0	0	414.6	414,557
7/5/2017	260.3	260,318	196.7	196,723	6.1	6,112	8.0	7,970	64.4	64,422	381.7	381,748
7/6/2017	277.8	277,829	320.7	320,678	0.0	0	0.0	0	0.0	0	438.5	438,547
7/7/2017	238.8	238,768	167.3	167,286	0.0	0	0.0	0	0.0	0	368.2	368,179
7/8/2017	212.0	211,953	325.5	325,487	0.0	0	66.0	65,964	52.5	52,501	452.5	452,496
7/9/2017	169.7	169,673	149.2	149,167	0.0	0	56.4	56,412	45.1	45,104	353.0	353,034
7/10/2017	301.2	301,231	313.5	313,524	0.0	0	0.0	0	0.0	1	507.5	507,530
7/11/2017	282.5	282,498	130.3	130,318	24.7	24,664	104.7	104,674	83.0	83,004	483.9	483,901

RECORD OF GROUND-WATER PUMPAGE FOR REMAINING WELLS

Project Name: Penn State University-19890106

Well ID[1]: Wells 2, 14, 16, 17, 24, and 26

Report Period: 04/17-03/18

Date	Well 2		Well 14		Well 16		Well 17		Well 24		Well 26	
	1,000's	Actual	1,000's	Actual	1,000's	Actual	1,000's	Actual	1,000's	Actual	1,000's	Actual
7/12/2017	228.9	228,891	238.7	238,681	0.0	0	13.8	13,773	10.9	10,920	501.6	501,580
7/13/2017	350.8	350,805	279.2	279,234	0.0	0	0.0	0	0.0	0	600.5	600,529
7/14/2017	172.6	172,574	472.8	472,759	0.0	0	2.2	2,241	179.0	179,010	222.2	222,159
7/15/2017	98.4	98,394	132.7	132,749	0.0	0	0.0	0	56.5	56,522	583.0	583,036
7/16/2017	76.1	76,088	148.0	148,019	0.0	0	70.6	70,561	18.4	18,430	502.0	502,041
7/17/2017	273.5	273,533	223.4	223,360	0.0	0	65.4	65,447	0.0	0	448.7	448,734
7/18/2017	210.9	210,925	180.9	180,912	0.0	0	55.9	55,861	44.7	44,676	703.2	703,170
7/19/2017	293.4	293,369	313.4	313,389	0.0	0	100.8	100,761	80.2	80,193	595.7	595,701
7/20/2017	151.2	151,169	427.0	427,004	39.4	39,392	0.0	0	0.0	0	527.1	527,127
7/21/2017	90.8	90,759	292.7	292,674	21.1	21,058	127.7	127,734	4.7	4,669	797.9	797,885
7/22/2017	280.5	280,488	253.2	253,172	0.0	0	0.0	0	0.0	3	428.3	428,319
7/23/2017	246.9	246,924	240.9	240,912	38.1	38,146	20.8	20,822	32.1	32,115	401.3	401,310
7/24/2017	269.1	269,107	283.5	283,492	96.1	96,088	0.0	0	0.0	0	391.6	391,625
7/25/2017	258.0	258,008	165.5	165,521	61.1	61,139	0.0	0	0.0	0	363.4	363,356
7/26/2017	281.2	281,222	148.1	148,066	45.4	45,372	0.0	0	0.0	0	405.0	404,955
7/27/2017	336.9	336,934	286.8	286,809	0.0	0	0.0	0	0.0	35	523.7	523,688
7/28/2017	101.8	101,842	381.2	381,220	0.0	0	166.0	166,045	0.0	0	550.8	550,811
7/29/2017	0.0	0	194.2	194,250	0.0	0	107.8	107,772	0.0	0	404.2	404,206
7/30/2017	68.9	68,943	81.8	81,799	10.5	10,467	18.9	18,908	0.0	0	509.7	509,665
7/31/2017	85.7	85,673	360.0	360,047	0.0	0	211.7	211,742	0.0	0	511.3	511,334
8/1/2017	236.1	236,067	311.4	311,396	0.0	0	80.8	80,772	0.0	0	399.6	399,564
8/2/2017	267.5	267,474	400.3	400,338	0.0	0	0.0	0	0.0	0	436.5	436,500
8/3/2017	271.9	271,918	264.3	264,284	62.2	62,238	117.7	117,744	4.4	4,377	506.3	506,264
8/4/2017	45.8	45,764	217.0	216,960	83.7	83,691	43.6	43,590	0.0	1	650.1	650,137
8/5/2017	259.4	259,449	181.6	181,631	1.7	1,671	86.7	86,672	0.0	0	396.7	396,676
8/6/2017	273.5	273,550	101.4	101,378	0.0	0	0.0	0	0.0	0	409.6	409,585
8/7/2017	252.5	252,493	98.6	98,598	0.0	0	0.0	0	0.0	0	367.2	367,156
8/8/2017	226.2	226,201	370.5	370,496	0.0	0	0.0	0	0.0	0	498.2	498,216
8/9/2017	119.0	119,029	101.3	101,338	0.0	0	0.0	0	0.0	1	529.8	529,766
8/10/2017	271.5	271,545	353.9	353,936	0.0	0	0.0	0	0.0	0	528.6	528,577
8/11/2017	294.0	293,981	481.2	481,159	0.0	0	0.0	0	0.0	0	491.8	491,809
8/12/2017	37.4	37,443	290.1	290,106	0.0	0	126.4	126,437	0.0	0	486.6	486,564
8/13/2017	88.6	88,573	55.8	55,821	46.6	46,612	120.8	120,805	0.0	0	384.6	384,560
8/14/2017	266.5	266,519	99.4	99,450	30.3	30,302	60.1	60,107	0.0	0	421.1	421,126
8/15/2017	293.4	293,399	157.4	157,441	61.8	61,830	119.4	119,425	0.0	0	495.4	495,358
8/16/2017	183.8	183,779	167.8	167,764	38.9	38,937	119.1	119,087	0.0	0	660.4	660,375
8/17/2017	327.9	327,937	204.3	204,312	99.5	99,534	203.5	203,493	162.5	162,454	535.0	534,982
8/18/2017	50.0	50,032	335.5	335,543	115.3	115,283	50.0	50,033	251.4	251,364	569.3	569,290
8/19/2017	113.7	113,718	265.9	265,867	25.2	25,230	0.0	0	239.2	239,176	470.5	470,489
8/20/2017	91.3	91,335	306.6	306,644	0.0	0	94.5	94,476	241.4	241,438	496.2	496,223

RECORD OF GROUND-WATER PUMPAGE FOR REMAINING WELLS

Project Name: Penn State University-19890106

Well ID[1]: Wells 2, 14, 16, 17, 24, and 26

Report Period: 04/17-03/18

Date	Well 2		Well 14		Well 16		Well 17		Well 24		Well 26	
	1,000's	Actual	1,000's	Actual	1,000's	Actual	1,000's	Actual	1,000's	Actual	1,000's	Actual
8/21/2017	0.0	0	554.7	554,663	117.1	117,124	75.8	75,836	302.4	302,383	705.8	705,808
8/22/2017	0.0	0	436.1	436,064	29.2	29,235	191.8	191,812	255.1	255,113	581.7	581,686
8/23/2017	198.9	198,867	429.2	429,201	108.8	108,776	311.2	311,175	265.9	265,926	396.9	396,860
8/24/2017	149.4	149,355	199.3	199,287	14.4	14,425	299.1	299,123	21.8	21,792	424.2	424,206
8/25/2017	311.2	311,216	115.5	115,493	88.9	88,883	261.3	261,260	0.0	0	529.9	529,895
8/26/2017	74.9	74,883	165.3	165,263	145.6	145,638	74.9	74,876	73.5	73,513	495.1	495,081
8/27/2017	156.9	156,902	323.7	323,681	49.5	49,481	0.0	0	83.7	83,721	454.4	454,378
8/28/2017	354.2	354,154	582.5	582,470	0.0	0	0.0	0	0.0	0	591.4	591,447
8/29/2017	89.5	89,491	335.5	335,461	0.0	0	289.2	289,181	0.0	0	608.9	608,854
8/30/2017	40.0	40,039	344.7	344,658	0.0	0	152.5	152,469	0.0	0	745.0	745,014
8/31/2017	0.0	0	432.4	432,353	0.0	0	386.0	386,027	0.0	0	691.6	691,574
9/1/2017	215.9	215,870	362.6	362,555	0.0	0	114.6	114,627	0.0	0	611.6	611,623
9/2/2017	297.6	297,647	125.1	125,076	18.9	18,911	36.4	36,352	0.0	0	486.3	486,284
9/3/2017	159.7	159,717	0.0	0	80.7	80,671	215.2	215,177	0.0	0	383.4	383,398
9/4/2017	65.2	65,154	194.8	194,786	32.2	32,182	225.6	225,613	0.0	45	414.6	414,631
9/5/2017	34.7	34,721	525.7	525,729	0.0	0	279.2	279,182	0.0	1	575.2	575,246
9/6/2017	236.2	236,242	329.5	329,503	0.0	0	291.5	291,450	0.0	0	414.7	414,749
9/7/2017	279.4	279,371	387.5	387,475	0.0	0	279.6	279,584	0.0	0	396.4	396,447
9/8/2017	224.0	224,036	312.8	312,834	0.0	0	224.2	224,243	0.0	0	319.5	319,521
9/9/2017	209.3	209,263	335.7	335,727	0.0	0	209.5	209,471	0.0	0	350.1	350,095
9/10/2017	61.0	60,966	237.3	237,341	68.9	68,908	181.4	181,415	0.0	0	296.2	296,172
9/11/2017	0.0	0	313.6	313,639	31.4	31,446	292.4	292,365	0.0	0	503.6	503,575
9/12/2017	151.2	151,168	160.1	160,128	72.6	72,588	308.3	308,328	4.9	4,867	561.2	561,188
9/13/2017	65.2	65,151	326.8	326,786	44.5	44,471	320.6	320,569	168.6	168,577	606.7	606,671
9/14/2017	0.0	0	404.6	404,560	15.6	15,566	290.4	290,435	66.1	66,054	545.4	545,355
9/15/2017	0.0	0	395.6	395,646	126.4	126,397	267.2	267,237	213.0	213,044	409.7	409,747
9/16/2017	0.0	0	385.5	385,505	24.3	24,339	285.2	285,207	179.2	179,236	514.4	514,446
9/17/2017	0.0	0	301.8	301,830	0.0	0	244.6	244,643	135.4	135,365	438.6	438,583
9/18/2017	0.0	0	459.0	458,987	95.4	95,409	329.7	329,733	56.0	55,993	564.2	564,177
9/19/2017	0.0	0	427.0	426,967	120.9	120,857	319.2	319,236	0.0	0	543.7	543,714
9/20/2017	0.0	0	446.4	446,380	138.2	138,229	328.3	328,313	0.0	0	604.0	603,992
9/21/2017	92.3	92,314	453.7	453,714	143.9	143,918	335.3	335,292	0.0	0	536.3	536,260
9/22/2017	40.1	40,063	431.6	431,611	138.4	138,431	281.8	281,818	0.0	0	484.3	484,282
9/23/2017	132.9	132,857	309.6	309,617	35.7	35,715	220.8	220,849	0.0	0	329.6	329,552
9/24/2017	223.9	223,933	270.9	270,877	0.0	0	224.3	224,349	0.0	0	335.8	335,790
9/25/2017	68.4	68,438	459.3	459,282	101.3	101,275	344.4	344,383	0.0	0	553.0	553,037
9/26/2017	0.0	0	334.3	334,264	88.9	88,926	363.9	363,889	0.0	0	566.6	566,569
9/27/2017	0.0	0	418.6	418,636	116.9	116,887	371.8	371,831	0.0	0	608.0	608,044
9/28/2017	0.0	0	398.6	398,639	108.7	108,698	362.0	362,010	0.0	0	580.5	580,475
9/29/2017	0.0	0	545.5	545,473	147.7	147,680	328.2	328,238	0.0	0	572.9	572,852

RECORD OF GROUND-WATER PUMPAGE FOR REMAINING WELLS

Project Name: Penn State University-19890106

Well ID[1]: Wells 2, 14, 16, 17, 24, and 26

Report Period: 04/17-03/18

Date	Well 2		Well 14		Well 16		Well 17		Well 24		Well 26	
	1,000's	Actual	1,000's	Actual	1,000's	Actual	1,000's	Actual	1,000's	Actual	1,000's	Actual
9/30/2017	0.0	0	267.2	267,203	14.4	14,446	241.5	241,519	95.3	95,320	407.2	407,205
10/1/2017	0.0	0	281.7	281,732	57.6	57,575	229.0	229,016	34.6	34,601	390.3	390,322
10/2/2017	0.0	0	408.2	408,203	25.9	25,864	283.7	283,750	0.0	0	528.2	528,219
10/3/2017	0.0	0	281.0	280,973	16.7	16,659	284.6	284,633	0.0	0	491.8	491,844
10/4/2017	0.0	0	564.9	564,855	158.6	158,553	343.3	343,317	0.0	0	588.2	588,166
10/5/2017	0.0	0	274.7	274,709	77.3	77,297	282.6	282,577	0.0	0	463.7	463,667
10/6/2017	32.8	32,844	529.5	529,516	128.8	128,848	323.9	323,851	0.0	0	554.7	554,714
10/7/2017	0.0	0	349.1	349,086	97.6	97,612	213.1	213,127	0.0	0	363.0	362,979
10/8/2017	0.0	0	441.5	441,506	122.1	122,116	268.2	268,239	0.0	0	460.8	460,832
10/9/2017	0.0	0	353.6	353,561	97.2	97,171	312.9	312,889	0.0	0	485.7	485,693
10/10/2017	0.0	0	486.6	486,648	132.9	132,945	294.8	294,832	0.0	0	508.0	508,021
10/11/2017	0.0	0	417.4	417,397	114.0	113,985	252.3	252,290	0.0	0	432.5	432,494
10/12/2017	182.5	182,478	138.8	138,772	111.5	111,478	245.3	245,345	126.7	126,661	434.6	434,624
10/13/2017	74.7	74,651	174.1	174,096	88.1	88,077	230.6	230,642	192.4	192,352	382.5	382,508
10/14/2017	0.0	0	174.4	174,448	50.7	50,699	223.1	223,088	25.8	25,841	338.3	338,284
10/15/2017	0.0	0	302.8	302,837	87.3	87,295	257.2	257,181	0.0	0	413.7	413,741
10/16/2017	0.0	0	350.9	350,949	25.3	25,297	277.5	277,525	116.8	116,848	483.4	483,414
10/17/2017	0.0	0	397.5	397,461	0.0	0	249.8	249,777	50.1	50,126	478.2	478,227
10/18/2017	156.6	156,590	111.9	111,862	75.2	75,197	265.6	265,563	126.8	126,830	445.3	445,251
10/19/2017	82.9	82,908	305.8	305,806	125.8	125,829	267.6	267,589	67.8	67,767	455.0	454,983
10/20/2017	0.0	0	446.3	446,266	123.5	123,497	271.2	271,168	0.0	0	463.8	463,842
10/21/2017	0.0	0	350.8	350,803	98.9	98,926	215.1	215,128	0.0	0	366.5	366,545
10/22/2017	108.6	108,589	293.9	293,943	95.0	94,981	87.9	87,856	0.0	0	304.3	304,305
10/23/2017	101.7	101,746	437.7	437,681	129.8	129,789	175.6	175,622	0.0	0	469.5	469,458
10/24/2017	0.0	0	253.4	253,388	70.1	70,105	325.7	325,698	0.0	0	499.6	499,576
10/25/2017	0.0	0	308.3	308,298	88.2	88,151	306.9	306,855	0.0	0	494.8	494,777
10/26/2017	0.0	0	309.7	309,730	85.0	84,976	342.7	342,726	0.0	0	517.0	516,958
10/27/2017	4.5	4,458	349.7	349,689	52.4	52,382	157.6	157,586	36.9	36,918	436.2	436,223
10/28/2017	0.0	0	239.8	239,828	66.4	66,394	238.4	238,422	61.7	61,655	505.2	505,179
10/29/2017	0.0	0	241.2	241,155	101.9	101,880	226.0	225,951	0.0	0	236.3	236,331
10/30/2017	0.0	0	268.1	268,062	80.0	80,019	250.1	250,126	112.1	112,132	374.5	374,549
10/31/2017	2.9	2,897	276.2	276,161	114.7	114,669	268.7	268,690	141.7	141,698	436.3	436,266
11/1/2017	109.7	109,691	68.6	68,645	74.5	74,547	285.5	285,530	124.6	124,628	431.3	431,311
11/2/2017	61.1	61,071	265.8	265,801	104.1	104,070	283.4	283,432	49.1	49,070	464.9	464,872
11/3/2017	85.5	85,502	196.0	196,004	23.6	23,623	248.2	248,194	71.1	71,084	364.9	364,871
11/4/2017	211.2	211,155	274.8	274,779	0.0	0	211.4	211,379	176.0	175,996	288.9	288,914
11/5/2017	90.7	90,730	145.0	144,963	0.0	0	54.7	54,668	151.4	151,363	274.8	274,793
11/6/2017	0.0	0	98.1	98,143	0.0	0	172.4	172,373	46.5	46,531	264.8	264,844
11/7/2017	0.0	0	326.4	326,421	96.1	96,110	303.6	303,616	0.0	0	478.0	478,043
11/8/2017	0.0	0	474.9	474,855	134.3	134,291	286.2	286,215	0.0	0	491.5	491,501

RECORD OF GROUND-WATER PUMPAGE FOR REMAINING WELLS

Project Name: Penn State University-19890106

Well ID[1]: Wells 2, 14, 16, 17, 24, and 26

Report Period: 04/17-03/18

Date	Well 2		Well 14		Well 16		Well 17		Well 24		Well 26	
	1,000's	Actual	1,000's	Actual	1,000's	Actual	1,000's	Actual	1,000's	Actual	1,000's	Actual
11/9/2017	0.0	0	323.0	323,034	97.3	97,322	244.5	244,544	0.0	0	441.2	441,208
11/10/2017	22.3	22,311	413.7	413,685	96.8	96,774	229.7	229,699	58.9	58,909	354.9	354,933
11/11/2017	0.0	0	372.4	372,444	0.0	0	276.0	276,030	170.1	170,118	503.4	503,423
11/12/2017	0.0	0	228.0	227,978	42.5	42,495	254.3	254,264	38.9	38,905	410.7	410,697
11/13/2017	50.5	50,454	235.7	235,742	126.7	126,739	226.3	226,347	170.0	170,031	299.3	299,322
11/14/2017	71.0	71,012	278.1	278,130	119.6	119,638	251.2	251,157	201.0	201,020	397.0	396,966
11/15/2017	0.0	0	351.4	351,443	117.2	117,172	234.8	234,829	191.4	191,371	323.2	323,235
11/16/2017	181.2	181,163	365.0	364,984	36.9	36,908	369.2	369,248	61.4	61,428	535.2	535,189
11/17/2017	36.5	36,475	273.0	272,963	66.6	66,606	230.3	230,270	0.0	0	365.0	365,027
11/18/2017	49.7	49,665	0.0	0	71.1	71,082	225.7	225,721	40.7	40,656	366.9	366,922
11/19/2017	75.6	75,597	0.0	0	59.2	59,169	76.4	76,365	102.3	102,344	145.0	145,009
11/20/2017	0.0	0	0.0	0	6.6	6,562	292.3	292,285	10.4	10,354	386.3	386,305
11/21/2017	85.3	85,252	188.8	188,786	0.0	0	235.7	235,700	0.0	0	167.1	167,097
11/22/2017	213.7	213,740	127.1	127,120	0.0	0	75.2	75,221	0.0	0	192.8	192,822
11/23/2017	170.1	170,134	0.0	0	64.4	64,353	64.3	64,266	64.4	64,431	149.5	149,538
11/24/2017	128.2	128,214	0.0	0	104.4	104,398	137.6	137,632	113.1	113,097	95.0	94,962
11/25/2017	0.0	0	0.0	0	12.8	12,804	154.0	154,012	0.0	0	222.3	222,309
11/26/2017	107.9	107,871	0.0	0	52.8	52,830	228.2	228,168	85.6	85,628	340.1	340,129
11/27/2017	35.8	35,772	267.6	267,568	116.8	116,824	195.5	195,454	53.5	53,542	377.7	377,669
11/28/2017	0.0	0	430.4	430,362	24.3	24,318	257.6	257,631	177.3	177,264	343.0	343,033
11/29/2017	148.0	148,028	332.4	332,403	0.0	0	236.2	236,208	201.2	201,163	271.2	271,193
11/30/2017	49.7	49,708	189.5	189,548	106.4	106,360	197.9	197,917	41.4	41,379	370.0	370,022
12/1/2017	113.9	113,908	225.4	225,359	83.2	83,197	229.0	228,966	110.0	109,994	326.0	325,965
12/2/2017	145.2	145,175	365.3	365,297	110.3	110,327	134.9	134,923	84.0	84,007	137.2	137,247
12/3/2017	152.8	152,825	140.4	140,367	142.9	142,891	175.4	175,372	122.8	122,819	178.7	178,704
12/4/2017	86.2	86,178	55.8	55,816	21.5	21,533	284.0	284,013	36.9	36,898	420.1	420,088
12/5/2017	84.2	84,207	440.9	440,905	29.2	29,151	145.8	145,776	0.0	0	468.3	468,346
12/6/2017	0.0	0	261.5	261,520	160.3	160,269	247.4	247,385	0.0	0	446.1	446,132
12/7/2017	0.0	0	353.9	353,947	137.8	137,818	254.4	254,434	0.0	0	449.1	449,098
12/8/2017	5.7	5,661	369.3	369,322	126.4	126,381	225.6	225,594	97.7	97,743	270.5	270,479
12/9/2017	0.0	0	196.1	196,101	61.5	61,458	242.8	242,810	103.4	103,387	358.6	358,570
12/10/2017	0.0	0	212.7	212,654	67.3	67,330	232.0	231,962	113.0	112,960	356.4	356,435
12/11/2017	0.0	0	306.8	306,796	94.4	94,394	291.0	291,028	162.3	162,310	435.5	435,484
12/12/2017	0.0	0	277.7	277,656	79.4	79,436	333.5	333,505	33.9	33,933	498.2	498,181
12/13/2017	157.2	157,201	372.8	372,804	37.4	37,389	184.1	184,146	122.3	122,294	523.2	523,172
12/14/2017	29.7	29,730	216.8	216,799	49.4	49,373	205.1	205,072	23.5	23,467	364.1	364,142
12/15/2017	41.0	40,980	152.5	152,504	28.3	28,327	267.8	267,847	0.0	0	375.0	374,955
12/16/2017	55.8	55,836	76.8	76,826	0.0	0	212.5	212,507	0.0	0	304.9	304,862
12/17/2017	70.3	70,250	56.0	55,956	0.0	0	201.8	201,796	0.0	0	297.2	297,245
12/18/2017	30.6	30,636	159.7	159,672	0.0	0	174.5	174,451	52.8	52,791	276.5	276,459

RECORD OF GROUND-WATER PUMPAGE FOR REMAINING WELLS

Project Name: Penn State University-19890106

Well ID[1]: Wells 2, 14, 16, 17, 24, and 26

Report Period: 04/17-03/18

Date	Well 2		Well 14		Well 16		Well 17		Well 24		Well 26	
	1,000's	Actual	1,000's	Actual	1,000's	Actual	1,000's	Actual	1,000's	Actual	1,000's	Actual
12/19/2017	0.0	0	306.3	306,342	154.3	154,336	21.3	21,306	186.5	186,527	0.0	0
12/20/2017	83.1	83,054	140.2	140,214	0.0	0	107.1	107,077	83.4	83,374	137.4	137,429
12/21/2017	0.0	0	0.0	0	0.0	0	282.6	282,603	0.0	0	392.1	392,072
12/22/2017	0.0	0	0.0	0	0.0	0	250.4	250,358	0.0	0	337.5	337,459
12/23/2017	0.0	0	0.0	0	0.0	0	204.8	204,763	0.0	0	279.3	279,337
12/24/2017	0.0	0	0.0	0	0.0	0	204.9	204,875	0.0	0	293.7	293,671
12/25/2017	0.0	0	0.0	0	0.0	0	215.0	215,025	0.0	0	300.8	300,802
12/26/2017	0.0	0	130.8	130,806	72.8	72,807	111.0	110,989	79.9	79,871	159.6	159,584
12/27/2017	0.0	0	125.0	125,032	70.7	70,686	109.5	109,486	75.8	75,831	159.1	159,132
12/28/2017	0.0	0	140.2	140,202	78.2	78,168	141.3	141,309	81.7	81,747	182.5	182,455
12/29/2017	34.2	34,180	279.3	279,259	94.9	94,860	68.7	68,683	171.3	171,255	0.0	0
12/30/2017	74.4	74,410	249.0	249,010	0.0	0	78.4	78,367	150.4	150,422	0.0	0
12/31/2017	99.1	99,079	169.5	169,479	0.0	0	133.3	133,335	98.7	98,684	193.7	193,747
1/1/2018	0.0	0	0.0	0	0.0	0	225.7	225,668	0.0	0	316.9	316,857
1/2/2018	0.0	0	58.7	58,748	17.5	17,537	291.8	291,836	0.0	0	368.0	367,962
1/3/2018	67.9	67,905	69.8	69,840	36.6	36,584	256.7	256,708	54.2	54,238	385.4	385,392
1/4/2018	108.4	108,402	185.3	185,265	119.0	118,995	106.1	106,088	25.0	25,036	175.0	174,951
1/5/2018	100.6	100,565	152.2	152,171	190.6	190,616	120.7	120,658	0.0	0	307.7	307,742
1/6/2018	0.0	0	165.1	165,054	151.8	151,849	79.1	79,064	0.0	0	427.6	427,608
1/7/2018	0.0	0	182.5	182,546	14.0	13,989	0.0	0	136.7	136,693	409.9	409,858
1/8/2018	0.0	0	471.4	471,390	106.1	106,109	143.3	143,326	63.0	62,974	494.0	493,989
1/9/2018	0.0	0	350.5	350,477	28.2	28,219	321.9	321,939	151.3	151,275	565.4	565,402
1/10/2018	0.0	0	319.7	319,701	0.0	0	261.2	261,221	143.6	143,573	470.0	469,983
1/11/2018	149.5	149,453	266.5	266,492	0.0	0	291.2	291,224	26.9	26,886	418.5	418,454
1/12/2018	33.4	33,416	410.4	410,356	0.0	0	249.2	249,228	187.7	187,659	288.4	288,423
1/13/2018	63.7	63,698	118.4	118,357	0.0	0	232.0	232,012	13.6	13,582	342.4	342,426
1/14/2018	233.8	233,803	323.1	323,113	0.0	0	268.0	268,028	0.0	0	382.5	382,514
1/15/2018	199.7	199,695	278.0	278,044	0.0	0	256.4	256,427	0.0	0	362.8	362,813
1/16/2018	45.3	45,279	308.1	308,083	71.8	71,788	272.6	272,590	0.0	0	433.8	433,829
1/17/2018	178.0	177,960	344.0	343,950	29.4	29,441	308.0	307,987	0.0	0	454.5	454,513
1/18/2018	69.0	69,004	421.1	421,114	0.0	0	318.4	318,408	143.8	143,820	544.3	544,344
1/19/2018	7.5	7,463	61.3	61,271	0.0	0	287.9	287,861	22.4	22,424	436.0	435,953
1/20/2018	123.8	123,835	170.6	170,614	0.0	0	295.3	295,271	0.0	0	428.5	428,462
1/21/2018	0.0	0	332.1	332,052	48.0	47,979	238.8	238,787	77.9	77,874	416.3	416,326
1/22/2018	0.0	0	405.4	405,380	115.8	115,787	307.3	307,304	0.0	0	509.9	509,886
1/23/2018	0.0	0	345.9	345,903	98.8	98,751	300.5	300,483	0.0	0	481.6	481,606
1/24/2018	169.9	169,936	273.9	273,901	11.3	11,261	298.9	298,888	0.0	0	413.6	413,594
1/25/2018	194.9	194,913	295.5	295,514	0.0	0	36.2	36,210	197.6	197,562	427.4	427,447
1/26/2018	226.2	226,167	323.2	323,233	0.0	0	244.0	243,955	42.5	42,489	428.0	428,042
1/27/2018	77.2	77,246	105.3	105,331	0.0	0	231.1	231,070	0.0	0	322.1	322,082

RECORD OF GROUND-WATER PUMPAGE FOR REMAINING WELLS

Project Name: Penn State University-19890106

Well ID[1]: Wells 2, 14, 16, 17, 24, and 26

Report Period: 04/17-03/18

Date	Well 2		Well 14		Well 16		Well 17		Well 24		Well 26	
	1,000's	Actual	1,000's	Actual	1,000's	Actual	1,000's	Actual	1,000's	Actual	1,000's	Actual
1/28/2018	78.4	78,450	235.9	235,867	36.0	35,998	288.3	288,334	0.0	0	406.7	406,694
1/29/2018	0.0	0	358.5	358,506	103.0	102,967	283.6	283,627	0.0	0	467.3	467,336
1/30/2018	25.6	25,572	351.7	351,721	27.5	27,450	301.9	301,876	131.3	131,262	521.3	521,321
1/31/2018	0.0	0	333.2	333,177	81.8	81,848	302.8	302,838	23.4	23,442	485.8	485,795
2/1/2018	0.0	0	301.5	301,457	100.7	100,655	289.9	289,915	0.0	0	427.2	427,187
2/2/2018	0.0	0	253.0	253,046	35.8	35,792	179.0	178,974	110.1	110,100	372.7	372,692
2/3/2018	0.0	0	304.3	304,282	37.1	37,090	185.1	185,124	111.4	111,411	385.6	385,621
2/4/2018	0.0	0	291.1	291,060	0.0	0	236.1	236,116	51.1	51,081	381.7	381,714
2/5/2018	37.7	37,714	300.5	300,484	20.5	20,478	165.2	165,235	0.0	0	408.5	408,474
2/6/2018	0.0	0	463.3	463,322	0.0	0	310.3	310,265	0.0	0	558.2	558,219
2/7/2018	0.0	0	288.7	288,738	0.0	0	224.4	224,376	0.0	0	568.1	568,054
2/8/2018	0.0	0	110.9	110,935	0.0	0	329.2	329,206	0.0	0	471.0	470,968
2/9/2018	0.0	0	212.2	212,210	12.6	12,596	322.3	322,313	0.0	0	542.2	542,203
2/10/2018	300.4	300,428	231.3	231,264	80.5	80,468	158.3	158,253	116.6	116,558	474.2	474,240
2/11/2018	76.1	76,075	303.1	303,109	14.2	14,170	29.7	29,685	99.6	99,583	193.5	193,547
2/12/2018	0.0	0	372.8	372,783	81.4	81,449	304.2	304,151	1.0	1,007	468.2	468,219
2/13/2018	0.0	0	285.9	285,929	31.4	31,436	328.8	328,799	83.9	83,931	536.8	536,761
2/14/2018	77.4	77,395	148.9	148,885	169.1	169,127	49.5	49,450	38.9	38,933	534.1	534,093
2/15/2018	0.0	0	198.8	198,791	169.1	169,086	0.0	0	0.0	0	644.8	644,790
2/16/2018	0.0	0	337.5	337,494	183.1	183,060	0.0	0	0.0	0	632.1	632,107
2/17/2018	0.0	0	505.6	505,646	136.4	136,395	0.0	0	0.0	0	539.5	539,482
2/18/2018	0.0	0	398.9	398,943	36.7	36,654	212.8	212,824	0.0	0	516.7	516,706
2/19/2018	157.7	157,735	64.7	64,683	0.0	0	290.4	290,354	125.1	125,063	493.7	493,721
2/20/2018	184.0	184,023	0.0	0	76.9	76,901	271.9	271,869	151.8	151,837	412.0	412,035
2/21/2018	81.5	81,484	253.6	253,567	112.1	112,073	296.8	296,775	185.2	185,219	398.2	398,154
2/22/2018	0.0	0	224.2	224,203	16.4	16,432	265.9	265,910	27.9	27,890	420.9	420,885
2/23/2018	0.0	0	465.7	465,655	58.8	58,796	261.9	261,862	0.0	0	601.8	601,822
2/24/2018	0.0	0	369.6	369,581	126.3	126,278	214.8	214,777	0.0	0	303.6	303,634
2/25/2018	0.0	0	366.7	366,704	134.8	134,751	201.7	201,700	0.0	0	281.4	281,362
2/26/2018	0.0	0	349.8	349,790	94.8	94,831	278.3	278,260	0.0	0	513.9	513,943
2/27/2018	0.0	0	395.7	395,684	146.4	146,400	188.1	188,144	0.0	0	376.8	376,842
2/28/2018	0.0	0	419.1	419,095	139.0	139,030	245.7	245,688	0.0	0	374.8	374,776
3/1/2018	0.0	0	337.4	337,427	93.8	93,839	266.8	266,831	0.0	0	479.9	479,934
3/2/2018	0.0	0	377.8	377,817	110.1	110,138	221.4	221,400	115.3	115,250	332.5	332,470
3/3/2018	0.0	0	250.4	250,364	115.3	115,347	151.6	151,553	0.0	0	99.2	99,179
3/4/2018	0.0	0	246.1	246,050	46.8	46,835	151.3	151,346	0.0	0	178.5	178,462
3/5/2018	83.0	82,988	259.2	259,205	0.0	0	182.8	182,839	0.0	0	120.5	120,508
3/6/2018	20.9	20,938	61.4	61,427	0.0	0	184.5	184,467	0.0	0	273.2	273,221
3/7/2018	2.2	2,249	176.9	176,913	79.3	79,336	172.4	172,369	37.9	37,897	180.2	180,239
3/8/2018	62.8	62,850	306.3	306,333	74.7	74,733	192.0	192,013	159.1	159,139	278.9	278,944

RECORD OF GROUND-WATER PUMPAGE FOR REMAINING WELLS

Project Name: Penn State University-19890106
Well ID[1]: Wells 2, 14, 16, 17, 24, and 26
Report Period: 04/17-03/18

Date	Well 2		Well 14		Well 16		Well 17		Well 24		Well 26	
	1,000's	Actual	1,000's	Actual	1,000's	Actual	1,000's	Actual	1,000's	Actual	1,000's	Actual
3/9/2018	0.0	0	104.5	104,521	110.1	110,113	68.5	68,458	122.6	122,598	135.1	135,125
3/10/2018	47.1	47,062	146.0	145,981	55.6	55,558	89.9	89,921	115.9	115,855	150.4	150,448
3/11/2018	121.9	121,900	252.9	252,900	64.7	64,700	190.6	190,600	71.3	71,300	225.0	225,000
3/12/2018	12.9	12,928	345.8	345,779	119.7	119,734	232.1	232,061	0.0	0	346.0	346,029
3/13/2018	0.0	0	264.3	264,250	55.6	55,648	261.6	261,565	41.7	41,735	499.0	499,042
3/14/2018	7.4	7,408	419.2	419,222	62.4	62,395	124.9	124,868	66.8	66,764	459.2	459,222
3/15/2018	0.0	0	221.4	221,439	195.1	195,140	127.5	127,477	171.2	171,211	506.7	506,652
3/16/2018	30.0	30,044	406.0	406,018	168.3	168,287	250.8	250,766	94.7	94,702	228.2	228,176
3/17/2018	0.0	0	370.0	369,974	124.6	124,633	211.9	211,895	0.0	0	315.3	315,279
3/18/2018	111.0	110,989	267.2	267,228	78.5	78,468	125.6	125,622	0.0	0	400.2	400,188
3/19/2018	45.3	45,259	339.2	339,214	95.9	95,888	209.0	209,046	0.0	0	490.2	490,222
3/20/2018	88.1	88,056	273.1	273,135	29.7	29,703	38.4	38,432	14.9	14,877	404.0	404,037
3/21/2018	20.6	20,624	363.8	363,789	138.4	138,444	252.6	252,570	90.8	90,815	279.0	278,991
3/22/2018	17.7	17,683	580.5	580,463	97.0	97,032	313.8	313,772	263.5	263,484	372.5	372,524
3/23/2018	123.0	122,967	244.3	244,341	18.6	18,551	244.1	244,104	127.7	127,712	398.3	398,348
3/24/2018	43.6	43,576	280.0	279,963	57.3	57,298	213.8	213,767	179.0	178,974	404.1	404,123
3/25/2018	100.0	99,958	184.7	184,672	50.9	50,914	75.1	75,102	152.6	152,562	332.5	332,486
3/26/2018	52.2	52,219	460.3	460,295	151.3	151,317	213.0	213,046	41.8	41,818	408.4	408,407
3/27/2018	0.0	0	72.5	72,476	21.7	21,707	292.5	292,514	0.0	0	435.9	435,891
3/28/2018	153.5	153,460	316.9	316,918	143.9	143,879	271.1	271,110	129.9	129,894	463.4	463,423
3/29/2018	242.0	241,982	75.4	75,383	201.8	201,833	250.1	250,085	40.7	40,685	354.6	354,577
3/30/2018	48.0	47,981	113.9	113,872	25.5	25,496	304.7	304,733	0.0	0	496.2	496,227
3/31/2018	0.0	0	325.2	325,167	102.8	102,821	196.4	196,374	0.0	0	224.8	224,812
Average (g	**89**	**88,577**	**229**	**229,005**	**64**	**63,515**	**191**	**190,935**	**78**	**77,691**	**381**	**380,974**
ft^3/day	11.8411	11841.061	30.6136817	30613.682	8.490736	8490.7361	25.524358	25524.358	10.389952	10385.83761	50.92898	50928.98259

Appendix C-1. Pumping rates for wells UN-2, UN-14, UN-16, UN-17, UN-24, and UN-26.

RECORD OF GROUND-WATER PUMPAGE AND WATER LEVELS

Project Name: Penn State University-19890106
Well ID[1]: WELL #37
Report Period: 04/17-03/18
Description of water level measurement point[2]:

Week Period	Pumpage (gallons)	Depth to Water (ft.)[3]
1/1/2017	0	88
1/8/2017	0	90
1/15/2017	0	84
1/22/2017	0	86
1/29/2017	0	75
2/5/2017	0	78
2/12/2017	0	73
2/19/2017	0	71
3/5/2017	0	76
3/12/2017	0	76
3/19/2017	0	78
3/26/2017	0	77
4/2/2017	0	61
4/9/2017	0	58.0
4/16/2017	126,000	65.0
4/23/2017	450,000	66.0
4/30/2017	0	70.0
5/7/2017	1,224,000	49.0
5/14/2017	900,000	53.0
5/21/2017	0	63.0
5/28/2017	522,000	65.0
6/4/2017	396,000	57.0
6/11/2017	1,242,000	63.0
6/18/2017	360,000	65.0
6/25/2017	864,000	66.0
7/2/2017	0	69.0
7/9/2017	0	67.0
7/16/2017	0	69.0
7/23/2017	0	87.0
7/30/2017	0	70.0

Week Period	Pumpage (gallons)	Depth to Water (ft.)[3]
08/06/17	1,692,060	82.0
08/13/17	605,700	77.0
08/20/17	457,670	77.0
08/27/17	195,960	78.0
09/03/17	1,037,080	86.0
09/10/17	12,650	84.0
09/17/17	2,832,210	64.0
09/24/17	1,336,550	100.0
10/01/17	1,992,660	83.0
10/08/17	841,780	100.0
10/15/17	655,080	94.0
10/22/17	500,910	92.0
10/29/17	0	92.0
11/05/17	0	68.0
11/12/17	0	-
11/19/17	0	70.0
11/26/17	0	68.0
12/03/17	0	75.0
12/10/17	0	72.0
12/17/17	0	-
12/24/17	0	75.0
12/31/17	0	81.0
1/7/2018	0	80.0
1/14/2018	0	79.0
1/21/2018	0	71.0
1/28/2018	0	73.0
2/4/2018	0	74.0
2/11/2018	0	73.0
2/18/2018	0	74.0
2/25/2018	0	43.0
3/4/2018	0	32.0
3/11/2018	0	39.0
3/18/2018	0	48.0
3/25/2018	0	52.0

Average (gal/day)	**49984.41096**
ft^3/day	6681.966041

Appendix C-2. Pumping Rates for well UN-37

Appendix D

Living Filter 10 Year Water Table Elevations

DATE	P-1	P-2	P-3	P-4	P-5	W-1	W-2	W-3	W-5	W-6	W-7	G-10	G-12
6/30/2008	941.2	994.04	1007.64	1015.59	1001.59	1020.98	1015.89	1026.35	1019.32	1007.76	1012.35	1011.06	995.97
9/29/2008	928.2	984.14	1000.04	1008.89	995.55	1016.18	1013.39	1023.95	1019.32	1002.36	1010.65	1008.26	1008.47
12/29/2008	924.4	981.74	996.94	1005.59	993.05	1013.98	1011.19	1022.35	1019.32	999.76	1008.05	1005.76	1006.27
3/30/2009	929.9	981.24	996.44	1004.09	992.05	1012.98	1009.19	1019.85	1019.32	998.75	1006.55	1004.26	1004.27
6/30/2009	927.1	978.34	994.14	1001.79	988.45	1009.38	1006.79	1016.95	1019.32	996.36	1004.35	1001.66	1002.57
9/29/2009	927.4	976.24	993.94	1001.09	987.05	1006.48	1003.69	1014.35	1019.32	993.26	1001.55	996.26	999.27
12/29/2009	927.9	977.24	992.44	999.09	984.05	1003.48	1000.69	1010.85	1019.32	990.26	999.05	996.26	996.271
3/30/2010	930.9	977.24	992.44	998.59	983.55	1002.48	999.69	1009.85	1019.32	990.26	998.05	995.26	995.77
6/30/2010	934.4	982.74	994.94	999.59	984.55	1002.98	999.19	1195.35	1159.32	990.76	997.55	995.76	995.77
9/29/2010	921.4	971.74	986.94	994.09	980.05	997.98	996.19	1006.35	990.32	985.76	993.55	991.76	991.77
12/29/2010	931.7	951.44	985.74	992.39	978.55	996.98	994.49		991.32	984.36	992.55	989.56	989.37
3/30/2011		969.04	983.14	989.69	976.65	996.98	993.19	956.85	995.62	985.46	991.15	989.96	959.27
6/30/2011	929.1	984.84	995.44	1000.79	986.05	1003.18	1002.09	1011.47	1000.22	991.08	995.55	996.46	996.07
9/29/2011	932.7	982.94	996.54	1024.09	987.75	1004.78	1000.59	1010.55	999.22	992.46	997.85	996.86	996.57
12/29/2011	950	987.34	1000.74	1004.99	991.05	949.28	1004.49	1014.95	999.52	995.66	1001.35	1000.76	1000.87
3/29/2012	944.2	993.64	1005.14	1012.29	996.85	1015.48	1009.59	1021.55	1009.52	1001.66	1007.25	1006.86	1006.67
6/29/2012	932.5	977.94	990.94	997.79	984.55	1017.18	1013.49	1023.85	1004.72	1003.46	1009.95	1009.56	1009.17
9/28/2012	930.2	986.54	1001.94	1011.69	998.05	1019.58	1016.99	1018.75		1005.36	1013.05	1011.76	1011.87
12/28/2012	932.3	983.94	1001.14	1010.29	996.45	1018.88	1016.59	1027.65	1009.42	1004.16	1012.45	1011.26	1010.87
3/29/2013	933.3	984.64	1000.64	1009.99	995.95	1017.88	1015.29	1026.15	1010.22	1003.95	1011.45	1010.06	1009.67
6/29/2013	936.3	984.64	999.84	1008.79	995.35	1016.58	1014.19	1024.55	1007.82	1003.36	1010.55	1009.36	1008.87
9/28/2013	936	986.24	1001.54	1009.49	995.15	1014.68	1011.89	1021.85	1007.92	1001.06	998.65	1006.26	1006.17
12/28/2013	926.7	978.44	994.04	1002.99	989.95	1009.28	1007.79	1017.55	1001.72	995.96	1004.25	1002.26	1001.97
3/29/2014	935	975.84	990.44	998.29	985.55	1005.18	1003.19	1012.95	999.2	992.53	1000.35	998.36	998.37
6/29/2014	932.5	977.94	990.54	997.79	984.55	1003.88	1001.69	1011.05	997.82	992.86	998.95	997.36	997.37
9/28/2014	950	869.84	1080.44	999.09	984.45	1002.48	999.09	1008.85	997.32	989.86	996.95	995.06	994.87
12/28/2014	931.3	976.64	992.14	998.59	983.35	1000.88	998.79	1008.05	994.62	989.06	997.05	994.06	993.87
3/29/2015	926	970.14	983.94	990.99	976.55	995.48	993.49	1002.15	987.62	983.56	991.15	989.36	988.77
6/29/2015	935.5	974.34	985.74	993.19	977.25	995.58	993.29	1002.15	990.22	984.76	991.25	989.46	989.37
9/28/2015	931.8	972.94	987.14	992.69	978.95	995.58	992.78	1000.95	992.52	984.46	990.55	989.06	988.87
12/28/2015	926.7	968.94	983.94	990.19	975.65	993.88	991.59	1000.05	987.62	982.76	989.45	987.26	987.27
3/28/2016	932.3	967.64	981.94	988.39	973.85	992.38	990.19	998.55	986.12	979.76	987.65	986.06	985.77
6/28/2016	927.3	967.54	981.24	987.69	973.85	992.18	989.79	998.25	987.92	981.26	987.85	985.86	985.87
9/27/2016	924.4	964.64	980.04	985.99	971.95	990.18	987.89	995.75	984.32	979.16	985.85	983.86	983.87
12/27/2016	920.9	960.94	976.04	982.69	969.15	986.88	984.49	992.75	980.72	974.76	982.35	980.06	979.77
3/28/2017	926.2	961.04	975.94	980.99	967.95	984.38	982.49	989.95	982.02	974.46	980.35	978.86	979.07
6/28/2017	934.7	966.2	978.5	984.4	970.2	986.4	983.3	991.1	982.6	976.2	980.4	980.3	979.4
9/27/2017	927.6	960.8	981.4	987.7	972.9	988.6	985.3	993.2	985.2	977.8	983.5	982	981.8
12/27/2017	922.1	963.34	977.64	984.39	969.75	986.98	984.29	991.95	981.82	975.86	982.25	980.36	980.47
3/28/2018	940.6	963.24	976.44	982.69	967.25	984.68	982.19	990.05	982.72	973.56	980.05	978.46	978.17
Average	**931.6076923**	**972.958**	**992.9055**	**998.2355**	**983.636**	**1001.331**	**1000.01025**	**1013.068462**	**1003.63641**	**990.39875**	**997.0925**	**995.577**	**994.419025**

Appendix D-1. 10 year Water Table Elevations from 2008-2018 and averages for all 13 Living Filter Wells.

Appendix E

2015 Concentration Maps by Layer

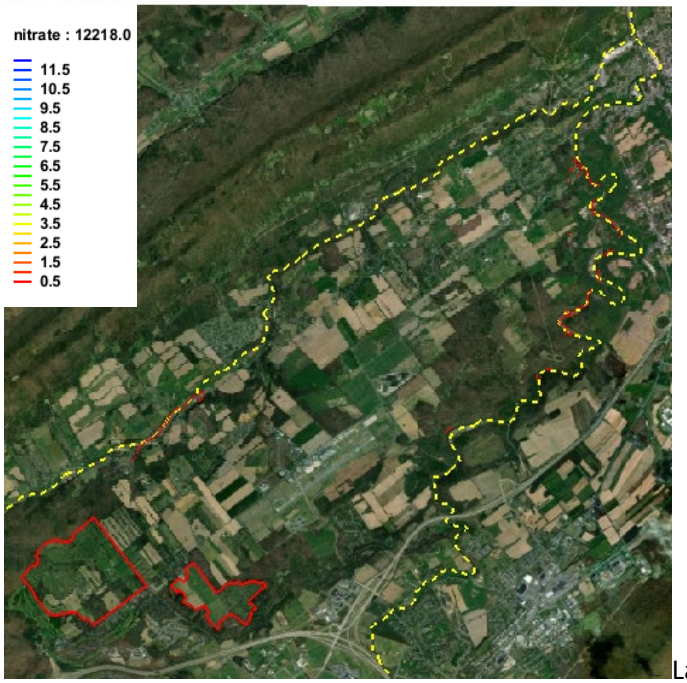

Layer 1

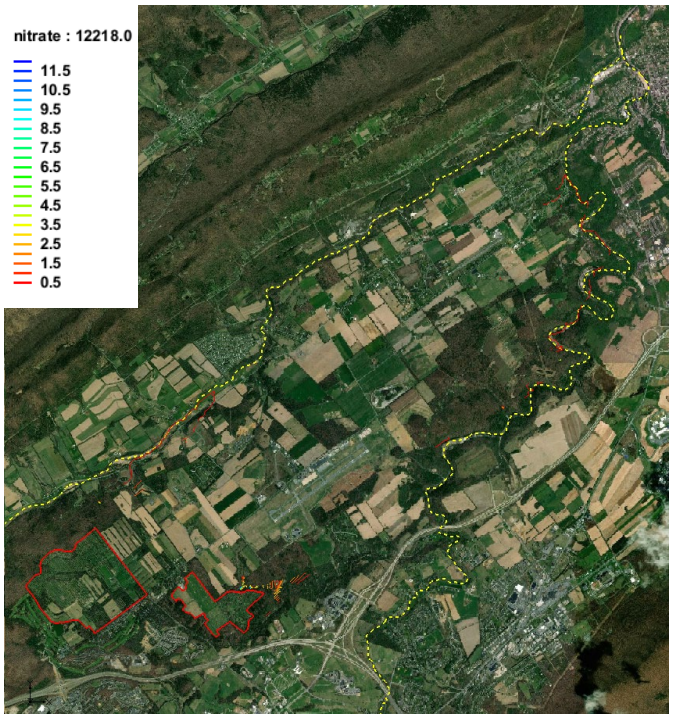

Layer 2

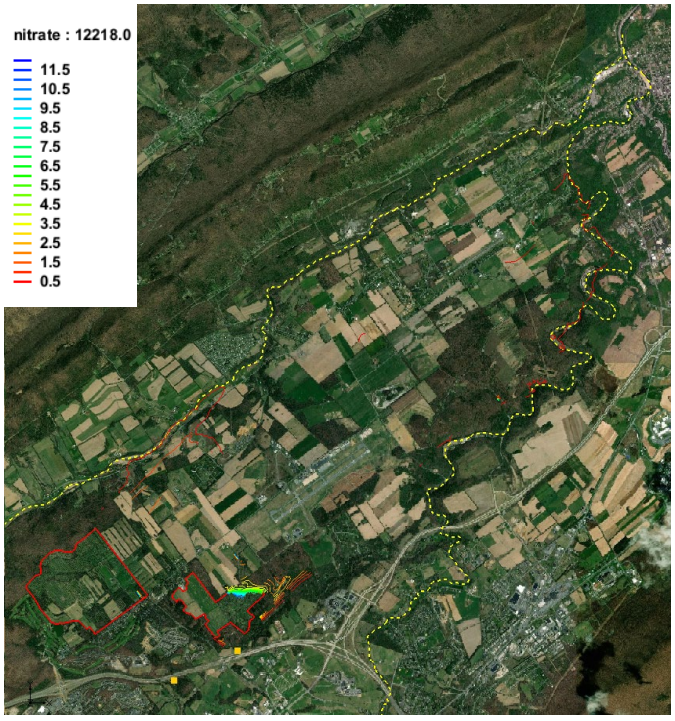

Layer 3

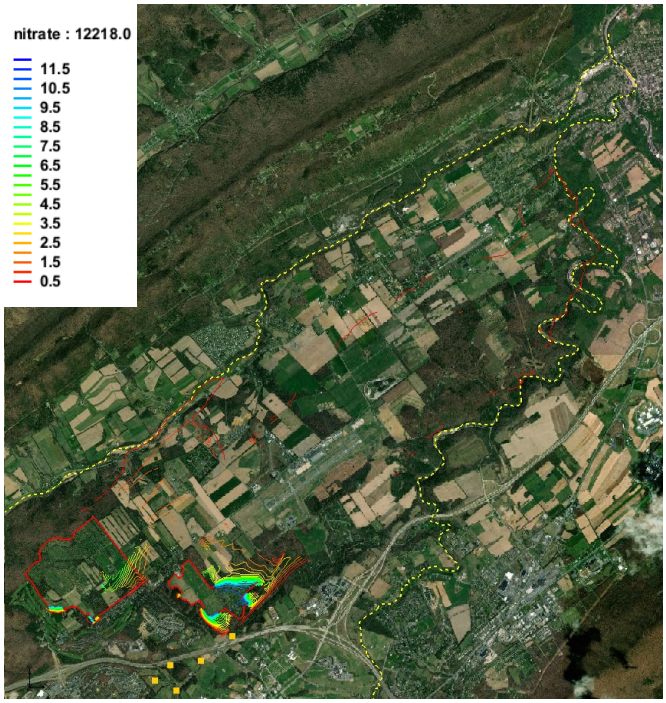

Layer 4

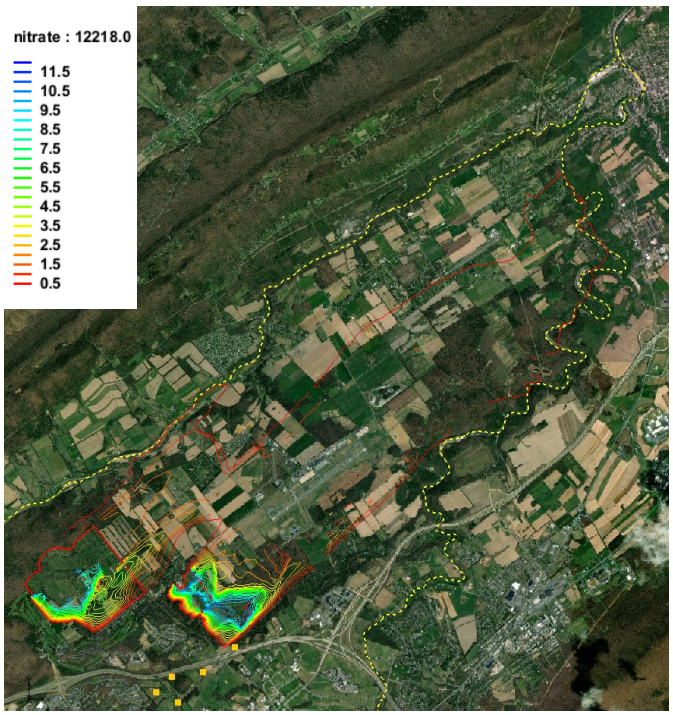

Layer 5

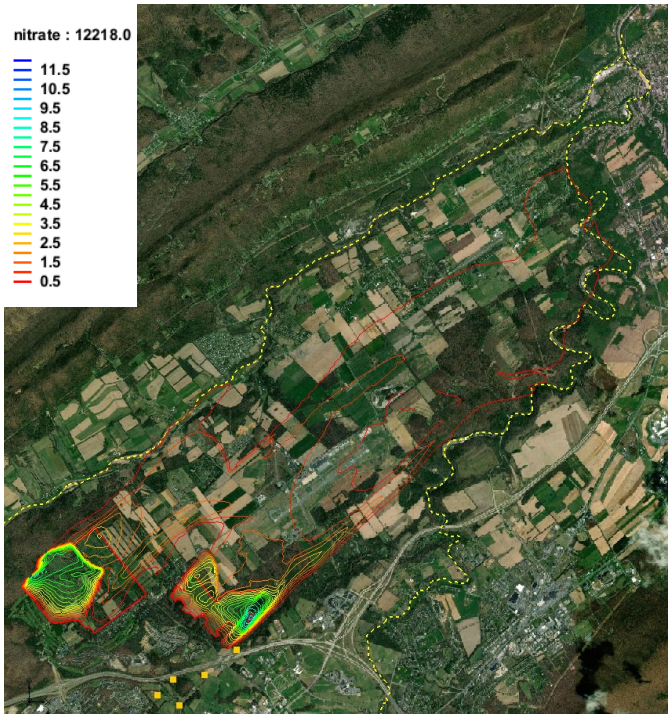

Layer 6

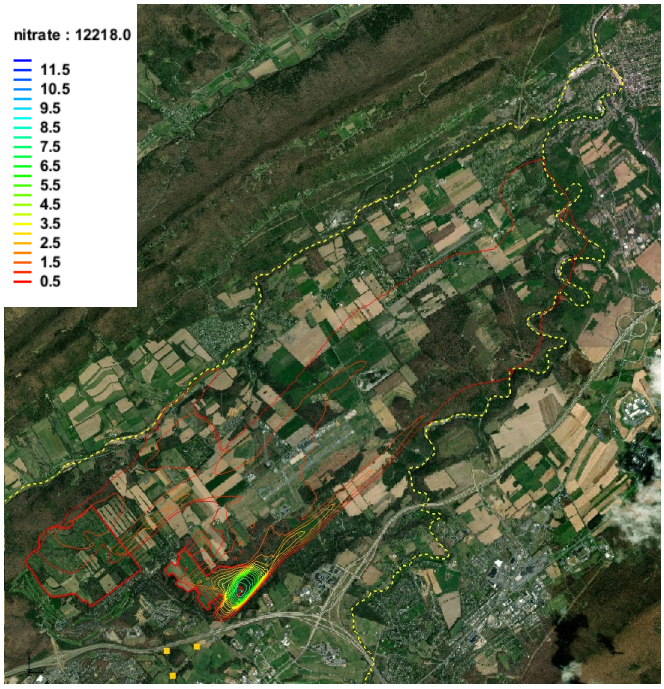

Layer 7

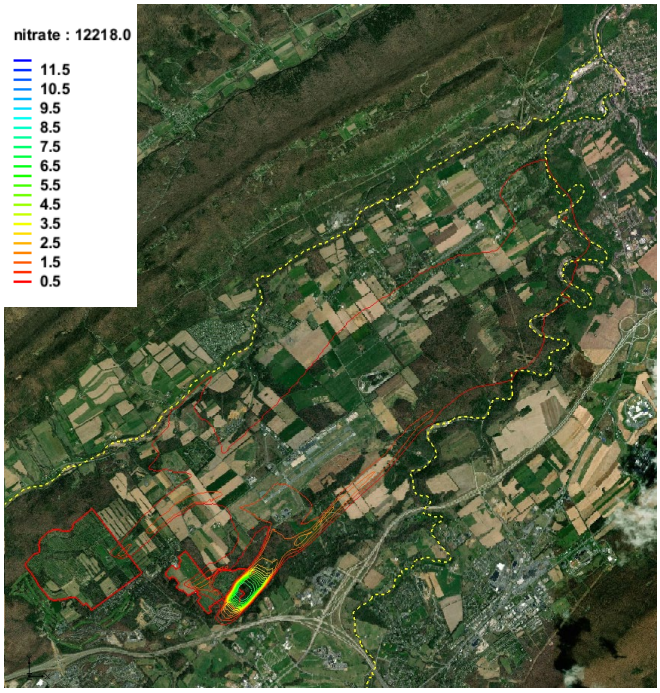

Layer 8

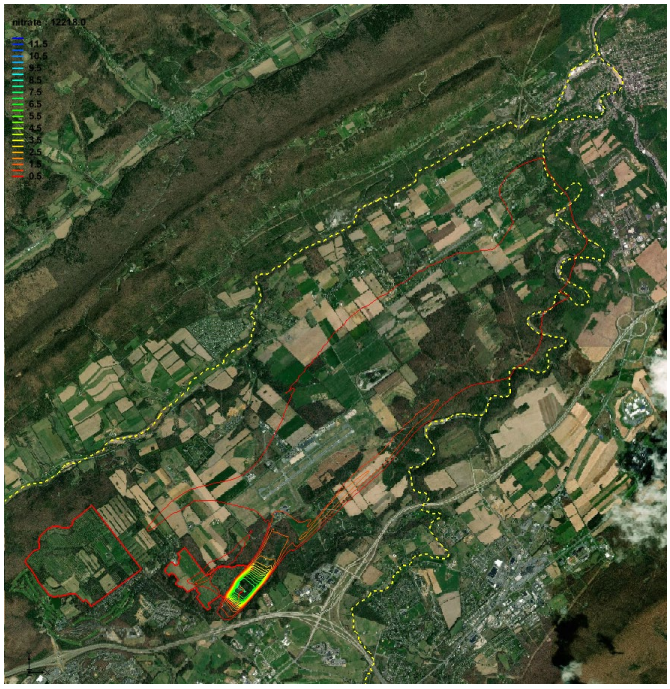

Layer 9

Appendix F

2035 Concentration Maps by Layer

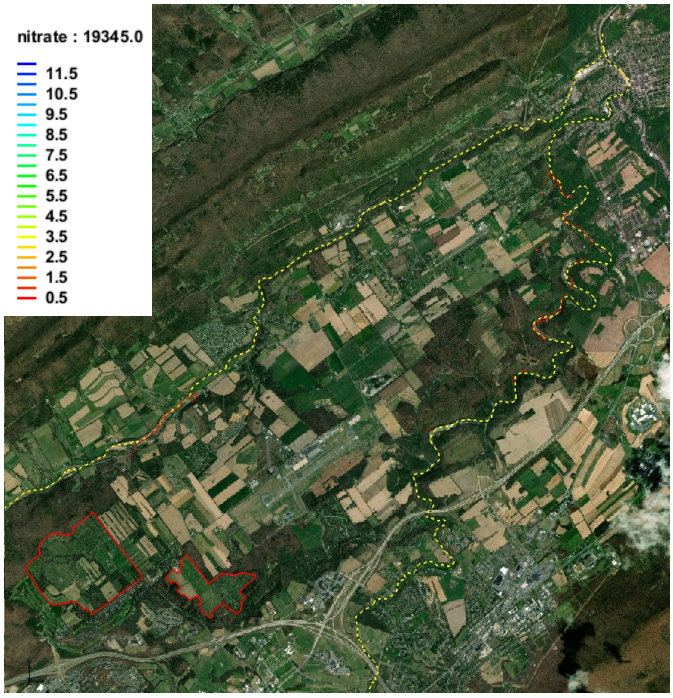

Layer 1

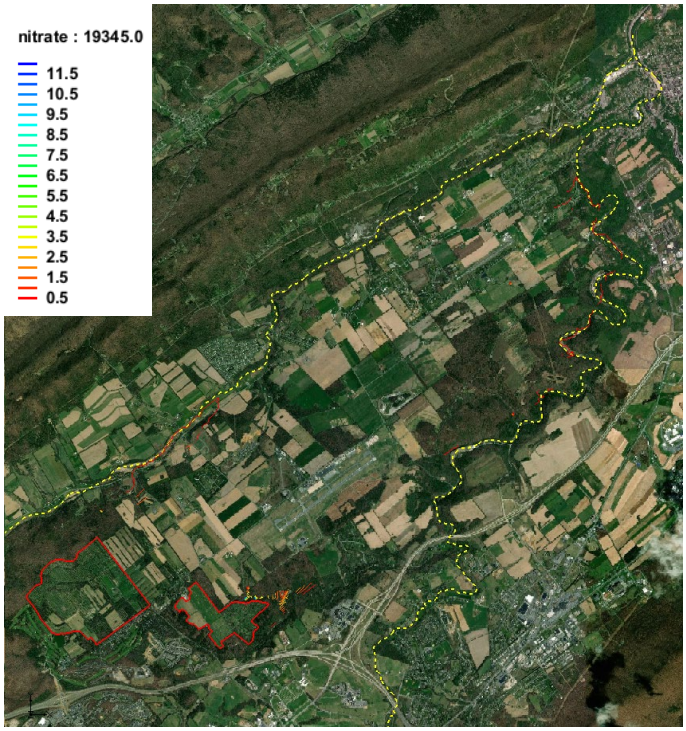

Layer 2

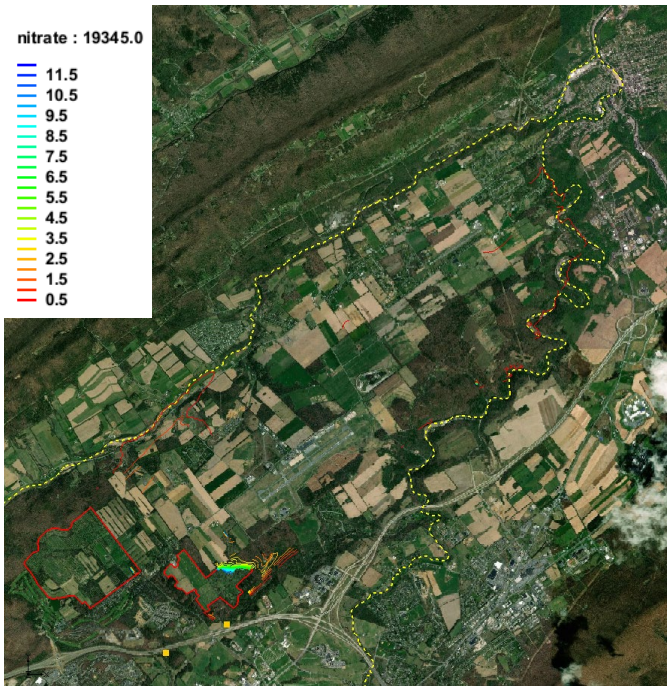

Layer 3

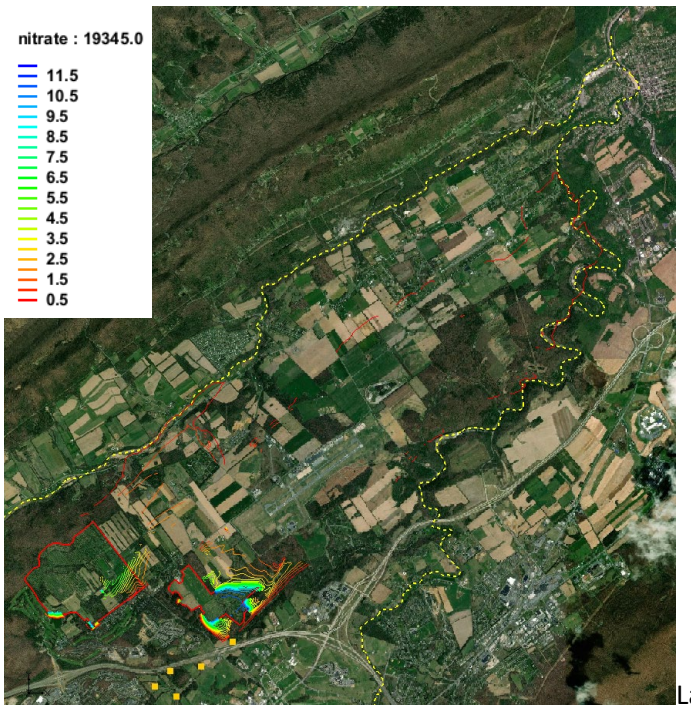

Layer 4

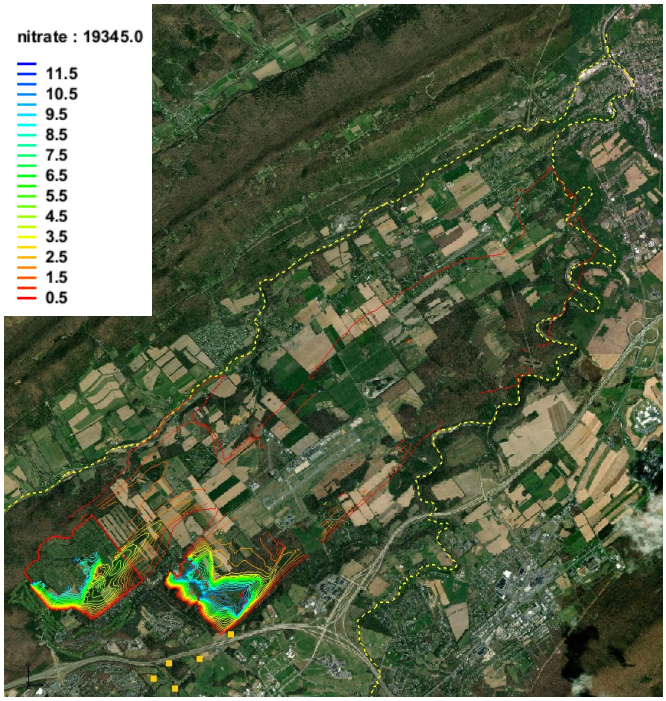

Layer 5

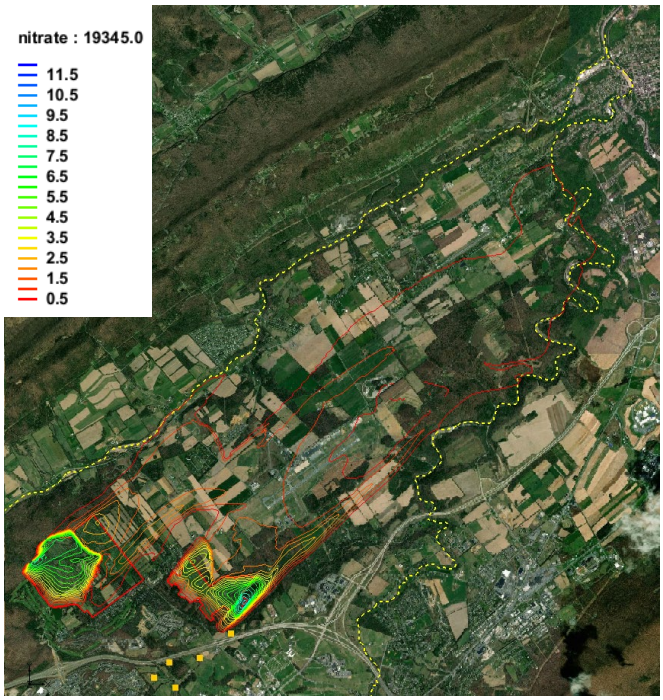

Layer 6

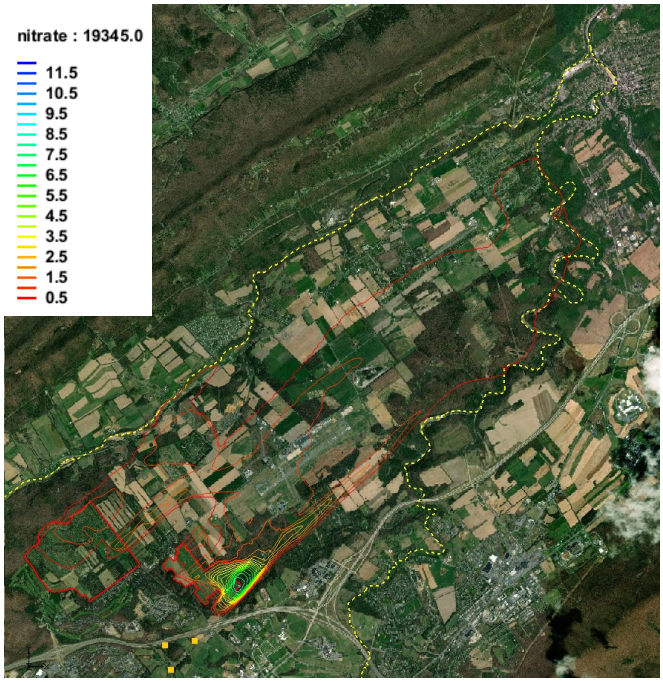

Layer 7

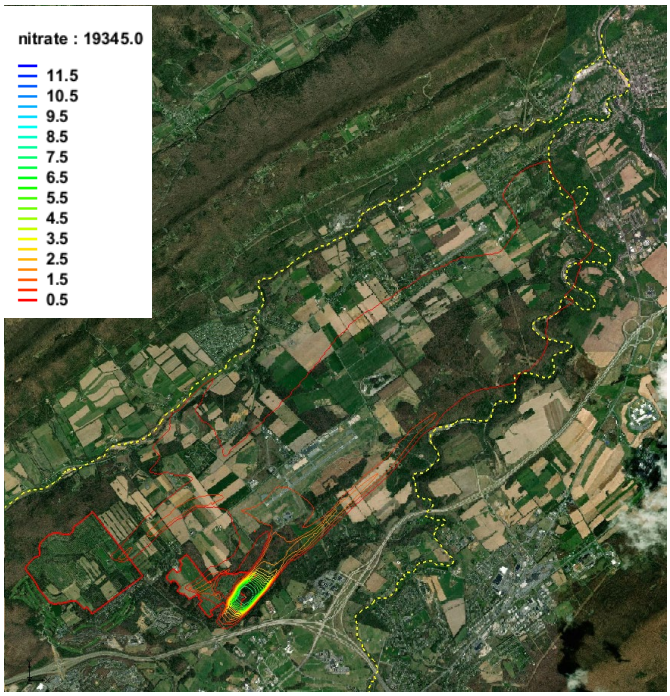

Layer 8

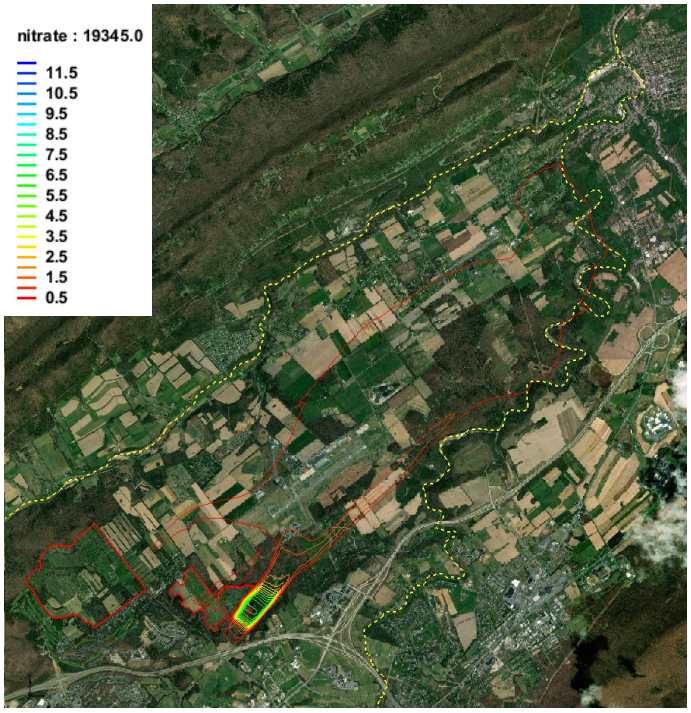

Layer 9

Appendix G

Model Parameters

Irrigation and Recharge Areas

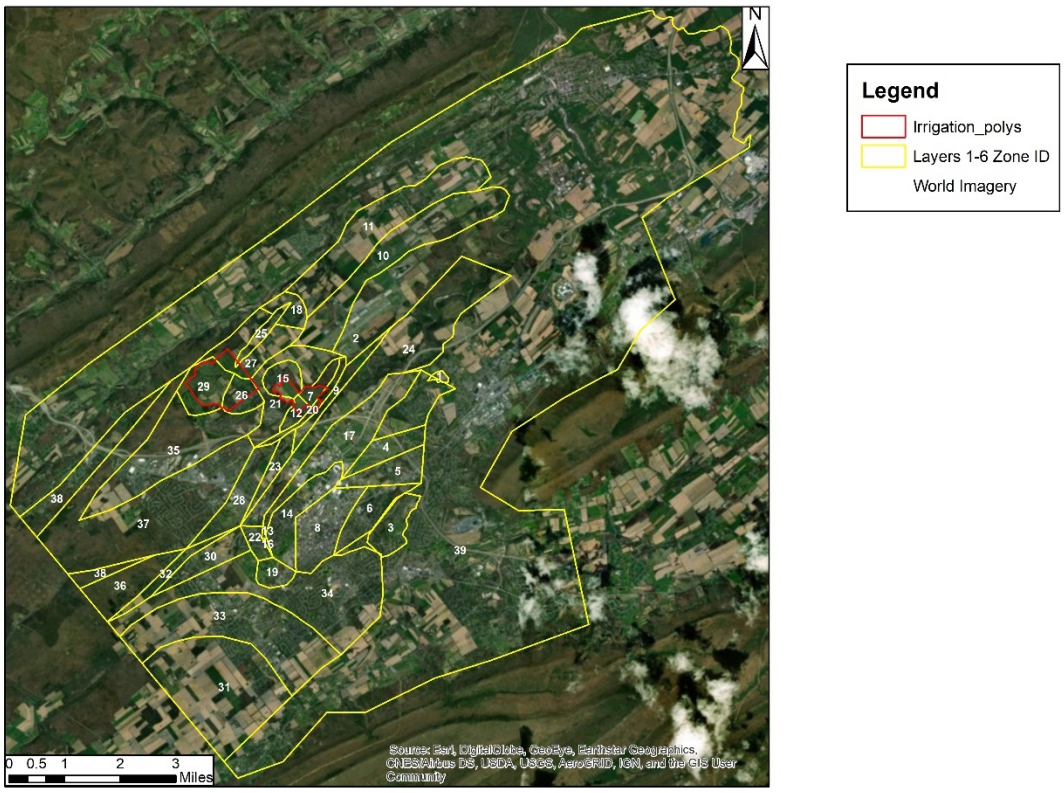

Conductivity zones for layers 1-6 and their corresponding values.

Spring Creek Watershed Layers 1-6 Properties					
ID	Horizontal Conductivity (ft/d)	Horizontal Anisotropy	Vertical Anisotropy	Porosity	Longitudinal Dispersivity
1	1	1	0.1	0.05	50
2	125	1	0.1	0.05	50
3	0.1	1	0.1	0.05	50
4	200	1	0.1	0.05	50
5	100	1	0.1	0.05	50
6	1	1	0.1	0.05	50
7	15	1	0.1	0.05	50
8	25	1	0.1	0.05	50
9	2250	1	0.1	0.05	50
10	1000	1	0.1	0.05	50
11	0.1	1	0.1	0.05	50
12	30	1	0.1	0.05	50
13	0.05	1	0.1	0.05	50
14	0.05	1	0.1	0.05	50
15	80	1	0.1	0.05	50
16	750	1	0.1	0.05	50
17	750	1	0.1	0.05	50
18	400	1	0.1	0.05	50
19	1.5	1	0.1	0.05	50
20	0.75	1	0.1	0.05	50
21	100	1	0.1	0.05	50
22	0.01	1	0.1	0.05	50
23	500	1	0.1	0.05	50
24	1000	1	0.1	0.05	50
25	650	1	0.1	0.05	50
26	400	1	0.1	0.05	50
27	400	1	0.1	0.05	50
28	0.25	1	0.1	0.05	50
29	200	1	0.1	0.05	50
30	10	1	0.1	0.05	50

31	10	1	0.1	0.05	50
32	25	1	0.1	0.05	50
33	1	1	0.1	0.05	50
34	1500	1	0.1	0.05	50
35	0.1	1	0.1	0.05	50
36	250	1	0.1	0.05	50
37	1	1	0.1	0.05	50
38	500	1	0.1	0.05	50
39	1	1	0.1	0.05	50
40	350	1	0.1	0.05	50
41	75	1	0.1	0.05	50
42	10	1	0.1	0.05	50

Irrigation and Recharge Areas

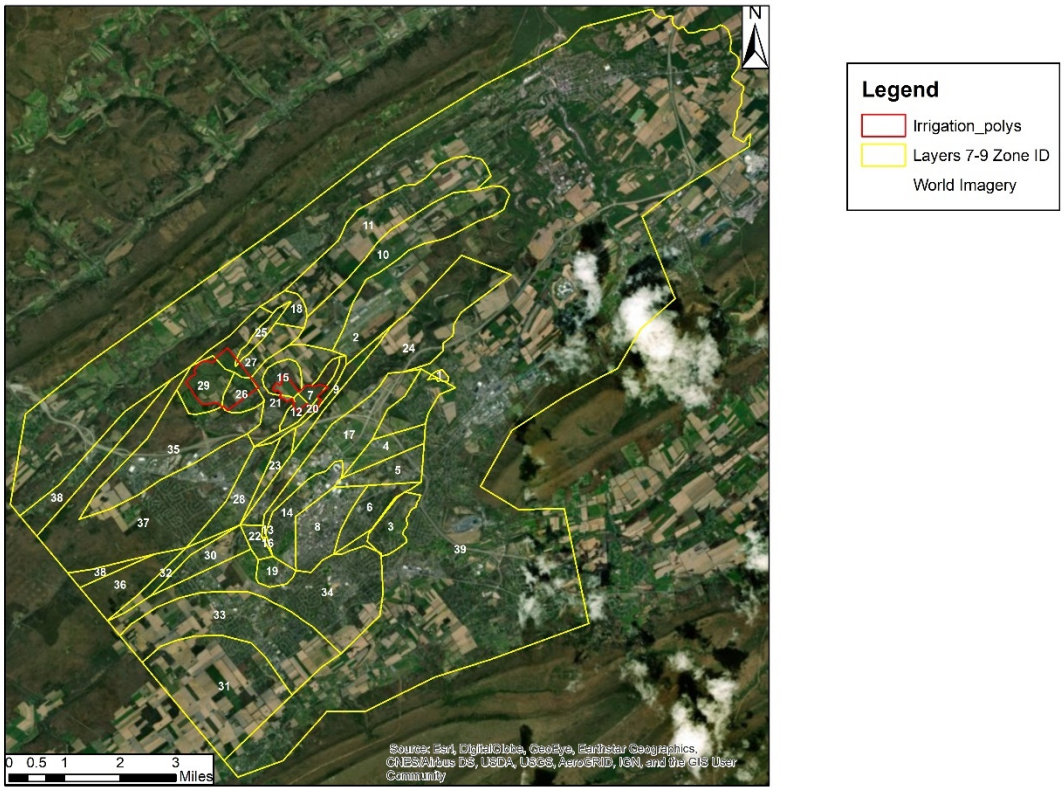

Conductivity zones for layers 7-9 and their corresponding values.

Spring Creek Watershed Layers 7-9 Properties					
ID	Horizontal Conductivity (ft/d)	Horizontal Anisotropy	Vertical Anisotropy	Porosity	Longitudinal Dispersivity
1	1	1	0.1	0.05	50
2	125	1	0.1	0.05	50
3	0.1	1	0.1	0.05	50
4	200	1	0.1	0.05	50
5	100	1	0.1	0.05	50
6	1	1	0.1	0.05	50
7	0.05	1	0.1	0.05	50
8	25	1	0.1	0.05	50
9	5	1	0.1	0.05	50
10	1000	1	0.1	0.05	50
11	0.1	1	0.1	0.05	50
12	5	1	0.1	0.05	50
13	0.05	1	0.1	0.05	50
14	80	1	0.1	0.05	50
15	50	1	0.1	0.05	50
16	1500	1	0.1	0.05	50
17	1.5	1	0.1	0.05	50
18	1	1	0.1	0.05	50
19	5	1	0.1	0.05	50
20	0.01	1	0.1	0.05	50
21	25	1	0.1	0.05	50
22	1000	1	0.1	0.05	50
23	750	1	0.1	0.05	50
24	100	1	0.1	0.05	50
25	400	1	0.1	0.05	50
26	1	1	0.1	0.05	50
27	2250	1	0.1	0.05	50
28	5	1	0.1	0.05	50
29	25	1	0.1	0.05	50
30	0.1	1	0.1	0.05	50
31	150	1	0.1	0.05	50

32	1	1	0.1	0.05	50
33	2250	1	0.1	0.05	50
34	3	1	0.1	0.05	50
35	350	1	0.1	0.05	50
36	75	1	0.1	0.05	50
37	10	1	0.1	0.05	50

Irrigation and Recharge Areas

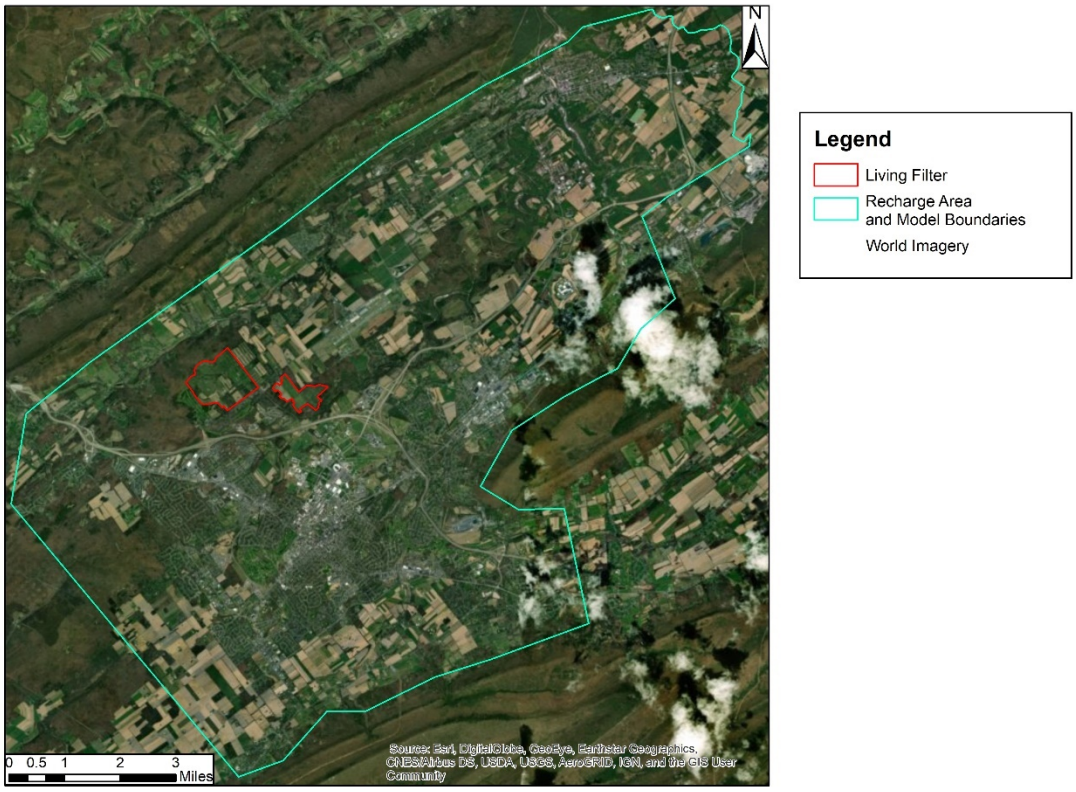

Size and shape of the model recharge areas along with their associated values

Spring Creek Watershed Precipitation Recharge Rate	
ID	**Recharge Rate (ft/d)**
1	0.0024

Adjusted Daily Irrigation Rate (ft/d)	
Days (d)	**Irrigation Rate (ft/d)**
0	0.014
11	0.008
41	0.007
72	0.008
117	0.015
133	0.015
181	0.013
194	0.012
228	0.015
266	0.015
304	0.014
315	0.015
345	0.013
376	0.008
406	0.007
437	0.014
482	0.016
498	0.016
529	0.015
566	0.013
590	0.013
648	0.017
650	0.014
699	0.016
711	0.012
742	0.009
772	0.008
803	0.011
861	0.016
864	0.016

895	0.015
943	0.012
956	0.012
1007	0.015
1015	0.013
1070	0.015
1076	0.011
1107	0.007
1137	0.007
1168	0.010
1223	0.015
1229	0.015
1260	0.014
1294	0.011
1321	0.012
1356	0.015
1380	0.013
1433	0.016
1441	0.011
1472	0.007
1502	0.006
1533	0.008
1575	0.015
1594	0.015
1648	0.014
1655	0.011
1686	0.013
1743	0.015
1745	0.013
1791	0.014
1806	0.010
1837	0.007
1867	0.006
1898	0.009
1949	0.016
1959	0.016
2002	0.014
2020	0.012
2051	0.014

2099	0.016
2111	0.016
2169	0.016
2172	0.011
2203	0.009
2233	0.008
2264	0.011
2316	0.017
2325	0.017
2372	0.015
2386	0.012
2417	0.014
2462	0.015
2476	0.015
2527	0.017
2537	0.012
2568	0.011
2598	0.009
2629	0.011
2681	0.017
2690	0.018
2741	0.016
2751	0.012
2782	0.015
2831	0.015
2841	0.014
2876	0.014
2925	0.009
2933	0.007
2987	0.006
3024	0.010
3042	0.015
3085	0.016
3097	0.014
3134	0.010
3151	0.012
3199	0.014
3234	0.012
3252	0.014

3286	0.010
3307	0.006
3358	0.005
3380	0.010
3419	0.015
3449	0.014
3477	0.013
3500	0.009
3524	0.011
3569	0.014
3602	0.012
3630	0.014
3661	0.009
3692	0.006
3722	0.006
3752	0.008
3785	0.015
3814	0.014
3827	0.013
3867	0.010
3888	0.011
3930	0.012
3967	0.011
3995	0.014
4024	0.009
4057	0.007
4088	0.005
4118	0.008
4147	0.013
4178	0.013
4204	0.012
4231	0.009
4266	0.011
4298	0.011
4302	0.009
4352	0.010
4386	0.008
4422	0.006
4429	0.005

4466	0.008
4500	0.012
4525	0.011
4563	0.010
4583	0.008
4624	0.010
4655	0.010
4683	0.008
4710	0.010
4753	0.006
4784	0.004
4819	0.003
4835	0.009
4855	0.014
4886	0.012
4924	0.010
5312	0.007
4987	0.011
5009	0.012
5047	0.010
5078	0.012
5108	0.008
5143	0.007
5178	0.005
5213	0.008
5240	0.013
5270	0.012
5296	0.011
5317	0.008
5353	0.009
5389	0.011
5417	0.010
5448	0.011
5478	0.009
5509	0.006
5544	0.005
5577	0.007
5606	0.012
5633	0.010

5663	0.010
5682	0.009
5718	0.009
5752	0.011
5787	0.010
5814	0.011
5843	0.009
5874	0.007
5905	0.005
5935	0.007
5967	0.013
5997	0.013
6028	0.012
6052	0.010
6087	0.011
6110	0.013
6143	0.010
6177	0.012
6206	0.009
6241	0.007
6269	0.006
6304	0.008
6334	0.012
6366	0.012
6390	0.011
6422	0.009
6457	0.010
6485	0.012
6514	0.010
6536	0.012
6570	0.009
6606	0.005
6641	0.004
6671	0.007
6705	0.012
6731	0.011
7127	0.011
6789	0.009
6816	0.011

6857	0.012
6884	0.010
6920	0.009
6949	0.009
6976	0.007
6995	0.005
7013	0.008
7026	0.010
7070	0.012
7097	0.012
7123	0.011
7145	0.008
7189	0.011
7215	0.011
7241	0.010
7272	0.012
7312	0.008
7346	0.006
7375	0.006
7396	0.008
7430	0.013
7461	0.012
7493	0.012
7517	0.009
7551	0.010
7587	0.012
7605	0.010
7641	0.012
7676	0.009
7703	0.006
7732	0.005
7755	0.007
7796	0.013
7822	0.012
7844	0.011
7878	0.009
7913	0.010
7943	0.011
7976	0.011

8007	0.013
8028	0.010
8067	0.007
8095	0.005
8123	0.007
8160	0.012
8180	0.011
8208	0.011
8231	0.008
8285	0.010
8314	0.013
8336	0.010
8361	0.012
8396	0.008
8425	0.008
8459	0.006
8487	0.010
8525	0.014
8560	0.012
8585	0.010
8614	0.008
8636	0.010
8677	0.011
8698	0.009
8726	0.011
8770	0.007
8803	0.005
8830	0.004
8854	0.006
8893	0.012
8915	0.012
8936	0.011
8964	0.009
8999	0.009
9041	0.012
9061	0.010
9090	0.011
9112	0.009
9154	0.005

9180	0.004
9215	0.007
9244	0.012
9264	0.013
9312	0.010
9328	0.009
9362	0.010
9391	0.012
9418	0.011
9454	0.013
9481	0.009
9516	0.006
9547	0.005
9573	0.009
9607	0.013
9636	0.013
9664	0.010
9698	0.009
9730	0.009
9761	0.012
9790	0.010
9824	0.010
9853	0.008
9880	0.006
9909	0.004
9944	0.009
9978	0.013
9999	0.012
10027	0.010
10062	0.009
10100	0.010
10135	0.012
10163	0.010
10184	0.012
10216	0.008
10253	0.006
10286	0.005
10302	0.007
10342	0.011

10372	0.010
10405	0.008
10435	0.007
10471	0.008
10500	0.009
10531	0.008
10555	0.009
10588	0.007
10617	0.005
10658	0.004
10708	0.010
10742	0.010
10786	0.007
10825	0.007
10848	0.008
10924	0.009
10940	0.007
10983	0.004
11058	0.006
11078	0.010
11108	0.010
11122	0.009
11163	0.008
11217	0.009
11246	0.006
11289	0.007
11309	0.006
11361	0.005
11413	0.005
11432	0.008
11464	0.009
11500	0.007
11584	0.008
11610	0.007
11647	0.008
11676	0.006
11766	0.006
11792	0.009
11826	0.008

11870	0.007
11946	0.008
11974	0.006
12003	0.007
12038	0.007
12130	0.007
12158	0.009
12200	0.007
12218	0.006
19345	0.006

Total N Application rate (mg/L)

Concentration of Total N in Effluent (mg/L)	
Days (d)	Total N Concentration (mg/L)
0	10
11	10
41	10
72	10
117	10
133	10
181	10
194	10
228	10
266	10
304	10
315	10
345	10
376	10
406	10
437	10
482	10
498	10
529	10
566	10
590	10
648	10
650	10
699	10
711	10
742	10
772	10
803	10

861	10
864	10
895	10
943	10
956	10
1007	10
1015	10
1070	10
1076	10
1107	10
1137	10
1168	10
1223	10
1229	10
1260	10
1294	10
1321	10
1356	10
1380	10
1433	10
1441	10
1472	10
1502	10
1533	10
1575	10
1594	10
1648	10
1655	10
1686	10
1743	10
1745	10
1791	10
1806	10
1837	10
1867	10
1898	10
1949	10
1959	10
2002	10

2020	10
2051	10
2099	10
2111	10
2169	3.22
2172	10
2203	10
2233	10
2264	10
2316	24.3
2325	10
2372	19.3
2386	10
2417	10
2462	20.3
2476	10
2527	19.3
2537	10
2568	10
2598	10
2629	10
2681	24.7
2690	10
2741	31.14
2751	10
2782	10
2831	21.2
2841	10
2876	14.7
2925	16.3
2933	12.1
2987	14.11
3024	36.8
3042	38.5
3085	21.02
3097	24.64
3134	10
3151	23.35
3199	55.91

3234	19.9
3252	23.05
3286	14.04
3307	12.1
3358	9.2
3380	20.2
3419	17.59
3449	36.5
3477	23.8
3500	6
3524	14.2
3569	17.2
3602	20.21
3630	31.1
3661	26
3692	12.92
3722	13.3
3752	18
3785	27
3814	19.1
3827	45.7
3867	21.1
3888	25.6
3930	18.83
3967	21
3995	40.9
4024	11.1
4057	22.8
4088	18.8
4118	12.6
4147	16.1
4178	32.3
4204	10
4231	27.3
4266	21.65
4298	10
4302	10
4352	10
4386	3.7

4422	12.71
4429	10.86
4466	4.52
4500	17.361
4525	16.354
4563	17.464
4583	19.247
4624	21.16
4655	13.719
4683	10.305
4710	12.348
4753	16.492
4784	8.642
4819	0
4835	5.52
4855	17.88
4886	14.78
4924	16.98
5312	12.11
4987	14.49
5009	26.146
5047	14.592
5078	16.59
5108	13.871
5143	15.346
5178	11.61
5213	15.5
5240	24.2
5270	25.01
5296	20.91
5317	16.4
5353	8.3
5389	3.5
5417	5.1
5448	21.8
5478	12.3
5509	14.24
5544	19.85
5577	21.7

5606	13.8
5633	16.6
5663	13.9
5682	18.124
5718	3.15
5752	6
5787	4.85
5814	6.7
5843	10.99
5874	9.1
5905	10
5935	10
5967	12.11
5997	6.14
6028	15.29
6052	14
6087	15.1
6110	18.9
6143	7.82
6177	13.597
6206	17.21
6241	7.41
6269	7.03
6304	7.65
6334	6.78
6366	7.5
6390	8.75
6422	5.22
6457	7.2
6485	7.65
6514	10.17
6536	7.65
6570	15.95
6606	5.21
6641	7.61
6671	2.84
6705	5.55
6731	6.41
7127	3.71

6789	12.61
6816	9.33
6857	5.65
6884	7.71
6920	5.84
6949	12.1
6976	5.33
6995	10
7013	6.82
7026	1.11
7070	6.031
7097	14.415
7123	10
7145	9.51
7189	12.091
7215	13.081
7241	13.28
7272	13.265
7312	15.15
7346	10.669
7375	11.829
7396	12.42
7430	14.416
7461	15.198
7493	15.451
7517	17.715
7551	10
7587	10
7605	10
7641	10
7676	10
7703	8.36
7732	6.063
7755	6.308
7796	8.94
7822	7.68
7844	11.337
7878	12.268
7913	20

7943	10
7976	6.76
8007	10
8028	10.94
8067	10
8095	10
8123	10
8160	10
8180	10
8208	10
8231	10
8285	10
8314	10
8336	10
8361	10
8396	10
8425	10
8459	10
8487	10
8525	10
8560	10
8585	10
8614	10
8636	10
8677	10
8698	10
8726	10
8770	10
8803	10
8830	10
8854	10
8893	12.66
8915	10.7
8936	10
8964	10
8999	10
9041	10
9061	10
9090	10

9112	10
9154	10
9180	10
9215	10
9244	10
9264	10
9312	10
9328	10
9362	10
9391	10
9418	10
9454	10
9481	10
9516	10
9547	10
9573	10
9607	10
9636	10
9664	10
9698	10
9730	10
9761	10
9790	10
9824	10
9853	10
9880	10
9909	10
9944	10
9978	10
9999	10
10027	10
10062	10
10100	10
10135	10
10163	10
10184	10
10216	10
10253	10
10286	10

10302	10
10342	10
10372	10
10405	10
10435	10
10471	10
10500	10
10531	10
10555	10
10588	10
10617	10
10658	10
10708	10
10742	10
10786	10
10825	10
10848	10
10924	10
10940	10
10983	10
11058	10
11078	10
11108	10
11122	10
11163	10
11217	10
11246	10
11289	10
11309	10
11361	10
11413	10
11432	10
11464	10
11500	10
11584	10
11610	10
11647	10
11676	10
11766	10

11792	10
11826	10
11870	10
11946	10
11974	10
12003	10
12038	10
12130	10
12158	10
12200	10
12218	10
19345	10